SPATIALLY RESOLVED AND BULK ZINC ANALYSIS IN BIOLOGICAL SAMPLES OF PATIENTS AT DIFFERENT STAGES OF ALZHEIMER'S DISEASE BY HIGH RESOLUTION INDUCTIVELY COUPLED PLASMA MASS SPECTROMETRY

A Dissertation

presented to

the Faculty of the Graduate School

at the University of Missouri

In Partial Fulfillment

of the Requirements for the Degree

Doctor of Philosophy

---

by

JIANG DONG

Dr. J. David Robertson, Dissertation Supervisor

DECEMBER 2008

The undersigned, appointed by the dean of the Graduate School, have examined the dissertation entitled

SPATIALLY RESOLVED AND BULK ZINC ANALYSIS IN BIOLOGICAL SAMPLES OF PATIENTS AT DIFFERENT STAGES OF ALZHEIMER'S DISEASE BY HIGH RESOLUTION INDUCTIVELY COUPLED PLASMA MASS SPECTROMETRY

presented by Jiang Dong,

a candidate for the degree of doctor of philosophy,

and hereby certify that, in their opinion, it is worthy of acceptance.

Dr. J. David Robertson

Dr. Sheryl A. Tucker

Dr. C. Mike Greenlief

Dr. Renee D. Jiji

Dr. J. Steven Morris

ACKNOWLEDGEMENTS

I would like to thank many people who have made the completion of this dissertation and my doctoral program possible. A great thanks goes to my advisor, Dr. J. David Robertson, for his advice, mentoring and support. Dr. Robertson has been a role model to me with his enthusiasms to science, his open mind, his optimism and his critical thinking skills. His unfailing inspiration and encouragement was very much appreciated. His demand in excellence in my work undoubtedly helped prepare me for the challenges down the road. I was very fortunate to be a member of his research group.

I am very grateful to my other committee members, Dr. Sheryl A. Tucker, Dr. C. Mike Greenlief, Dr. Renee D. Jiji and Dr. J. Steven Morris for their assistance, support, kindness and suggestions. I enjoyed getting to know them better and appreciate their time and willingness to help. Their support made it possible for me to complete this dissertation in time.

A special note of appreciation goes to Amanda Crafford for introducing me to the world of ICP-MS. I thank her for her patience and effort during the training.

This project could not have been done without the support from Dr. Mark Lovell at the University of Kentucky Alzheimer's Disease Center. I especially thank Dr. Lovell for providing the precious samples used in this project.

Many thanks go to the Analytical Chemistry Group members at MURR, especially Jim Guthrie, Barry Higgins and Bryan Higgins for their invaluable guidance and support. It was a great pleasure getting to know and working with them.

I would also like to thank all the members of Dr. Robertson's Research Group, from whom I have learned a lot and whose friendships made the program fun. My gratitude extends to the whole Chemistry Department at MU. I acknowledge the financial support from the department and thank the professors, staff and students for all the ways that they have assisted me.

TABLE OF CONTENTS

ACKNOWLEDGEMENTS ii
LIST OF ILLUSTRATIONS vii
LIST OF TABLES viii
ABBREVIATIONS x
ABSTRACT xii
1. Alzheimer's Disease 1
1.1 Background 1
1.2 Risk factors 2
1.3 Different stages of AD 2
1.4 Pathological features 3
1.4.1 Amyloid plaques, Amyloid β peptide (Aβ) and Amyloid Precursor Protein (APP) 3
1.4.2 Neuofibrillary tangles and tau protein 4
1.5 AD diagnosis 4
1.6 Current treatment 6
1.7 Suggested mechanisms 7
1.7.1 Genetic defects 7
1.7.2 Amyloid cascade theory 8
1.7.3 Trace element imbalances 9
2. Zinc studies in AD 10
2.1 Zinc studies in AD 10
2.1.1 Zinc studies in AD brain 10
2.1.2 Zinc studies in AD serum 11
2.1.3 Zinc studies in AD cerebrospinal fluid barrier (CSF) 11
2.2 Zinc in biosystem and normal zinc homeostasis 12
2.3 Zinc pools 13
2.4 Proteins and channels to mediate Zn homeostasis 14
2.5 Specific aims 15

2.5.1 Development of a novel laser ablation inductively coupled plasma mass spectroscopy (LA-ICPMS) method for spatial quantification of Zn in soft tissue samples 15

2.5.2 Quantification of Zn in MCI senile plaques (SP) and neurofibrillary tangles (NFT) using the developed LA-ICPMS method 16

2.5.3 Human brain Zn levels in the progression of AD 17

2.5.4 Brain Zn levels in an APP/PS1/ZnT-1 mouse model 18

2.5.5 Serum and CSF Zinc levels in the progression of AD 18

3. Experimental 20

3.1 Inductively coupled plasma mass spectrometry (ICP-MS) introduction 20

3.1.1 Advantages and disadvantages of ICP-MS in trace element analysis 20

3.1.2 Basic principles of high resolution ICP-MS (HR-ICPMS) 20

3.2 Neutron activation analysis (NAA) introduction 24

3.3 Laser ablation ICP-MS (LA-ICP-MS) analysis of Zn in senile plaques (SP) and neurofibrillary tangles (NFT) 26

3.3.1 LA-ICP-MS introduction 26

3.3.2 Major challenges with LA-ICP-MS 28

3.3.3 Metal Standards 29

3.3.3.1 Thin film metal standards 29

3.3.3.2 Conformation of zinc concentrations by neutron activation analysis (NAA) 32

3.3.3.3 Homogeneity tests 33

3.3.3.4 Calibration Graphs 37

3.3.4 SP and NFT samples 40

3.4 Serum, cerebrospinal fluid (CSF) and brain tissue 42

3.4.1 ICP-MS analysis of serum, CSF and brain tissue 42

3.4.2 Method development with ICP-MS analysis 46

3.4.2.1 Precleaned trace metal free polypropylene vials 46

3.4.2.2 Acid strength effect and suitable internal standard 46

3.4.2.3 Effects of sample size and shaking time in serum analysis 52

3.4.3 Serum sampling and preparation 53

3.4.4 CSF sampling and preparation 55

3.4.5 Brain tissue sampling and preparation 56
3.4.5.1 Human Brain sampling and preparation 56
3.4.5.2 Mouse Brain sampling and preparation 57
3.4.6 Analytical Procedures 60
4. Results 62
4.1 Introduction to Statistical Analysis to Compare Group Means 62
4.1.1 Comparison of two groups 62
4.1.1.1 Independent-samples *t*-test 62
4.1.1.2 Paired-samples *t*-test 62
4.1.1.3 Three assumptions for *t*-test 63
4.1.1.4 Calculations and Decisions 63
4.1.2 More than Two Groups - Analysis of Variance (ANOVA) 64
4.1.2.1 Three assumptions in ANOVA 64
4.1.2.2 Violation of assumptions in ANOVA 65
4.1.2.2.1 Violation of normality 65
4.1.2.2.2 Violation of Homogeneity of Variance 65
4.1.2.2.3 Violation of independence of observations 66
4.1.2.3 Interaction in ANOVA 66
4.1.2.4 Post-Hoc Procedures 67
4.2 Laser ablation of crown ether complex standards 67
4.2.1 Method validation (Precision and Reproducibility of Thin Film Standards) 67
4.3 Laser ablation of soft tissue samples 68
4.3.1 Laser ablation of MCI Senile Plaques (SP) 68
4.3.2 Laser ablation of MCI Neurofibrillary Tangles (NFT) 72
4.4 Bulk Brain Tissue Analysis 77
4.4.1 Mouse Brain 77
4.4.1.1 Method validation 77
4.4.1.2 Statistial analysis method 77
4.4.1.3 Comparison of all subjects 78

4.4.1.4 Comparison of data segregated by sex 78
4.4.2 Human Brain 79
4.4.2.1 Method validation....79
4.4.2.2 Statistical analysis method 80
4.4.2.3 Comparison of all subjects 81
4.5 Serum 82
4.5.1 Method validation 82
4.5.2 Statistical analysis method 83
4.5.3 Comparison of all subjects 83
4.5.4 Comparison of data segregated by sex 84
4.6 CSF....86
4.6.1 Method validation 86
4.6.2 Statistical analysis method 87
4.6.3 Comparison of all subjects 87
4.6.4 Comparison of data segregated by sex 88
5. Discussion 91
5.1 Laser ablation 91
5.2 LA-HR-ICPMS analysis of Zn in MCI SP and NFT....93
5.3 Mouse Brain study 95
5.4 Human brain study 96
5.5 Serum and CSF study....98
5.6 Possible Zn roles in AD....99
APPENDICES.... 102
REFERENCES.... 113
VITA 131

LIST OF ILLUSTRATIONS

Figure Page

3.1 A schematic of the VG Axiom HR-ICP-MS 22

3.2 NAA spectrum of 34.1 ppm Zn standard 33

3.3 Five thin film standards cut for homogeneity studies 34

3.4 Example spectrum of 25.9 ppm zinc thin film standard 38

3.5 Zinc calibration curve obtained by ablation of standards with a 10 μm diameter laser spot size (n=4 per concentration) 39

3.6 Signal fluctuation of 25.9 ppm Zn standard during the day 40

3.7 Influence of nitric acid concentration on multi-elements signal strength 49

3.7 Influence of nitric acid concentration on multi-elements signal strength 50

3.8 A picture of digestion insert and vessel 59

4.1 Example of the brain tissue section that was analyzed 70

4.2 Zinc signal response from SP ablation of an MCI tissue section 70

4.3 Example of the brain tissue section after being ablated 74

4.4 Zinc signal response from NFT ablation of an MCI tissue section 74

4.5 Zn calibration curve for human brain study 80

LIST OF TABLES

Table Page

3.1 General LA and ICP-MS settings for experiments conducted on metal crown ether standards and biological tissue samples 36

3.2 Ion percentage as a function of plasma temperature and ionization potential, calculated using Saha equation 51

3.3 Effects of shaking and sample volume on Zn concentration 53

3.4 Instrumental operating conditions for the Axiom HR-ICP-MS 61

4.1 The relative standard deviations (%RSD) of zinc metal crown ether standards over a 2 month period 68

4.2 Senile plaque sample subject demographic data 69

4.3 Average and standard deviation of the zinc concentrations (ppm) in MCI SP and MCI Neuropil 71

4.4 Average and standard deviation of the zinc concentrations (ppm) in Control Neuropil 71

4.5 Neurofibrillary tangle sample subject demographic data 73

4.6 Average and standard deviation of the zinc concentrations (ppm) in MCI NFT and MCI Neuropil 75

4.7 Average and standard deviation of the zinc concentrations (ppm) in Control Neuropil 76

4.8 Zinc concentrations (ppm) in the original mouse brain samples by groups 78

4.9 Zinc concentrations (ppm) in the original mouse brain samples by sex and group 79

4.10 Human brain subject demographic data 81

4.11 Zinc concentrations (ppm) in the original human brains by groups 82

4.12 Serum sample subject demographic data 84

4.13 Zinc concentrations (ppm) in the original serum samples by groups 84

4.14 Serum sample subject demographic data by sex 85

4.15 Zinc concentrations (ppm) in the original serum samples by sex and group 86

4.16 CSF sample subject demographic data 88

4.17 Zn concentrations (ppb) in the original CSF samples by groups..... 88

4.18 CSF sample subject demographic data by sex..... 90

4.19 Zn concentrations (ppb) in the original CSF samples by sex and group..... 90

5.1 Comparison between the relative standard deviation of the standard sample used for Feldmann et al., cryogenically cooled ablation chamber soft tissue studies with normalization by carbon ratio and the Spurr's standard sample utilized in our LA-HR-ICPMS without ablation chamber cooling or carbon normalization of the signal..... 92

5.2 Comparison of the concentrations of zinc obtained from the testing of senile plaques using μ-PIXE and LA-ICP-MS. The μ-PIXE data was obtained by testing 9 separate subjects, 10 plaques per subject. The LA-ICP-MS was obtained for zinc by analyzing 5 subjects, 10-14 plaques per subject 94

ABBREVIATIONS

AD - Alzheimer's disease

ADL – activities of daily living

APP - amyloid precursor protein

Aβ - amyloid β peptide

BBB - blood-brain barrier

BCB - blood-cerebrospinal fluid barrier

CDR - clinical dementia rating

CER - cerebellum

CPS - counts/second

CSF - cerebrospinal fluid

CT - computerized tomography

DRS - dementia rating scale

EAD - early Alzheimer's disease

ESA - electrostatic analyzer

FAAS - flame atomic absorption spectrometry

fMRI - functional magnetic resonance imaging

FWHM - full width half maximum

GFAAS - graphite furnace atomic absorption spectrometry

HPG - hippocampus/parahippocampal gyrus

HPGe - high-purity gamma-ray detectors

ICP-MS inductively coupled plasma mass spectrometry

ICP-OES inductively coupled plasma optical emission spectrometry

LAD - late Alzheimer's disease

LA-ICPMS laser ablation inductively coupled plasma mass spectrometry

LMMA - laser microprobe mass analysis

LOD - limits of detection

LOQ - limits of quantification

MCI - mild cognitive impairment

MMSE - Mini Mental State Exam

MRI - magnetic resonance imaging

MT/T - metalloprotein/thionein

MTF-1 - metal response element-binding transcription factor-1

N - neuropil

NAA - neutron activation analysis

NC - normal control

NFT - neurofibrillary tangle

OPT - optical projection tomography

PET - positron emission tomography

PIXE- particle induced X-ray emission

PMI - post mortem interval

ppb - parts per billion

ppm - parts per million

PS1 - presenilin proteins 1

PS2 - presenilin proteins 2

RSD - relative standard deviation

SD - standard deviation

S.E.M. - standard error of the mean

SEM - scanning electron microscopy

SEM-EDX scanning electron microscopy and energy dispersive X-ray analysis

SIMS - secondary ion mass spectrometry

SIM - single ion monitoring

SMTG - superior and middle temporal gyrus

SP - senile plaques

SPECT - single photon emission computed tomography

SRM - standard reference material

XRD - X-ray diffraction

XRF - X-ray fluorescence spectrometry

ZIP - Zrt-Irt like protein

ZnT - zinc transporter

SPATIALLY RESOLVED AND BULK ZINC ANALYSIS IN BIOLOGICAL SAMPLES OF PATIENTS AT DIFFERENT STAGES OF ALZHEIMER'S DISEASE BY HIGH RESOLUTION INDUCTIVELY COUPLED PLASMA MASS SPECTROMETRY

Jiang Dong

Dr. J. David Robertson, Dissertation Supervisor

ABSTRACT

One hypothesis that has gained considerable attention in the pathogenesis of Alzheimer's disease (AD) is trace element toxicity, and various elements, including zinc, have become the foci of renewed interest.

The first study is analysis of spatially resolved zinc from senile plaques (SP) and neurofibrillary tangles (NFT) using laser ablation high resolution inductively coupled plasma mass spectrometry (LA-HR-ICPMS). By using matrix matched thin film standards, zinc was quantified in SP, NFT and adjacent neuropils in subjects with mild cognitive impairment (MCI). In addition, zinc was quantified in neuropils from age-matched normal control (NC) subjects. There are significant increases of zinc in MCI SP and MCI NFT compared to surrounding neuropils, suggesting a role of zinc in the pathogenesis of AD.

The second study is bulk zinc analysis in human serum, cerebrospinal fluid (CSF) and brain tissues from subjects with mild cognitive impairment (MCI), early AD (EAD), late-stage AD (LAD) and age-matched normal control (NC) subjects using HR-ICPMS. There are significant changes in zinc levels from subjects with MCI compared to subjects from NC group. The studies indicate that zinc homeostasis is altered early in the progression of AD and may play a role in the pathogenesis of AD.

1. Alzheimer's Disease

1.1 Background

As the average life expectancy of human beings continues to increase, Alzheimer's disease (AD) has become a major concern among the elderly. In 1906, Dr. Alois Alzheimer, a German doctor after whom AD is named, noticed changes in the brain tissue of a woman Auguste D., who had died of an unusual mental illness. He found abnormal clumps of material (now called amyloid or senile plaques) and tangled bundles of fibers (now called neurofibrillary tangles) in that patient's brain. Today, these plaques and tangles in the brain are the key markers of AD and their presence is used to confirm a diagnosis of AD at autopsy.

Alzheimer's disease is the most common form of dementia, a brain disorder that affects people's daily activities. Estimates indicate that around 3% of Americans between ages 65 and 74, 19% ages between 75 and 84, and 47% of individuals over age 85 are victims of AD [1]. Around 4.5 million Americans and 8 million people worldwide suffer from AD [2]. In addition, it is estimated that 14.3 million Americans will have the disease by 2050 [2]. AD is a slow disease. The time the disease lasts till death varies from 2 to 20 years after diagnosis. On average, AD patients live from 8 to 10 years after they are diagnosed. The average cost of care for an individual with AD is $174,000 [3]. At over $100 billion per year, AD is the third most costly disease in the U.S., after heart disease and cancer. The federal government estimated spending approximately $647 million for AD research in fiscal year 2005.

1.2 Risk factors

Advanced age is the greatest risk factor for AD and the risk of developing AD almost doubles every 5 years after age 65. Genetic factors include presenilin (PS) 1 and 2 and amyloid precursor protein (APP) mutations [4, 5], and the presence of apolipoprotein E4 alleles [6]. Additional risk factors for AD include head injury [7], low educational attainment and low linguistic ability early in life [8, 9], diabetes [10-12], hyperlipidemia [13], hypertension [14], heart disease [15], smoking [16, 17], elevated plasma homocysteine [18] and obesity [19].

1.3 Different stages of AD

Alzheimer's disease is characterized by a progressive decline in multiple cognitive functions. It is thought to start with mild memory problems and end with severe brain damage. Mild cognitive impairment (MCI) [20] is widely considered to be a transition stage between normal aging and dementia. It is different from both AD and normal age-related memory change. Individuals with MCI experience memory loss to a greater extent than one would expect for age, yet they do not satisfy the criteria for dementia or probable AD. According to Petersen et al. [20], the clinical criteria for diagnosis of amnestic MCI include: a) memory complaints, b) objective memory impairment for age and education, c) intact general cognitive function, d) intact activities of daily living, and e) the subject is not demented. Current data suggest that conversion from MCI to dementia occurs at a rate of 10 to 15% per year [21] with around 80% conversion by the sixth year of follow up. About 5% of diagnosed MCI subjects remain stable or convert to normal [22, 23]. MCI progresses to early AD (EAD). EAD is clinically characterized by a) a decline in cognitive function from a previous

higher level, b) declines in one or more areas of cognition in addition to memory, c) a clinical dementia rating scale score of 0.5 to 1, d) impaired activities of daily living (ADL) and e) a clinical evaluation that excludes other causes of dementia. Further progression of the disease leads to late stage AD (LAD) characterized by severe dementia with disorientation, profound memory impairment, global cognitive deficits and immobility.

1.4 Pathological features

Pathologically, AD is characterized by the presence of large numbers of senile plaques (SP), neurofibrillary tangles (NFT), neuropil thread formation, and neuron and synapse loss, particularly in the hippocampus, amygdala, entorhinal cortex, neocortex and associated area of the neocortex. The senile plaques are composed of beta amyloid (Aß) peptides and the neurofibrillary tangles are intracellular deposits of hyperphosphorylated tau protein filaments.

1.4.1 Amyloid plaques, Amyloid β peptide (Aβ) and Amyloid Precursor Protein (APP)

The Aß peptides are derived from the transmembrane protein amyloid precursor protein (APP) [24]. Amyloid precursor protein is now known to have neuroprotective and neurotrophic functions. It is involved in cell adhesion [25], cell-cell and cell-matrix interactions, and modulates the outgrowth of neuritis [26]. The APP bound to neuronal membranes is normally cleaved by α-secretase into a large soluble fragment APPα and a carboxy terminal P3 fragment which remains bound to the membrane. The latter is then cleaved by γ-secretase to form another soluble fragment and a smaller

membrane anchored fragment. In AD subjects, APP is first cleaved by β-secretase and yields a smaller soluble fragment APPβ and a larger membrane associated fragment, which is then cleaved by γ-secretase and produces the insoluble 40- or 42-amino acid peptide forms of amyloid-ß ($Aß_{40}$ or $Aß_{42}$) fragments and a small membrane associated fragment. More recent studies suggest that in addition to insoluble Aß present in SP, soluble Aß oligomers are present in the AD brain that may represent the main toxic form of Aß, thus implicating the soluble oligomers in the disease process [27-29].

1.4.2 Neuofibrillary tangles and tau protein

Neuofibrillary tangles are mainly found in the neocortex, hippocampus, basal forebrain and the brain stem [30]. Like amyloid plaques, neuofibrillary tangles (NFTs) are the result of abnormal aggregation of proteinaceous material. However, unlike the extracellular Aβ pathology, NFTs are intracellular deposits of paired helical filaments mainly composed of hyperphosphorylated tau protein [31]. Tau is a microtubule associated protein. Under normal conditions, tau is bound to microtubules and helps assemble and stabilize the microtubules that convey cell organelles, glycoproteins and other important materials through the neuron. In AD, tau becomes detached from microtubules and aggregates into NFTs, which may disturb the normal processes [32]. As NFTs develop within neurons, they fill the intracellular space and are believed to kill the affected neurons.

1.5 AD diagnosis

The definitive diagnosis of AD can only be made by brain autopsy. It is desired to detect AD as early as possible although the etiology and pathogenesis of neuron

degeneration and loss of AD patients remain unknown.

AD is usually associated with memory impairment and old age. However, only some of those who have memory impairment as they age develop AD. Different types of tests are used to rule out other causes of symptoms that are similar to those of AD. Among them are laboratory tests, imaging tests, and neuropsychological tests.

Such causes of dementia as nutritional deficiencies, infection, metabolic disorders and drug effects can be detected with laboratory tests. Examples of laboratory tests include complete blood cell count, sedimentation rate, vitamin B_{12} and folic acid levels, β-amyloid peptide ($A\beta_{42}$) level, total tau-protein level, phosphorylated tau level and syphilis serologic testing.

Imaging tests are utilized to rule out other memory disorders, such as tumors, multi-infarct dementia and stroke. Imaging tests include positron emission tomography (PET), single photon emission computed tomography (SPECT), optical projection tomography (OPT), magnetic resonance imaging (MRI), and functional MRI (fMRI).

Neuropsychological tests enable a clinician to analyze and document a patient's cognitive status, as well as attention, perception, motor, problem solving and language skills. There are many types of neuropsychological tests for dementia, such as the Mini-Mental State Exam (MMSE) and Clinical Dementia Rating (CDR) scale. MMSE [33] is commonly used because of its simplicity and low cost. There are also some rating scales for characterizing subjects in different stages of AD. The Clinical Dementia Rating (CDR) [34] is a popular scale to classily subjects from normal to AD. Patients start from normal (CDR 0) to questionable dementia (CDR 0.5) to mild dementia (CDR 1) to moderate dementia (CDR 2) and to severe dementia (CDR 3).

The general recognition that MCI may represent a transition state between normal cognitive decline due to aging and dementia offers possibilities for early diagnosis and potential treatment with the aim of delaying the onset or preventing dementia.

1.6 Current treatment

Currently, there is no medical treatment that can cure or stop the progression of AD. There are five medications approved by the Food and Drug Administration (FDA) to treat the cognitive and behavioral symptoms of AD. The cholinergic system is essential for memory and learning and is progressively destroyed in AD patients. Cholinesterase inhibitors work by preventing the breakdown of the brain chemical acetylcholine. Tacrine, the first cholinesterase inhibitor, approved in 1993, is no longer clinically used because of possible side effects, such as liver damage. Other cholinesterase inhibitors include donepezil (Aricept), galantamine (Razadyne) and rivastigmine (Exelon) [35]. They are recommended for treatment of mild to moderate AD patients. The benefits of these drugs are far from dramatic. They only slow down the progression of AD and do not affect the underlying disease process.

Memantine is the fifth approved drug to treat AD. It is also the only approved drug for the treatment of moderately severe to severe AD [36]. Excessive activation of N-methyl-D-aspartate (NMDA) receptors may underlie the degeneration of cholinergic cells. Memantine is a fast NMDA- receptor antagonist. It blocks the NMDA receptor in the presence of sustained release of low glutamate concentrations and thus attenuates NMDA receptor function.

Even though there is no cure today, new compounds are being tested constantly. Most disease-modifying therapies are based on the amyloid hypothesis. Following this hypothesis, prevention of AD can be achieved by decreasing the production of Aβ, by increasing the clearance of Aβ formed or by prevention of aggregation of Aβ into amyloid plaques [37]. Since individuals with MCI are at a very high risk of developing Alzheimer's disease [21], it is expected that future clinical trials will focus increasingly on early intervention.

1.7 Suggested mechanisms

Alzheimer's disease has been a subject of intense scrutiny and, while the etiology and pathogenesis of neuron degeneration and loss are still unkown, it is now clear that AD is a disease of multiple, etiologic factors. Numerous mechanisms have been suggested for the cause of AD, such as genetic defects [4, 38], the amyloid cascade hypothesis [39], the oxidative stress hypothesis [40], trace element imbalance [41], or some combination of the above.

1.7.1 Genetic defects

Genes that cause rare, inherited forms of AD were discovered about 15 years ago. A very small fraction of AD cases are caused by autosomal dominant mutations in the genes encoding presenilin (PS) proteins 1 and 2 and the APP [42]. Mutations in PS1, PS2 and APP genes result in an increase in the production of Aß peptides [42]. Mutations in PS1 and PS2 are autosomal dominant and highly penetrant. They cause Alzheimer's disease (AD) symptoms before age 65, in some cases with onset of symptoms less than 30 years of age [43]. Soon after, the ApoE gene was found to

strongly influence the risk of AD and it was demonstrated that subjects carrying ApoE ε4 nearly doubles the chance to develop AD whereas individuals not carrying ApoE ε4 allele decreases the risk of AD by 40% [44]. Currently, ApoE4 is the only well established genetic risk factor for sporadic AD [44]. But the biological mechanisms involving apoE in learning and memory processes are unclear [45] . A major focus of research today is to identify genes that contribute to a person's risk of developing Alzheimer disease [46]. Geneticists think there are additional genes that have weaker effects, based on the observation that a person who has a first-degree relative with AD is at twice the risk for developing AD.

1.7.2 Amyloid cascade theory

It is unclear whether Aß deposition or NFT formation occurs first and initiates the disease cascade. The majority of AD researchers support the amyloid cascade hypothesis, which proposes that formation and aggregation of Aβ peptide into plaques are decisive events in the pathogenesis of AD. The rest of the disease process, including formation of NFT, is then thought to result from an imbalance between Aβ production and Aβ clearance. It has been shown in *in vivo* studies that Aβ protein can aggregate spontaneously into amyloid fibrils. The longer forms of Aβ undergo more self-aggregation than the shorter forms [47]. Aggregated Aβ is insoluble and is deposited extracellularly and forms senile plaques. Although the amyloid hypothesis is popular and can explain AD pathogenesis, it does not account for some observations. For example, the number of amyloid deposits in the brain does not correlate well with the degree of cognitive impairment that the patient experiences in life [48]. Also, the $A\beta_{42}$ is normally found in the CSF [49] and so according to the cascade theory, it should be precipitated and the lesions in AD should be uniform throughout

the brain. This is, however, not the case as SP are predominately found in the hippocampus, amygdala, entorhinal cortex, neocortex and associated area of the neocortex in AD.

1.7.3 Trace element imbalances

There is considerable evidence for an imbalance in transition metal homeostasis in AD. Although aluminum toxicity was proposed about 30 years ago as the major etiological factor in AD, its relevance to AD remains controversial [50, 51]. Iron and copper have been proposed to contribute to AD through excess production of damaging reactive oxygen species [52]. Most recently, calcium imbalance was related with AD and gained renewed interest [53-55]. Trace Zn toxicity hypothesis in AD was initiated in 1981 when Burnet [56] proposed that Zn deficiencies led to dementia. In 1994, Bush observed that concentrations of Zn above 300 nM rapidly destabilized $A\beta_{40}$ solutions and induced amyloid formation *in vitro* [26] and proposed a role for cerebral Zn in the neuropathogenesis of AD.

2. Zinc studies in AD

2.1 Zinc studies in AD

2.1.1 Zinc studies in AD brain

Any element that is less than 0.01% of the organism is called a trace element. Many metabolic disorders in humans are accompanied by alterations of trace element concentrations in biological fluids and tissues. Interest in Zn and its possible role in the pathogenesis of AD was initiated in 1981 when Burnet [56] proposed that Zn deficiencies led to dementia. Burnet [56] suggested that administration of additional zinc could prevent or delay the onset of dementia in subjects genetically at risk, even though its clinical efficacy and benefits were yet to be determined. Although initial studies of AD and control brain tissue showed significantly decreased Zn in the hippocampus, inferior parietal lobule and occipital cortex of LAD subjects [57-60], later studies using short post mortem interval (PMI) tissue specimens from well characterized LAD and control subjects consistently showed significant elevations of Zn in LAD hippocampus, amygdala, and multiple neocortical areas [24, 25, 61-64]. The inconsistencies may be due to a number of factors including differences in methodology and technical difficulties encountered during tissue processing. In 1994, Bush observed that concentrations of Zn above 300 nM rapidly destabilized $A\beta_{40}$ solutions and induced amyloid formation *in vitro* [26], although later studies found that higher Zn concentrations are required [31, 32] for significant aggregation (fibril formation). From this observation, Bush proposed a potential role for cerebral Zn in the neuropathogenesis of AD. Support for the role of Zn in the development of AD also comes from three other observations. The first observation comes from increased

Zn in SP compared to neuropil and an elevation of Zn in LAD neuropil compared to age-matched control subjects [65, 66]. Second, ZnT-3 knockout mice crossed with transgenic animals carrying the APP2576 gene show markedly decreased amounts of amyloid plaques when compared to wild type APP2576 mice [67]. ZnT-3 is a zinc transporter that is thought to be the primary protein responsible for loading Zn^{2+} into synaptic vesicles [68] and synaptic zinc is thought to contribute to the deposition of amyloid plaques [67]. Third, solubilization of Aβ deposits from postmortem nervous tissue of AD cases and controls is significantly enhanced by the presence of zinc chelators [47].

2.1.2 Zinc studies in AD serum

The reasons for elevated Zn in the AD brain consistently observed in the most recent literature are unclear. Although several studies have attempted to relate changes in peripheral Zn to elevated brain levels, these studies yield highly variable results. The main source of Zn^{2+} to the brain parenchyma is the blood-brain barrier (BBB). Haines et al. [49], Molina et al. [69] and Shore et al. [70] showed no significant differences between AD and control serum Zn. The study of Haines et al. [49] included control subjects whose Mini Mental Status Examination (MMSE) scores were considered cognitively impaired. Jeandel et al. [71] showed a significant decrease in Zn and other nutrients and antioxidant properties in AD serum. However, their AD group may have contained malnourished subjects. In contrast, Rulon et al. [72] and Gonzales et al. [73] showed significant elevations of Zn in AD serum.

2.1.3 Zinc studies in AD cerebrospinal fluid barrier (CSF)

Besides the BBB, the transfer of Zn^{2+} to the brain also occurs at a slower rate across the blood-cerebrospinal fluid barrier (BCB) [74]. The choroidal epithelial cells

constitute the BCB. The BCB, primarily located in the choroid plexus [75], separates the systemic circulation from the CSF compartment. It restricts the entrance of substances from the blood to the CSF, actively secretes CSF, and produces and secretes various polypeptides, such as transthyretin, vasopressin, and transferrin [76, 77]. The importance of BCB in the etiology of certain chemical-induced neurotoxicity has received increased attention [78, 79]. As to CSF levels of zinc, there is also a controversy. For CSF Zn analysis, Hershey et al. [80] found decreased CSF Zn levels in 33 AD patients compared to 2 control groups. However, Monlina et al. [81] questioned that the 2 control groups studied by Hershey et al. might not have been properly chosen. One control group contained 16 neurologic demented subjects, among which 9 had Parkinson's disease, 4 had alcoholic dementia, 2 had normal pressure hydrocephalus and 1 had olivopontocerebellar atrophy. Later, Sahu et al. [82] reported absence of significant differences in the CSF Zn levels between AD patients and controls and concluded that Zn was unlikely to be related to the etiology of AD. Kapaki et al. [83] reported decreased CSF Zn in 5 AD patients compared with 28 non age-matched controls. Molina et al. [81] compared CSF Zn levels in 26 patients with AD and 28 matched controls and found significantly decreased CSF Zn in AD patients as compared with controls. Rao et al. [84] found significantly decreased CSF Zn in 9 AD patients as compared with 11 controls. Recently, Kovatsi et al. [85] measured CSF Zn levels in 15 healthy controls, 16 MCI patients and 26 AD patients. They found significantly lower CSF Zn in the AD group in comparison to the control group and the MCI group.

2.2 Zinc in biosystem and normal zinc homeostasis

Zinc is an essential trace element that is redox inert with structural, catalytic and

regulatory roles [86-88]. Zinc interacts with over 300 enzymes and proteins, including transcription factors, which are critical for cell survival and could be linked to apoptotic processes [89]. The average wet weight of Zn in mammalian brains is 10 µg/g [89]. The concentration of Zn is around 150 µM in neuron cytoplasm and 15 µM in serum [90]. The free Zn in the cytoplasm is in the nM level measured with fluorescent methods [89]. The physiological range of Zn in the neuron is very narrow. Excess Zn is neurotoxic and deficiency inhibits cell growth; both extremes induce cell death. The main source of Zn^{2+} to the brain parenchyma is the blood-brain barrier where brain capillary endothelial cells respond to changes in Zn status by increasing or decreasing Zn uptake [91]. The transfer of Zn^{2+} also occurs at a slower rate across the blood-cerebrospinal fluid barrier [74]. There is increased transport across the barrier in case of Zn deficiency and decreased transport in the case of Zn excess.

2.3 Zinc pools

There are three cellular Zn pools in the brain: a) a membrane bound metalloprotein (MT) pool accounting for about 80% or more of total cellular Zn; b) a vesicular pool localized in nerve terminal synaptic vesicles which accounts for about 5–15% of total cellular Zn; and c) free cytosolic pool in the cytoplasm (about 5%) [92]. The vesicular pool is thought to be the most important when considering disruptions in Zn homeostasis [93-96] because Zn is released during neurotransmission and may reach concentrations of 300 µM in the synapse. Unless these Zn gradients are immediately sequestered, they could potentially induce neurodegeneration.

2.4 Proteins and channels to mediate Zn homeostasis

Investigations of the expression and distribution of Zn transport and sequestration proteins in AD provide additional evidence for disrupted Zn metabolism in AD. In general, Zn homeostasis is mediated by 3 families of proteins: a) metallothionein (MT)/thionein (T), b) Zrt-Irt like (ZIP) proteins, and c) zinc transporter (ZnT) proteins. The MT/T system accounts for the major portion of cellular Zn in the brain and can sequester Zn or release it during signal transmission or deficiency states [97]. MetallothioneinIII (MTIII) is a brain-specific member of the metallothionein family of metal-binding proteins and expression of MTIII has been reported to be altered in AD brain [98]. MTIII is deficient in AD brain tissue [99, 100] which may impair the buffering capacity of the cortical tissue and contribute to the extracellular pooling of Zn that occurs in AD. Although the transport of Zn from brain extracellular environments to intracellular compartments in neurons and glia is not completely understood, it is thought to involve members of the Zrt-Irt like (ZIP) family of proteins [101]. ZIP proteins are predicted to have 8 transmembrane domains with a histidine-rich intracellular loop between domains 3 and 4 [102] and are part of the plasma membrane or membranes of intracellular organelles. To date, 14 mammalian ZIP proteins that function to increase intracellular Zn by increasing Zn uptake (ZIP 1-5; 7 – 15) or by releasing Zn from intracellular stores when Zn is deficient (ZIP 6 and 7) have been identified using mouse and human sequence analysis. In addition to ZIP proteins, neuronal Zn uptake may also be mediated by 4 known Zn-permeable membrane spanning channels: a) voltage-dependent Ca^{2+} channels [103]; b) Ca^{2+}-permeable channels gated by certain types of kainite [104] or 2-amino-5-methyl-4-isoaxazolylpropionate (AMPA) receptors; c) Ca^{2+}-permeable channels gated by N-methyl-D aspartate (NMDA) receptors [105]; and d) Na^{+}/Zn^{2+}

exchangers [106]. Export and sequestration of Zn are carried out by the ZnT family of proteins that are predicted to have 6 transmembrane domains with a histidine-rich loop between transmembrane domains 4 and 5. To date, 8 ZnT proteins have been identified [107]. ZnT-1 is located at the plasma membrane and is expressed in the brain and other organs. Its expression is induced in the presence of elevated cytoplasmic Zn through direct binding of Zn to the Zn-finger domain of metal response element-binding transcription factor-1 (MTF-1) [108]. ZnT-1 is thought to remove Zn to the extracellular space when cytoplasmic Zn levels become elevated [109, 110]. ZnT-1 is significantly depleted in MCI HPG but significantly elevated in LAD HPG [111]. Although the reason for decreased ZnT-1 in MCI remains unclear, recent *in vivo* studies show animals on Zn-deficient diets demonstrate decreased ZnT-1 but increased Zn levels in brain [74, 112]. ZnT 2-7 are responsible for Zn sequestration into intracellular compartments. ZnT-3 is expressed in the brain and testis and is particularly abundant in the hippocampus, amygdala, neocortex, and olfactory bulb, where chelatable Zn occurs in high concentrations [68].

2.5 Specific aims

2.5.1 Development of a novel laser ablation inductively coupled plasma mass spectroscopy (LA-ICPMS) method for spatial quantification of Zn in soft tissue samples

There has been considerable interest in the potential role of Zn in the pathogenesis of AD since 1981 when Burnet [56] first proposed Zn deficiencies led to dementia. Since that time numerous studies have quantified Zn levels in gross brain specimens from LAD and control subjects and obtained conflicting results using instrumental neutron

activating analysis (INAA), inductively coupled plasma mass spectroscopy (ICP-MS), and graphite-furnace atomic absorption spectrometry. Although multiple studies show alterations of Zn at the bulk level, the cellular localization of Zn alterations in AD is unclear. Studies of Zn distribution in AD have primarily focused on the association of Zn with senile plaques (SP). Using micro-particle induced x-ray emission (micro-PIXE) Lovell et al. initially showed increased Zn in senile plaques compared to adjacent neuropil and an elevation of Zn in LAD neuropil compared to age-matched control subjects [65]. Several subsequent studies have confirmed those findings in AD [113-116] and in amyloid plaques in Tg2576 transgenic mice expressing mutant amyloid precursor protein (APP) [117, 118]. However, these studies were done with micro-particle induced x-ray emission (micro-PIXE). Micro-PIXE has a spatial resolution as high as 1 μm but the detection limit can not go lower than 1 ppm for any element. Laser-ablation inductively coupled plasma mass spectrometry (LA-ICPMS) has the potential of providing better detection limits than micro-PIXE. So the first objective was to develop a method that can be employed at the University of Missouri that will have better detection limits than miro-PIXE. The sub ppm LOD is not needed for Zn in soft tissue samples, but the to-be-developed technique will hold great potential for neurotoxins like Pb and Hg.

2.5.2 Quantification of Zn in MCI senile plaques (SP) and neurofibrillary tangles (NFT) using the developed LA-ICPMS method

Studies of Zn distribution in AD brain have primarily focused on late AD. There is no study focused on the transitional mild cognitive impairment (MCI) stage. Also, previous studies of Zn distribution in AD have primarily focused on the association of

Zn with senile plaques (SP) [65]. There is no study of Zn in NFT. The developed LA-ICPMS method will be used to quantify Zn in SP, NFT and adjacent neuropils in tissue samples from well characterized MCI patients. To compare Zn in neuropils from MCI patients and age-matched normal control, Zn in neuropils from age-matched normal control subjects will also be measured.

2.5.3 Human brain Zn levels in the progression of AD

Early studies of AD and control brain showed significantly decreased Zn in the hippocampus, inferior parietal lobule and occipital cortex of LAD subjects [57-60]. Later studies using short post mortem interval (PMI) tissue specimens from well characterized LAD and control subjects consistently showed significant elevations of Zn in LAD hippocampus, amygdala, and multiple neocortical areas [24, 25, 61-64]. Alzheimer's disease is a chronic disorder with a slowly progressive course that is characterized by an inevitable deterioration in cognitive function. The brains of patients with Alzheimer's disease show extensive neuronal loss, the accumulation of ß-amyloid, and extracellular senile plaques and intracellular neurofibrillary tangles in the hippocampus and frontal and temporal cortexes. Minor pathological changes may appear decades before clinical symptoms occur, and they may also be found in middle-aged and elderly persons without obvious symptoms of the disorder. To develop new methods to prevent and treat Alzheimer's disease, the possible underlying mechanisms from MCI to LAD must be well understood. However, there have been no published studies of brain Zn concentrations in MCI brain. To determine if alterations of brain Zn occur in the progression of AD, brain Zn concentrations in thoroughly evaluated, well-characterized, living MCI, and probable AD patients and age-matched normal control (NC) subjects will be analyzed using ICPMS.

2.5.4 Brain Zn levels in an APP/PS1/ZnT-1 mouse model

Because ZnT-1 functions to remove cytoplasmic Zn to the extracellular space, it is possible that introduction of increased ZnT-1 expression into the APP/PS1 mouse model of Aß deposition would lead to accelerated production, oligomerization, and deposition of Aß. Dr. Lovell and his colleagues have crossed APP/PS1 mice with ZnT-1 overexpressing mice to generate stable APP/PS1/ZnT-1 mice. Preliminary characterization of APP/PS1/ZnT-1 mice shows ~20% overexpression of ZnT-1 and a ~ 5-fold increase in Aß plaque deposition compared to APP/PS1 mice beginning at 3 months. The concentrations of Zn concentrations will be quantified in mouse brain and correlated with ZnT-1 to determine if there is a correlation between Zn levels and ZnT-1 in the transgenic mouse brain.

2.5.5 Serum and CSF Zinc levels in the progression of AD

Alzheimer's disease is a chronic disorder with a slowly progressive course that is characterized by an inevitable deterioration in cognitive function. Minor pathological changes may appear decades before clinical symptoms occur, and they may also be found in middle-aged and elderly persons without obvious symptoms of the disorder. Previous studies of ZnT proteins show alterations of ZnT-1, ZnT-4, and ZnT-6 in the progression of AD [119, 120]. Of particular interest is the observation of a significant decrease of ZnT-1, the protein responsible for maintaining low intracellular Zn in the hippocampus/parahippocampal gyrus (HPG) of subjects with MCI that rebounds to a significant increase in LAD HPG [111]. The main source of Zn^{2+} to the brain parenchyma is the blood-brain barrier (BBB). To determine if alterations of serum Zn occur in the progression of AD and contribute to alterations of ZnT-1, serum Zn concentrations will be analyzed in thoroughly evaluated, well-characterized, living

MCI, and probable AD patients and age-matched NC subjects using ICPMS. Besides the BBB, the transfer of Zn^{2+} to the brain also occurs at a slower rate across the BCB. To determine if CSF Zn levels are altered in the progression of AD and if low extra-parenchymal Zn is observed in MCI, Zn concentrations will be quantified in ventricular CSF obtained from short post mortem interval (PMI) autopsies of well characterized MCI, EAD, and LAD patients and NC subjects using ICPMS.

3. Experimental

3.1 Inductively coupled plasma mass spectrometry (ICP-MS) introduction

3.1.1 Advantages and disadvantages of ICP-MS in trace element analysis

For trace element analysis, flame atomic absorption spectrometry (FAAS), graphite furnace atomic absorption spectrometry (GFAAS), inductively coupled plasma optical emission spectrometry (ICP-OES), inductively coupled plasma mass spectrometry (ICP-MS) and X-ray fluorescence spectrometry (XRF) are generally used methods. Since the commercialization of ICP-MS in 1984 [121], ICP-MS has been used extensively in trace element analysis in biological samples. Compared to other techniques, ICP-MS is ideal for trace element analysis because of its ultra low detection limits and wide dynamic range. It is capable of simultaneous multi-element analysis and isotopic ratio measurements. Also, ICP-MS analysis has the advantage of high throughput. These characteristics have made ICP-MS an ideal choice for routine analysis of body fluids and tissues because these samples are available in small amounts. However, ICP-MS is a destructive technique. In most cases, samples need to be digested and converted to solutions. It also suffers from isobaric, molecular and doubly-charged ion interferences. The signal strongly depends on sample matrices and plasma conditions. The biological applications of ICP-MS have been reviewed extensively [121-127].

3.1.2 Basic principles of high resolution ICP-MS (HR-ICPMS)

A quadrupole mass spectrometer typically has a mass resolving power of 300-400. The mass resolving power is defined by:

$$\text{Resolving power} = \frac{Mass_{element}}{Width_{peak}} \qquad \text{Equation 3.1}$$

Where the peak width ($Width_{peak}$) is the width at 10% of the peak's height.

The resolving power of a quadrupole is adequate for the majority of routine applications. However, the resolving power with a quadrupole is not adequate to solve challenging application problems that require excellent detection limits, high resolving power and high precision. High resolution, magnetic based ICP-MS to separate analyte ions from spectral interferences were on the markets in the late 1980s, offering mass resolving powers as high as 10,000. Traditional high resolution magnetic-sector based instruments have two different designs, standard or reverse Nier-Johnson geometry. They share the same basic principles. Both of them have an electromagnet and an electrostatic analyzer (ESA). In the Nier-Johnson design, the ESA is positioned after the electromagnet. In the standard design, which is the case in University of Missouri Research Reactor (MURR), the ESA is positioned before the electromagnet.

A schematic of the VG Axiom HR-ICP-MS used for this work is shown in Figure 3.1. The inductively coupled plasma (ICP) consists of high temperature plasma of ionized argon that is inductively coupled and maintained by a liquid cooled copper coil. For the VG Axiom ICP-MS, the power is supplied to the coil by a remotely located 2 kW 27 MHz RF generator. This generates an intense magnetic and electrical field within the coil. The plasma is lit by high-energy electrons from a high voltage Tesla spark and a stable, self-sustaining plasma forms immediately at the end of the torch. The electron temperatures can reach as high as 8000 to 10000 K. The sample is injected into the plasma in the form of an aerosol and is able to interact with the high

temperature plasma for 2 to 3 milliseconds. The molecules and particles in the samples are broken down to atoms and subsequently ionized due to collisions with energetic argon ions. Argon has a first ionization potential of 15.76 eV, which is higher than most elements. Because of this, the ionization process is extremely effective.

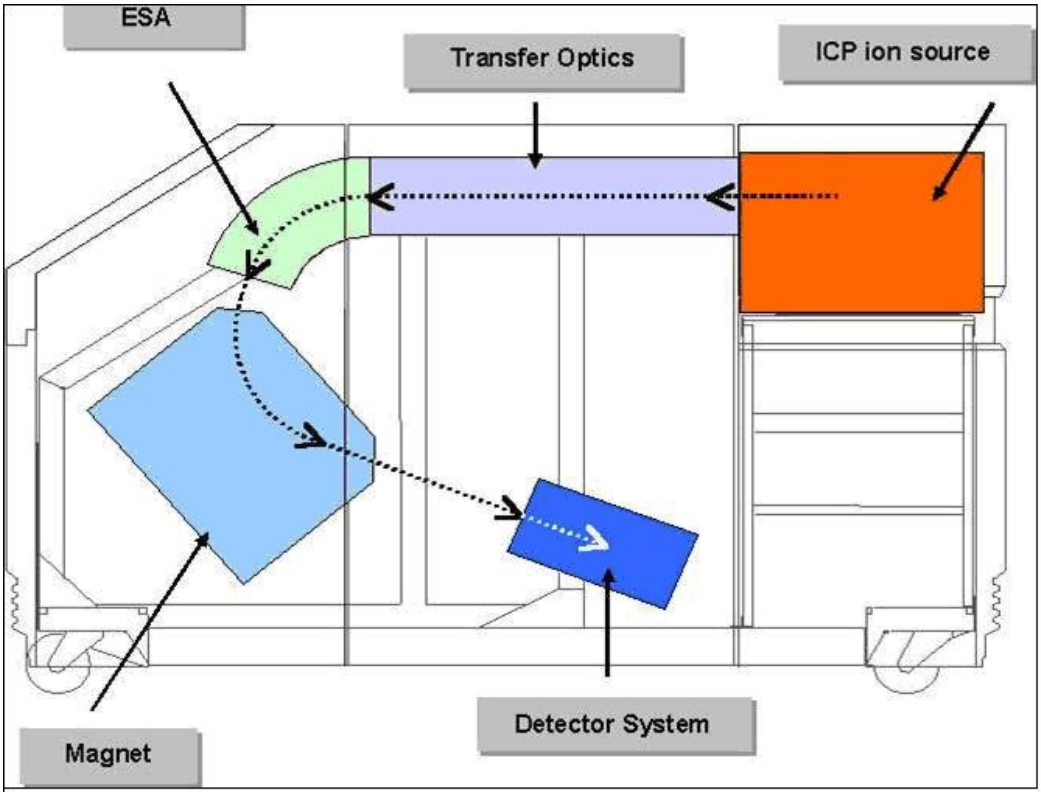

Figure 3.1 A schematic of the VG Axiom HR-ICP-MS.

The plasma is placed across the tip of a water-cooled Nickel sample cone. At the tip of the sample cone, there is a small hole with a diameter of 1 mm, which leads into the inside of the mass spectrometer. The space behind the sample cone is the expansion chamber. It is evacuated to a pressure of around 1 -1.5 mB. Another cone named the

skimmer cone is place behind the sample cone. It has a steeper angle and a smaller hole with a diameter of 0.7 mm. Behind the skimmer cone is the mass spectrometer, maintained at a pressure of less than 1.0×10^{-7} mB. The ions that pass through the skimmer cone orifice are accelerated by a high voltage potential gradient and passed through a series of focus lenses. The ESA separates ions according to their kinetic energy. Only ions with a certain amount of kinetic energy can pass the ESA. The resultant energy spread of the ion beam is less than 60 eV. The electromagnet then separates ions according to their mass to charge ratio. The high resolution spectrometer in MURR operates in peak hopping mode. Only the mass peaks of analytes will be scanned rather than the whole mass range. This is accomplished by varying the accelerating voltage as well as its changing rate. Peak quantitation is typically performed by taking multiple data points over a preset mass window and integrating over a fixed period of time. The high resolution is achieved by using two mechanical slits. One is at the entrance to the mass spectrometer and the other one is at the exit before the detector. Higher resolution is achieved by using narrower slits. As the resolution increases, the transmission decreases. The magnetic sector mass analyzer consists of a curved radially flattened stainless steel tube. By varying the field strength of the magnet, it is possible to select ions of different mass to charge ratios. Only when the radius of the ion trajectory is the same as the radius of the flight tube will the ion exit the dipole magnet. The Axiom HR-ICP-MS has two detectors. The primary detector is an electron multiplier. When an ion hits the multiplier it sets off an electron cascade which will cause a signal reading in the electronics system. It is so sensitive that it can measure a single ion. The second detector is the Faraday cup. It is less sensitive and more prone to noise than the electron multiplier. When a very large signal is detected, the detector will switch to Faraday cup to protect the electron

multiplier.

3.2 Neutron activation analysis (NAA) introduction

NAA is a one of the most sensitive analytical method for multi-element analysis. The basic principles of NAA are incident neutrons interact with the stable analyte nucleus. The radioactive analyte nuclides produced in this activation process are not stable and in most cases they will emit beta particles and gamma rays with a unique half-life. The energy of the emitted gamma rays can be used to identify isotopes and the intensity can be used to quantify the amount of the isotopes. There might be some interference from gamma rays of the same or similar energy. In this case, an alternative emission line can be chosen or by waiting for the short lived isotopes to decay before counting. At the University of Missouri Research Reactor (MURR), high-purity gamma-ray detectors (HPGe, 25% relative efficiency) are used to measure the emitted gamma rays coming from the sample.

For example, when a sample that contains zinc is irradiated, a fraction of the ^{68}Zn atoms in the sample will capture a neutron and become ^{69m}Zn. The ^{69m}Zn atoms are radioactive and have a half-life of 13.76 hours. When the ^{69m}Zn atoms decay to ^{69}Zn, a 438.6 keV gamma ray is emitted 94.77% of the time. The amount of zinc in the original sample can be determined by measuring the number of 438.6 keV gamma-rays emitted from the sample in a given time interval after the sample has been exposed to a flux of neutrons for a certain amount of time.

$$^{68}\mathrm{Zn} + \mathrm{n} \rightarrow {}^{69m}\mathrm{Zn}$$

$$^{69m}\mathrm{Zn} \rightarrow {}^{69}\mathrm{Zn} + \gamma\ (438.6\ \mathrm{keV})$$

The measured count rate (R) of the gamma rays from the decay of a specific isotope in the irradiated sample can be related to the number of atoms (n) of the original, stable isotope in the sample through Equation :

$$R = \varepsilon I_{\gamma} n \varphi \sigma (1 - e^{-\lambda t_i}) e^{-\lambda t_d} \qquad \text{Equation 3.2}$$

R = measured gamma-ray count rate (counts per second)

ε = absolute detector efficiency for the emitted gamma ray

I_γ = absolute gamma-ray abundance

n = number of atoms of isotope ^{A}Z in sample

φ = neutron flux (neutrons·cm^{-2}·sec^{-1})

σ = neutron capture cross section (cm^2) for isotope ^{A}Z

λ = radioactive decay constant (s^{-1}) for isotope ^{A+1}Z

t_i = irradiation time (s)

t_d = decay time (s)

If the neutron flux φ, neutron capture cross section σ, absolute detector efficiency ε, and absolute gamma-ray abundance I_γ are known, the number of atoms n of isotope ^{A}Z in the sample can be calculated directly. In most cases, however, concentrations of unknown samples are determined by the comparator method. The standards are first irradiated and the characteristic gamma ray is monitored. The sample of interest is irradiated simultaneously with the standard or under the same conditions and the same gamma ray monitored. The gamma-ray count rate of the unknown sample is then compared to that of standards of known concentration. The equation is:

$$\frac{R_{sam}}{R_{std}} = \frac{M_{sam}(e^{-\lambda t_d})_{sam}}{M_{std}(e^{-\lambda t_d})_{std}} \qquad \text{Equation 3.3}$$

R_{sam} = gamma-ray count rate from the sample (counts per second)

R_{std} = gamma-ray count rate from the standard (counts per second)

M_{sam} = mass of element in sample (g)

M_{std} = mass of element in standard (g)

λ= radioactive decay constant (s^{-1}) for isotope ^{A+1}Z

t_d = decay time (s)

Compared to other elemental analysis techniques, NAA has the advantages of superior sensitivity, miminal matrix effects, simple sample preparation and less opportunity for laboratory contamination of the sample. Because of its high sensitivity, high precision and accuracy, NAA is routinely used by the National Institute of Standards and Technology (NIST) to certify elemental concentrations in standard reference materials (SRMs). The primary disadvantage of NAA is the limited access to a neutron source.

3.3 Laser ablation ICP-MS (LA-ICP-MS) analysis of Zn in senile plaques (SP) and neurofibrillary tangles (NFT)

3.3.1 LA-ICP-MS introduction

Total metal concentration for an affected tissue section can be obtained from bulk tissue analysis by microwave digestion with ICP-MS analysis. However, bulk analysis is incapable of providing detailed trace metal information from small biological structures, such as AD SP and NFT in these tissue sections. Spatially resolved trace

metal analysis must be conducted to determine where within these tissues trace element imbalances are occurring.

Histochemical staining techniques can be used to image element distributions in tissue samples. However, this method is not sensitive enough to detect elements at trace level and it lacks multi-element detection ability [128].

Laser microprobe mass analysis (LMMA), micro-proton induced X-Ray emission (micro-PIXE), secondary ion mass spectrometry (SIMS) and scanning electron microscopy (SEM) with energy dispersive X-ray analysis (EDX) have been used to analyze trace metal content within biological tissues. However, these established methods suffer from either low precision or poor detection limits. LMMA has been used to study the features associated with neurological diseases such as AD [129, 130]. LMMA provides good sensitivity and detection limits, and when coupled with a time-of-flight (TOF) mass spectrometer, it can simultaneously detect all elements of interest. This technique provides a spatial resolution of around 1 μm needed for examining the pathological structures associated with these diseases [130]. However, the detection limits for most LMMA instruments are in the upper ppm range (1-100ppm). Micro-PIXE provides multi-elemental detection with a spatial resolution of 1 μm and detection limits of 1 ppm. However, the mass range is limited as only those elements higher than sodium can be accurately quantified [131]. SIMS has huge matrix effects and molecular ion formation rates making it very difficult to obtain quantitative data [132]. EDX is similar to PIXE, but EDX utilizes a finely focused beam of electrons as a probe instead of the beam of protons used by PIXE. Due to the use of an electron beam, the main drawback of EDX is the presence of high background or Bremsstrahlung radiation, which decreases its detection capabilities [131]. To determine

trace element concentrations in the small pathological structures associated with these diseases, detection limits of lower than 1 ppm are often needed.

LA-ICP-MS is a semi-quantitative analytical technique capable of multi-elemental detection. This sensitive technique has detection limits for most elements in the lower ppm range, and a spatial resolution of 5 μm or lower depending upon the laser system employed. It is becoming a popular analytical technique for direct determination of elements in biological samples.

Laser-ablation inductively coupled plasma mass spectrometry (LA-ICPMS) has the potential of providing better detection limits than micro-PIXE. So the first objective was to develop a method that can be employed at the University of Missouri that will have better detection limits than the techniques outlined above. The sub ppm LOD is not needed for Zn analysis in soft tissue samples, but the to-be-developed technique will hold great potential for toxins like Pb and Hg related with other diseases.

3.3.2 Major challenges with LA-ICP-MS

The majority of the samples that have been examined by LA-ICP-MS are geological samples such as rocks, obsidians, archeological artifacts or hard biological tissues such as tree rings, teeth, and bivalve shells [133]. A small number of soft biological tissue samples have been tested in the recent past. There are, however, a number of challenges associated with the application of laser ablation ICP-MS to soft biological tissues.

First, there are fluctuations associated with the use of laser ablation on soft biological tissue samples. These samples can be difficult to test due to the fact that the tissue

samples are very thin and may contain water. The presence of water can alter the sample during the ablation process due to evacuation of water in surrounding area brought about by thermal heating from the laser [133]. This alteration of the sample can then cause signal fluctuations from variation in ablated sample mass. Further fluctuations in the ablation process can be caused by inconsistency in laser power, surface effects, and changes in absorption coefficient of the laser within sample and between two different types of tissue samples [133]. Most soft tissue studies employ ^{12}C or ^{13}C as an internal standard [133] to correct for fluctuations in the ablation process and to improve precision. The VG Axiom ICP-MS instrument is not a time of flight system. It can analyze one isotope at a time when coupled with laser ablation system; therefore carbon normalization was not an option.

Second, the major limitation to establishing LA-ICP-MS as a quantitative technique for the analysis of soft biological tissues is the lack of adequate standards. There are currently no commercially available "soft tissue" metal standards certified at the spatial resolution that can be achieved with laser ablation. The ideal standard should be matrix matched to the tissue sections to be studied so that it couples with the laser in a similar fashion, and be homogeneous at the spatial resolution being investigated.

3.3.3 Metal Standards

3.3.3.1 Thin film metal standards

One of the challenges for the application of LA-ICPMS in soft tissue samples is the lack of suitable standards. The most widely used materials for the quantization of biological materials are cryo-sections of albumin, ion chelation beads [134], matrix-matched laboratory standards [135, 136], homogeneous certified reference materials [137] and metal crown ethers embedded in Spurr's media [134, 138]. The

cryo-sections of albumin have the best matrix match to the biological tissues but were not used as standards for this study because the metals are inhomogeneously distributed throughout the albumin. Ion chelation beads have the lowest relative sensitivity coefficient of the three materials and are not matrix matched to the tissue samples [134]. Matrix-matched laboratory standards were developed and used to quantify element concentrations in biological tissue samples by Becker J.S. et al. [139]. Brain tissue samples were spiked with selected standard solutions. The spiked brain tissues were homogenized, centrifuged and frozen at -50°C. Frozen brain samples were cut with a microtome to a thickness of 20 μm and mounted onto glass slides. This method seems easy and promising. However, it is not easy to make the spiked solutions homogeneously distributed in tissue samples. Homogeneous certified reference material (CRM LGC 7112, Pig Liver) was used to analyze Cu and Zn in sections of sheep liver by Feldmann et al. [133]. Pellets of certified biological reference materials were used to analyze trace elements in rat brain tissues by Jakson et al.[140].

Metal crown ether complexes like those used by Lovell et al. in laser-ablation time-of-flight mass spectrometry were employed as standards for our study [134]. Metal crown ethers serve as good standards for laser studies of biological materials because they exhibit little interference with the analyte of interest, mimic chelation of metals in brain tissue, can be used with a wide variety of elements, and are well defined chemically and structurally [134]. Most importantly the standard and sample matrices are similar and the standards are homogeneous at 5 μm [134]. The metal crown ether standards can be incorporated into thin films with a thickness equivalent to standard pathology tissue sections, making tissue sample preparation easier and less time consuming.

In this study we have chosen metal crown ethers imbedded in Spurr's media to be

used as standards for thin human tissue sections. Crown ether complex preparation was modeled after that of Lovell [134] and Spurr [138]. The crown ether chosen for these experiments is 15-crown-5 ether ($C_{10}H_{20}O_5$), due to its lack of interference with metals of interest [134]. Metal to crown ether match was based upon previous studies in the literature. The zinc complex was formed as a 1:1 complex using 15-crown-5 (Acros Organics) and $Zn(NO_3)_2 \cdot 6H_2O$ (Acros Organics). The crown ether complex was prepared by dissolving one mmole of 15-crown-5 ether in 5 mL of diethyl ether (Fisher) and combining it with one mmole of zinc nitrate hexahydrate (MW = 297.46 g/mol) dissolved in 5 mL of absolute ethanol (AAPER). The hydrated metal salts generally dissolved more readily in the absolute ethanol than their anhydrous counterparts. The two solutions were thoroughly mixed for 10-30 minutes and transferred to a glass Petri dish. The solution was then placed in a 70 ℃ oven until a solid was observed. The white solid was then stored in a sealed container until needed. The metal crown ether complex of interest was then added by weight to Spurr's low viscosity embedding medium (Electron Microscopy Sciences) and thoroughly mixed with a vortex mixer. The zinc concentrations in the standards were less than 100 ppm in Spurr's medium. A small portion of the Spurr's metal complex was cast into molds and the rest of the standard solution was used to create the thin film standards.

A small portion of the Spurr's metal crown complex was cast into a flat embedding molds obtained from Electron Microscopy Sciences measuring 14mm(L) x 5mm(W) x 4mm(D). These complexes cast in the embedding molds were then polymerized in a 70°C oven for 12-16 hours. The Spurr's metal complex blocks were then removed from the embedding molds and stored in plastic containers. The zinc concentrations in block standards were analyzed with NAA. The portion of the liquid Spurr's metal crown complex that was left after block casting was then allowed to cure to an

adequate viscosity without noticeable change in volume and cast as a 12.4 μm thick film on a Mylar carrier using a TTC-1200 tape caster (Richard E. Mistler, Inc.). The resulting thin films were then heated in a 70°C oven for 12-16 hours, until the thin films had completely polymerized. The finished thin film metal standards on the Mylar carrier were then cut to size and mounted on glass slides. The mounted standards were then placed on the sample holder inside the ablation chamber for examination.

3.3.3.2 Conformation of zinc concentrations by neutron activation analysis (NAA)

The exact concentrations of the zinc metal standard blocks were verified by NAA. A Spurr's block containing only the crown ether 15-crown-5 and a blank Spurr's block were also prepared and tested to ensure that no zinc signal was associated with these materials. A certified high purity zinc liquid standard (High Purity Standards) was diluted into three separate samples containing 0.005, 0.01, and 0.02 mg of Zn. These samples bracketed the estimated zinc mass range of the block standards (0.005 - 0.015 mg of Zn) tested. The samples were analyzed using 2/5 dram high-density polyethylene vials. In the case of the high purity liquid standards, paper pulp was added to the vials to absorb the liquid. The 2/5 dram vials containing the certified standards and the block samples were then packed into individual rabbits and irradiated for 5 minutes in a thermal flux of approximately $8x10^{13}$ $n \cdot cm^{-2} \cdot s^{-1}$. Following a four-hour-decay, the samples were counted for ten minutes. The background counts from chloride were negligible after the four-hour decay. Figure 3.2 shows an NAA spectrum of a 34.1 ppm Zn standard. Dead times were less than 1.1% for all samples tested. The mass of Zn was quantified using the 438.6 keV peak from the decay of ^{69m}Zn with a half-life of 13.76 hours. Using the calibration curve

developed from the certified standards, the mass of Zn in the block standards was determined. The average weight percent of Zn in the standards was determined and their concentrations calculated. The Zn concentrations in the standards ranged from 2.9 to 41.0 ppm. The average response factor for Zn was $(118\pm3)\times10^4$ counts per second per microgram.

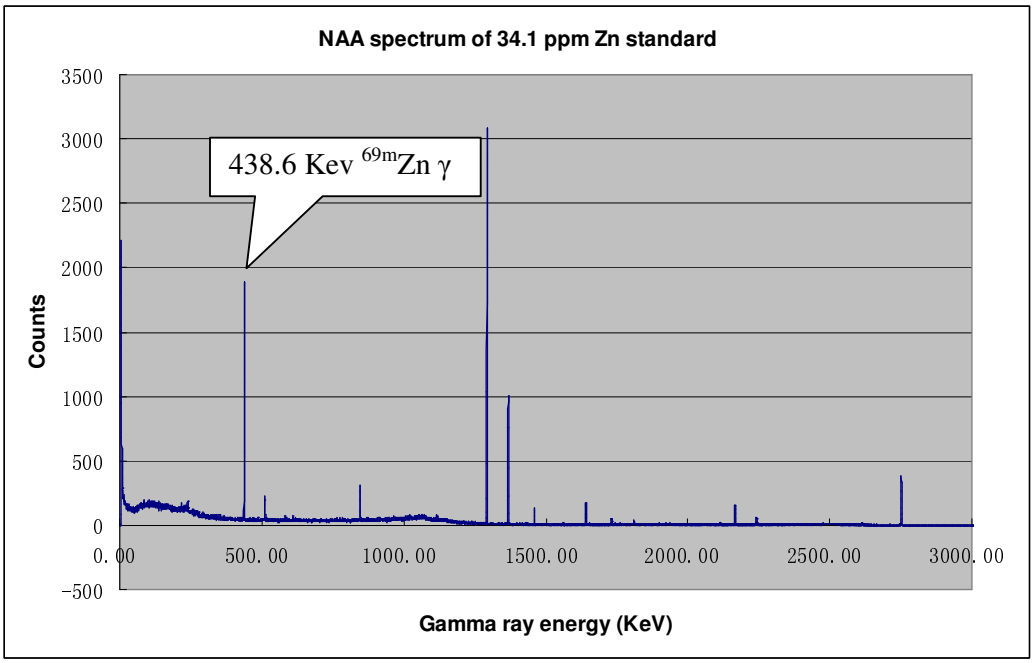

Figure 3.2 NAA spectrum of 34.1 ppm Zn standard.

3.3.3.3 Homogeneity tests

It was important that the developed metal standards be homogenous at a diameter of 10 μm, the same spatial resolution that was used to examine the biological tissues. Homogeneity studies were conducted on a single Zn concentration standard. The metal standard film that was to be tested was cut into five different sections, one section from the middle of the film and one section each from the left and right side at

both the top and the bottom of the film, shown in Figure 3.3. These sections were cut out and mounted individually on glass slides.

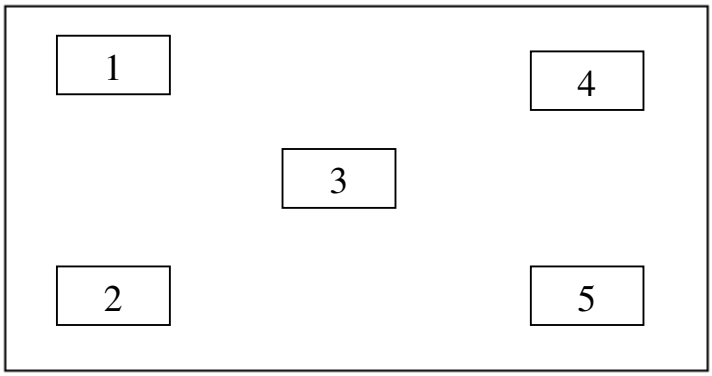

Figure 3.3 Five thin film standards cut for homogeneity studies.

The LA-HR-ICP-MS measurements were made using a VG Axiom high-resolution ICP-MS and a Merchantek 213 nm Nd:YAG laser-ablation system. The LA and ICP-MS settings used to perform these homogeneity experiments can be found in Table 3.1. The instrument reading (counts/second, (CPS)) was obtained in single ion monitoring (SIM) mode. In SIM mode the magnet is set to scan over a very small range of mass, recording only the ions that are consistent with this mass unit and pre-selected resolution. A 10 μm diameter laser spot size was used and a series of four successive 30 μm long line scans are ablated from the surface of the 12.4 μm-thick films. Background metal levels are measured before the laser scan, between scans, and at the end of the scan series. The signal was then integrated over the peak areas and background corrected using Microsoft Excel in a similar way as peak integration in high-performance liquid chromatography. The resulting integrated signals were averaged, standard deviations derived and the relative standard deviations between the

five separate thin film sections were determined. The relative standard deviation served as our method of precision between the five separate thin film sections. The relative standard deviation determined from the five cut out sections from the Zn film was 8.5%.

Table 3.1 General LA and ICP-MS settings for experiments conducted on metal crown ether standards and biological tissue samples

ICP-MS Instrument Settings	
Instrument	VG Axiom High Resolution ICP-MS
RF power (W)	1400
Plasma gas (Ar) flow (L/min)	14
Auxiliary gas (Ar) flow (L/min)	1.2
Nebulizer gas flow (L/min)	1.2 – 1.4
Resolution	1000
Torch	Quartz
Scanning mode	Single Ion Monitoring (SIM)
Spray Chamber	Cinnabar cyclonic spray chamber
Ion optics	Optimized on ^{115}In
Sampler/skimmer cone	Nickel
Detector	Continuous dynode electron multiplier

Laser Ablation Settings	
Carrier gas	Argon
Laser	Merchantek Nd:YAG
Wavelength	213 nm, 5^{th} harmonic of an 1064 nm Nd:YAG laser
Focus	Sample surface
Viewing	Internal CCD camera
Pulse energy	40% - 60% power
Frequency	10 – 20 Hz
Laser spot size	10 μm
Scan length	30 μm
Scan Speed	10 μm/sec

3.3.3.4 Calibration Graphs

For metal crown ethers to be effectively used as standards in these experiments it was important that the various concentrations of the standards responded in a linear fashion. The calibration curve for Zn standards was created using the settings in Table 3.1. In many cases, the maximum sensitivities are obtained in ICP-MS by selecting the most abundant isotope of an element. Zinc has five stable isotopes at mass numbers 64, 66, 67, 68 and 70 with abundances of 48.6%, 27.9%, 4.1%, 18.8% and 0.6%, respectively. The most abundant ^{64}Zn has a direct interference from ^{64}Ni which occurs in high abundance in the system as the sample cone and skimmer cone are made of nickel. To separate ^{64}Zn (m/z = 63.9292) from ^{64}Ni (m/z = 63.9280), the resolution has to be set at least 54000, which exceeds the 10000 limit for the VG Axiom High Resolution ICP-MS (HR-ICP-MS). For this reason, ^{66}Zn, with an abundance of 27.9%, was then chosen as the analyte and the instrument resolution was set at 1000 to avoid possible polyatomic interferences.

For these analyses, a 10 μm diameter laser spot size was used and a series of five successive 30 μm long line scans are ablated from the surface of the 12.4 μm-thick films. Due to the size (20 – 50 μm in diameter) of the pathological structures (SPs and NFTs) in the biological tissue samples, the scan length was initially established at 30 μm. Examining the standards and the biological tissue samples in the same manner allows for a direct comparison between the two.

Figure 3.4 is an example of one of the Zn standards that were tested. These scans were performed using four successive 30 μm long line scans with a 10 μm laser spot diameter on a 25.9 ppm zinc thin film standard. The background signal is less than 50 CPS. A large ablation signal is observed well above the background level. The relative

standard deviation between these four scans was 8.2%.

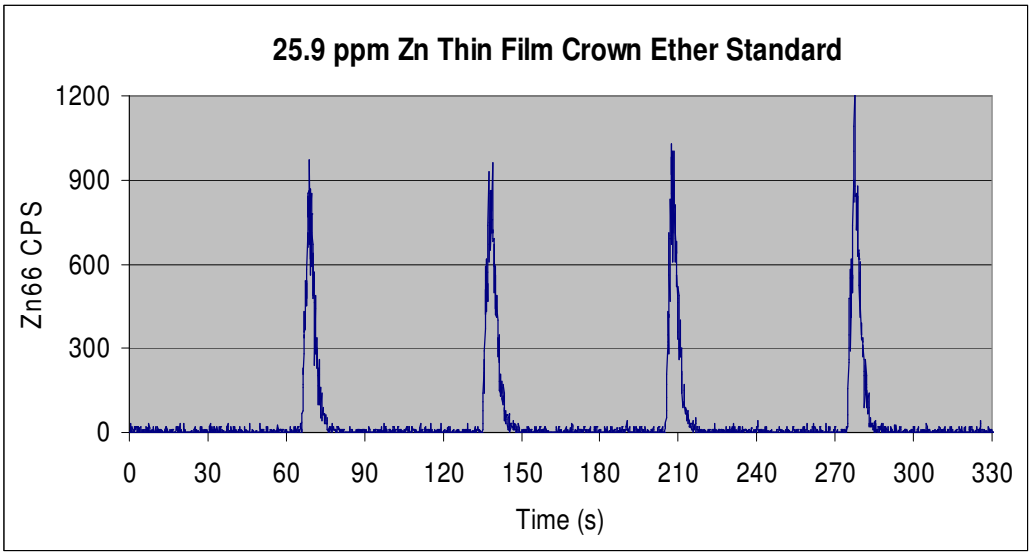

Figure 3.4 Example spectrum of 25.9 ppm zinc thin film standard.

On the following calibration curve each point is the average, with standard deviation, of the integrated peak area (background subtracted) of four (n=4) successive 30 μm long line scans. The limits of detection (LOD) for these metal standards were calculated by taking 3 times the square root of the background signal over one full width half maximum (FWHM) of the peak signal divided by the slope determined by the calibration curve for Zn. When ablation was not occurring there is a background signal that is less than 50 CPS from the instrument. This background signal was subtracted from all data, which resulted in a "zero" background level when the laser was not ablating material from the samples. As a result of the "zero" background level all of the calibration curves were forced through zero.

The zinc calibration curves were determined by analyzing the developed standards in SIM mode using ^{66}Zn (65.93 amu). These standards were analyzed with a 10 μm

diameter laser spot as seen in Figures 3.5. The LOD for Zn was 87 ppb.

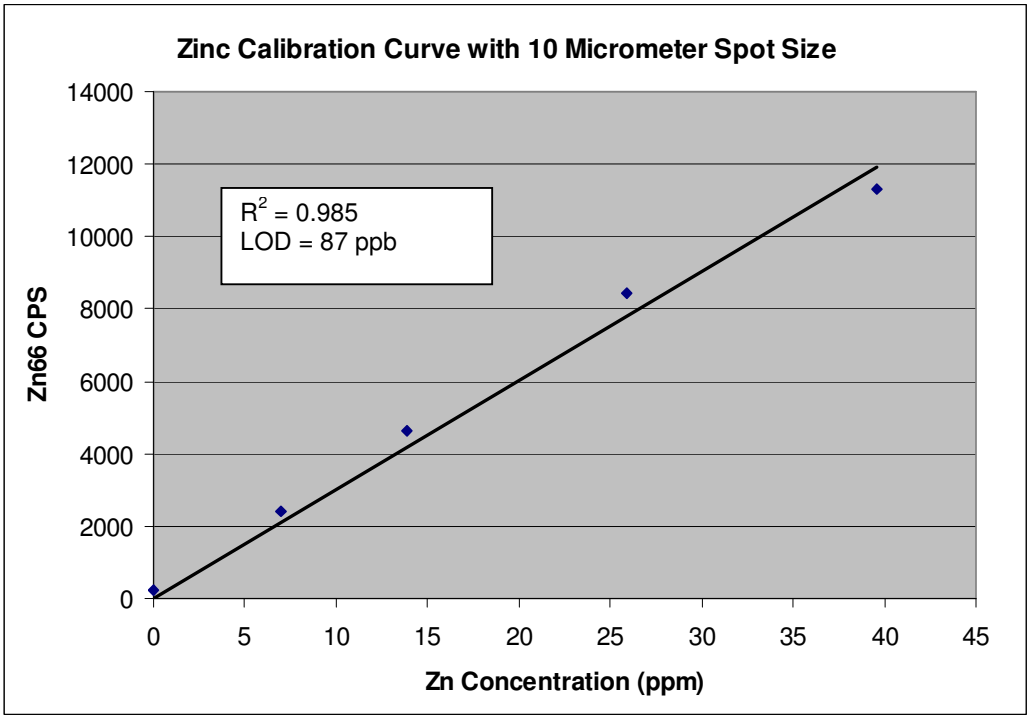

Figure 3.5 Zinc calibration curve obtained by ablation of standards with a 10 µm diameter laser spot size (n=4 per concentration) .

It was found later that the laser power systematically decreases when it is on. This trend will give lower CPS for the same standard ablated later in the day. Without correction, the Zn CPS reading for any sample analyzed during the day will be erroneous because the established Zn calibration curve at the beginning will be used to calculate Zn concentration. Figure 3.6 shows an example of how the CPS of 25.9 ppm Zn standard decreases during a typical day. To correct this, 25.9 ppm Zn standard was analyzed at the beginning, followed by other Zn calibration standards. The 25.9 ppm Zn standard was analyzed again when all the standards were finished and was

analyzed about every 1 to 2 hours during the rest of the analysis. The lineal line was drawn between each two data points. The 25.9 ppm Zn standard serves as a correction standard in the whole analysis. At any time during the interval, the CPS for the 25.9 ppm Zn standard can be calculated and was compared to the initial CPS reading at the beginning. A correction factor was calculated and used to compensate the decreased CPS reading resulting from decreased laser power.

Figure 3.6 Signal fluctuation of 25.9 ppm Zn standard during the day.

3.3.4 SP and NFT samples

The brain tissue samples from AD and control subjects used in these studies were obtained through the Neuropathology Core of the NIA-funded University of Kentucky-Alzheimer's Disease Research Center (UK-ADRC). The subjects were derived primarily from patients followed in the Clinical Core of the UK- ADRC.

Control subjects were derived from a volunteer control group of 446 subjects who had agreed to donate their brain tissue at death. Approximately 15 deaths occurred in the group each year. Each control subject underwent annual mental status testing, and physical and neurological examination every other year. Samples used in analyses had a post mortem interval (PMI) less than 4 hr. Diagnosis of MCI and control brains were determined by the Neuropathology Core of the UK-ADRC. All MCI patients demonstrated progressive intellectual decline and meet NINDS-ADRDA Workgroup criteria for the clinical diagnosis of MCI. The well recognized and validated screening tests for cognitive impairment [1], the Mini-Mental Status Examination (MMSE) and the clinical dementia rating (CDR), were administered as a part of the annual evaluation of subjects for the UK-ADRC. Histopathologic examinations of multiple sections from neocortex, hippocampus, entorhinal cortex, amygdala, basal ganglia, nbM, midbrain, pons, medulla, and cerebellum using hematoxylin and eosin and the modified Bielschowsky stains along with 10D-5 (for Aß) and α-synuclein immunochemistry were carried out on all subjects.

Human brain tissue samples were taken from the hippocampus of MCI subjects using pure titanium knives. These tissue samples were then placed in formalin for fixation and embedded with paraffin. A Shandon Finesse microtome was used to microtome 10 µm sections from the tissues and these sections were placed on Plus slides. The sections were then deparaffinized in xylene 3 times for 10 minutes each followed by 100% ethanol 2 times for 5 minutes each, 95% ethanol 2 times for 5 minutes each, 80% ethanol for 5 minutes and distilled/deionized water. The sections were washed with distilled/deionized water 3 times and incubated in 3% hydrogen peroxide/methanol for 30 minutes at room temperature. Following incubation the sections were washed with distilled/deionized water 3 times and incubated a second

time for 3 minutes in 88% formic acid and rinsed for 5 minutes in running water. The sections were pretreated with pepsin (Biomedia) for 10 minutes at 37°C, then washed 2 times for 2 minutes each in automation buffer (Biomedia) and blocked with 15% filtered horse serum in automation buffer for 1 hour at room temperature. The sections were incubated with the primary antibody, beta amyloid (Novacastra) at a 1:100 dilution, in 15% horse serum/automation buffer overnight at 4°C in a humidity chamber. The sections were then washed 2 times for 5 minutes each in automation buffer and incubated with horseradish peroxidase conjugated anti mouse IgG (made in house) at a 1:200 dilution in 1:70 horse serum/automation buffer for 1 hour at room temperature. The sections were then washed in automation buffer 2 times for 5 minutes each and the color was developed using prepared diamino benzadine (Dako). The samples were then washed with water and allowed to air dry for LA-ICP-MS measurements.

3.4 Serum, cerebrospinal fluid (CSF) and brain tissue

3.4.1 ICP-MS analysis of serum, CSF and brain tissue

One challenge for standard ICP-MS analysis is sample preparation. K.S. Subramanian reviewed general sample preparation methods for atomic spectroscopic techniques [123]. Ideally, sample preparation procedure should be as easy as possible. The more complex the sample preparation, the more sample preparation time and the more chance of contamination. For biological fluids, direct analysis may cause the blocking of the nebulizer and the partial blockage of the sampling orifice because these biological fluids contain high levels of proteins and salts. For example, human serum

contains 6-8% protein and 1% inorganic salts by mass [141]. Serum is the fluid that separates from clotted blood or blood plasma that has been allowed to stand. It is similar in composition to plasma but lacks fibrinogen and other substances that are used in the coagulation process [142]. CSF is a complex medium, secreted from blood which supports the functions of the brain and spinal cord. CSF is produced at a rate of 0.5 L per day. CSF cushions the brain and spinal cord, providing protection against trauma. The composition of CSF is similar to blood plasma but contains less albumin and glucose. It contains many biochemical and chemical components, including leucocytes, 0 to 5.3 counts/μL; free amino acids, 9.6 to 15.2 mg/L; proteins, 156 to 333 mg/L; total fatty acids 42 to 98 μmol/L; glucose, 480 to 860 mg/L; and various enzymes, vitamins, inorganic substances [143]. In addition to the potential for nebulizer clogging and blockage of the sampling orifice, the high percentage solids and salts also have a strong matrix effect on the readings in that they may cause spectral interference from polyatomic ions.

For human body fluids, the easiest way to prepare samples is dilution with suitable diluents. Dilution will deteriorate detection limits but it will not affect the performance greatly because ICP-MS has detection limits of ppb to ppt level for most elements. Zn has been analyzed in human serum by different dilution factors ranging from 5 to 100 with ultrapure water [121], nitric acid [121, 124, 142-150] or customized diluant [151, 152] that is appropriate for a broad range of clinical samples. Sample digestion with concentrated nitric acid accompanied with heat is preferred to simple dilution because it provides more accurate and reproducible results [150]. Dombovari J. et al. [149] and Krachler M. et al. [153] digested serum samples using closed-vessel microwave digestion with HNO_3 and H_2O_2. They used Teflon crucibles to hold serum samples and put the crucibles in digestion vessels. Helal A.I. et al [148] used microwave

digestion to digest serum samples. They added 5 mL of HNO_3 and 2 mL of H_2O_2 to 0.2 mL of serum samples. Recently, Kassu A. et al. [146, 147] used dry ashing to digest serum samples. They added 1 mL of concentrated HNO_3 to 200 µL serum sample and heated the sample at 120 ºC for 5 h on an aluminum heating block. The sample was further heated to near dryness at 200 ºC after removing the Teflon ball. Finally, the residue was dissolved with 2 mL of 0.1 M HNO_3. Although dry ashing removes the organic matrix content of serum samples effectively, contamination and loss of volatile analytes are possible because of the high temperature used and open system if the samples are not prepared carefully.

In general, trace metal concentrations in CSF are lower than those in serum. Simple dilution may also cause nebulizer blockage and partial blockage of the sampling orifice and a digestion method is needed to destroy organic materials in the sample. Thompson J. et al. [144] digested 1 mL CSF with 0.2 mL concentrated HNO_3 using a microwave. All samples were diluted to a final volume of 3 mL. Melo et al. [154] diluted 140 – 200 µL of CSF with ultrapure water to 2.90 mL and then added 100 µL concentrated HNO_3 to digest CSF samples. More recently, Gellein K. et al. [152] digested 0.5 mL of CSF with 0.5 mL of concentrated HNO_3 on a block heater at 110 ºC for 1 h. Then the digestion mixture was diluted to 13 mL.

For tissue samples, direct analysis is possible with laser ablation. But the small amount of sample taken by these methods may not represent the whole sample. For ICP-MS analysis, tissue samples need to be digested in most cases. They can be digested by use of hot plates and furnaces. But these methods are time-consuming and may contaminate the samples. Microwave digestion is widely considered the best method to dissolve tissue samples. Closed-vessel microwave digestion provides efficient mineralization, lowers contamination risk and lowers blank values [145].

Compared to $HClO_4$ and H_2SO_4, HNO_3 produces less spectral interferences [123]. In general, a two-step program is necessary to avoid overheating and damage to the digestion vessels. Lyon T.D.B. et al. digested 0.5 g freeze-dried tissue sample in a Teflon 'bomb' with 1 mL nitric acid. Their microwave could hold 6 'bombs' at a time [155, 156]. Vanhoe [121] determined 11 elements in bovine livers by a two-step microwave digestion. Panayi A.E. et al. [157] digested 50 to 150 mg of dried brain in Teflon PFA microwave digestion vessels with 2 mL of concentrated HNO_3. The digested solution was transferred to acid cleaned polypropylene tubes and diluted to a volume of 10 mL with DI water. The samples were diluted by a factor of 5 finally. Krachler et al. [145] tested trace elements in tissue samples and reference materials with open-focused and closed-pressurized digestion systems. Both systems gave good results when compared to reference values. However, closed digestion system needed less HNO_3 and H_2O_2 and gave more precise data because no volatile analytes are lost. The combination of HNO_3 and H_2O_2 works for a lot of samples [145]. Gelinas Y. et al. used 1 mL of HNO_3 and 0.5 mL of H_2O_2 to digest 50 mg of tissue samples with microwave digestion bomb [158]. Traditional microwave digestion system is not suitable for a large number of samples because only 6 to 24 digestion vessels are available in one digestion cycle. Recently, a new microwave digestion system with 80 digestion vessels has been frequently used by Bocca et al [159-161]. They also used disposable screw-cap tubes for sample digestion instead of commonly used bombs or Teflon vessels, which made the cleaning cycle unnecessary.

3.4.2 Method development with ICP-MS analysis

3.4.2.1 Precleaned trace metal free polypropylene vials

To analyze trace level Zn in samples, special care must be taken to reduce the background Zn levels in trace-metal-free polypropylene tubes (Stockwell, Scottsdale, AZ). 2-3 mL of 2% HNO_3 was added to each tube and the tubes were caped tightly. These tubes were placed in a rack and the rack was then placed on a shaker table with the tubes oriented parallel to the direction of shaking. After 2 hours' shaking, the rack was flipped over and shaken for another 2 hours. The acid was discarded from each tube and the tube was then rinsed with ultrapure water (18 MΩ-cm DI H_2O). The above procedure was then repeated for another cycle. Before cleaning, the Zn background in each tube is between 0.6 – 7.3 ng, which corresponds to 0.06-0.73 ppb if the final solution volume is 10 mL. After the cleaning procedure, the Zn level in each tube is between 0.1 – 2.2 ng, which corresponds to 0.01 - 0.22 ppb if the final volume of the digested solution is 10 mL.

3.4.2.2 Acid strength effect and suitable internal standard

For ICP-MS analysis, two calibration methods are used in general: traditional external calibration and standard addition with suitable internal standards (IS). The advantage of standard addition method is that the standard elements added undergo the same signal suppression or enhancement as the analyte of interest originally in the sample.

The selection of the internal standard is important in obtaining reliable data. To be considered suitable internal standards, several basic requirements must be met. First, the internal standard must be absent or at very low concentration in real samples. Second, the internal standard should not create spectral interferences. Third, the

internal standard should not react with the analytes of interest.

Internal standard is used to compensate for instrumental drift during analysis. The instrumental drift may result from deposition around cone orifices or deposition on lenses. Lenses are used to focus ions into the detector. Ions with higher mass will be less focused than those with lower masses. A good internal standard should have similar mass as analyte of interest. Besides instrumental drift, there are variations in the plasma energy during the analysis. The internal standard must have a similar ionization potential of the isotope under investigation.

Internal standards such as Sc and Y were used to overcome the instrumental drift for Zn analysis in serum, CSF and tissue samples. Sc and Y have similar masses compared to Zn. But the first ionization potentials for Sc and Y are 6.54 and 6.38 eV, respectively and may not be able to correct for matrix effects for Zn which has a first ionization potential of 9.4 eV.

A series of spike recovery tests were performed. The final volumes of the solutions were varied to get different nitric acid concentrations. Sc and Y were used as internal standards in order to compensate for any instrumental drift. The recovery is consistently higher for 2% nitric acid solution than that of 4% nitric acid solution if both of them are calibrated by 2% nitric acid standard solutions.

Campbell M.J. et al. found a systematic underestimation of Zn in a candidate biological reference material IAEA 392 Algae by external calibration ICP-MS despite the use of internal standards [162]. Their recovery for Zn is only 55.4%. They proposed a non-spectroscopic suppression of the Zn in the digest solution is caused by different concentrations of nitric acid in digestate and standard solutions.

A series of solutions were prepared containing 10 ppb of Be, Sc, Mn, Fe, Co, Cu, Zn, Ge, As, Se, Y, In in 0%, 0.2%, 0.5%, 1.0%, 1.5%, 2.4%, 4%, 7.4% HNO_3 , respectively. These solutions were analyzed by HR-ICP-MS and raw counts were recorded. The raw counts of each element were divided by their counts in 0% HNO_3 solution. No internal standard adjustment was applied. Fig. 3.7 shows a significant suppression of Zn at higher nitric acid concentration levels where other analytes (Sc and Y) are largely unaffected, making these internal standards ineffective for Zn.

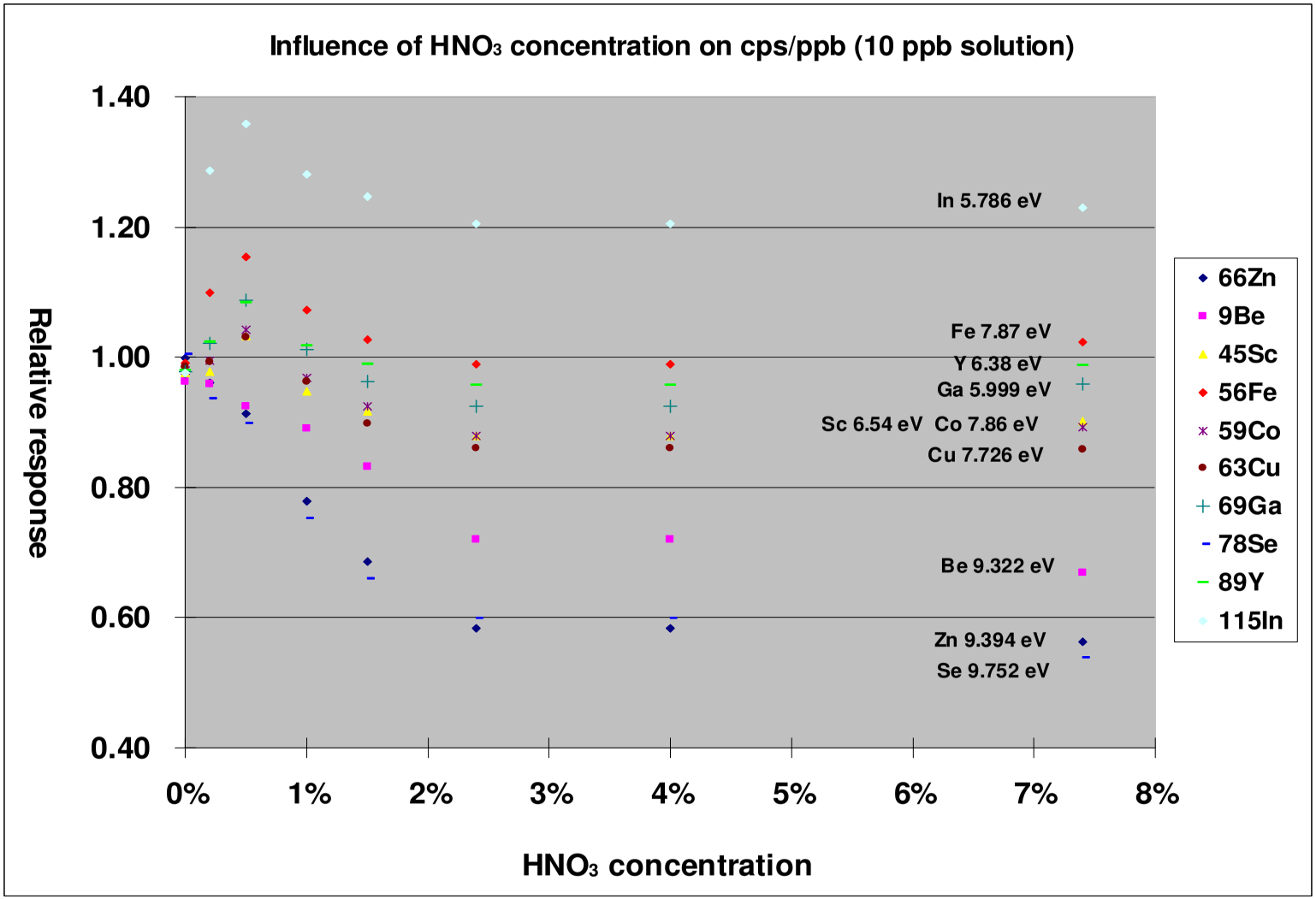

Figure 3.7 Influence of nitric acid concentration on multi-elements signal strength..

M.J. Campbell et al. [162] proposed that nitric acid of higher concentration has more effect in reducing the plasma energy. The first ionization potential of Zn (9.4 eV) is higher compared to other analytes. A decrease in plasma energy would result in a significant decrease in the degree of ionization for Zn than other easily ionized analytes. The Saha equation can be simplified and used to estimate the degree of ionization.

$$\frac{N_i}{N_0} = \frac{2Z_1(T)}{Z_0 N_e} \frac{2\pi mkT}{h^2} e^{-E/kT} \qquad \text{Equation 3.4}$$

N_i - number densities of ions

N_0 - number densities of atoms

N_e - number densities of free electrons

m - electron mass

Z_1- partition function

Z_0 - partition function

E - first ionization potential

T - temperature.

Using this equation, Houk [163] calculated the degree of ionization of elements for a plasma temperature of 7500 K and electron density of 10^{15} cm^{-3}. McCurdy E. et al. [164] calculated the degree of ionization of elements for a plasma temperature of 5000 to 8000 K and showed that reducing plasma temperature can dramatically decrease ionization efficiency of many elements, especially those with high first ionization potentials. Table 3.2 shows the degree of ionization of elements with different first

ionization potentials under different temperature at an electron density of $6.65\times10^{16}\,cm^{-3}$.

Table 3.2 Ion percentage as a function of plasma temperature and ionization potential (Ip), calculated using Saha equation

		Plasma temperature			
Element	Ip (eV)	5000	6000	7000	8000
Cs	3.89	100.0%	100.0%	100.0%	100.0%
Ba	5.21	100.0%	100.0%	100.0%	100.0%
In	5.79	39.9%	100.0%	100.0%	100.0%
Al	5.98	25.7%	100.0%	100.0%	100.0%
Y	6.38	10.1%	100.0%	100.0%	100.0%
Sc	6.54	7.0%	100.0%	100.0%	100.0%
Co	7.86	0.33%	9.9%	100.0%	100.0%
Cd	8.99	0.02%	1.1%	18.1%	100.0%
Be	9.32	0.01%	0.6%	10.5%	94.1%
Zn	9.39	0.01%	0.5%	9.3%	85.0%
Se	9.75	0.0%	0.3%	5.1%	50.4%
As	9.81	0.0%	0.2%	4.6%	46.2%
Hg	10.43	0.0%	0.1%	1.7%	18.8%

Stewart I.I. et al. [165] reported that robust conditions, such as low nebulizer gas flow rates and high powers improve the capability of the plasma to accept a change in the concentration of the acid matrix without affecting the analyte signal significantly.

The first ionization potentials of Be (9.32 eV), Se (9.75 eV) and Cd (8.993 eV) are

close to the first ionization potential for zinc (9.394 eV). However, Se has numerous interferences from polyatomic ions and there is around 0.1 ppm Se in human serum which makes it impossible to use Se as an internal standard for Zn measurements. While Be seems to be the best choice based upon ionization energy, matrix-induced analyte signal changes are not uniform for all elements, but depend on the mass of the element. Be has a relatively low mass to charge ratio (m/z) compared to Zn. For this reason, Cd with a first ionization potential of 8.993 eV was chosen as internal standard for Zn. To our knowledge, this is the first study using Cd as the internal standard for Zn in ICP-MS analysis of biological samples.

3.4.2.3 Effects of sample size and shaking time in serum analysis

One challenge in the analysis of biological samples is ensuring that the sample aliquot is representative of the entire sample. The sample must be homogeneous so that the results generated from the subsample are representative of the entire sample. Sampling tests were performed on serum sample 419c and the results are presented in Table 3.3. It is clear that mixing of the serum sample on the vortex mixer for twenty seconds produces a much more homogeneous sample than no shaking. Likewise, increasing the aliquot size from 50 to 100 μL resulted in much better reproducibility as can be seen from the lower standard deviation.

Table 3.3 Effects of shaking and sample volume on Zn concentration

No shaking, 50 µL serum	ppm	20 s shaking, 50 µL serum	ppm
419c trial 1	1.47	419c trial 1	0.62
419c trial 2	0.64	419c trial 2	0.61
419c trial 3	0.70	419c trial 3	0.73
Average of 419c	0.93	Average of 419c	0.66
SD of 419c	0.46	SD of 419c	0.07
%SD of 419c	49.5	%SD of 419c	10.1

No shaking, 100 µL serum	ppm	20 s shaking, 100 µL serum	ppm
419c trial 1	0.77	419c trial 1	0.60
419c trial 2	0.60	419c trial 2	0.59
419c trial 3	1.22	419c trial 3	0.58
Average of 419c	0.86	Average of 419c	0.59
SD of 419c	0.32	SD of 419c	0.01
%SD of 419c	36.9	%SD of 419c	1.9

3.4.3 Serum sampling and preparation

Fasting serum samples were collected from 18 mild to moderate probable AD patients (9 men, 9 women), 19 MCI patients (9 men, 10 women) and 16 age-matched normal control subjects (9 men, 7 women) through the University of Kentucky Alzheimer's Disease Center (UK-ADC) using University of Kentucky Institutional Review Board approved protocols. All AD patients were followed longitudinally in the Clinical Core of the UK-ADC and had annual mental status testing, and physical and neurological examinations. Probable AD patients demonstrated progressive intellectual decline and

met NINCDS-ADRDA Workgroup criteria for the clinical diagnosis of probable AD [166]. Control subjects were from a population of 446 normal participants followed longitudinally in the healthy brain aging clinic of the UK-ADC. Control subjects had neuropsychologic testing, and physical, and neurological examinations annually. All control subjects had neuropsychologic scores in the normal range and showed no evidence of memory decline. Histopathologic examination of control subjects generally showed only age-associated changes and Braak staging scores of I to III.

Control subjects met NIA-Reagan Institute low likelihood criteria for the histopathologic diagnosis of AD. Patients with MCI were derived from the control group and were followed longitudinally in the UK-ADC clinic. MCI patients were normal on enrollment and developed MCI during follow-up. The clinical criteria for diagnosis of amnestic MCI are those of Petersen et al. [20] and include: a) memory complaints, b) objective memory impairment for age and education, c) intact general cognitive function, d) intact activities of daily living (ADL), and e) the subject is not demented. Objective memory test impairment was based on a score of ≤ 1.5 standard deviations from the mean of controls on the CERAD Word List Learning Task [167] and corroborated in some cases with the Free and Cued Selective Reminding Test [168]. The major distinction between MCI and control subjects is a significant increase in neuritic plaques in neocortical regions and a significant increase in NFT in entorhinal cortex, hippocampus and amygdala in MCI [169]. Braak staging scores of MCI subjects typically ranged III to IV.

Immediately after coagulation, the blood samples were centrifuged at 800 g for 20 minutes at room temperature. The upper supernatant serum samples were aliquoted into 2 mL aliquots and immediately stored in precleaned trace metal free polypropylene vials at -80 °C until used for analysis. For blank corrections, identical

vacutainer tubes were filled with an equal volume of distilled/deionized water.

Human serum contains about 90% water, 7% proteins, 2% low molecular mass organic compounds and 1% inorganic substances, which are usually ionic, present either as simple salts or bound to plasma proteins. Human serum samples were removed from freezer and allowed to thaw at room temperature in a hood for 2 to 3 hours. After being vortexed for 20 seconds, 100μL of serum sample was pipetted and dispensed into the bottom of a preweighed and precleaned trace metal free polypropylene tube and then weighed. To estimate recovery, 150 μL of 1ppm Zn standard solution was used to spike duplicate samples. The samples were weighed and centrifuged for 2 minutes. This forces any serum on the sides of the tube into the very bottom. 300 μL of Optima grade HNO_3 and 100 μL of Fluka TraceSelect grade H_2O_2 were then added to each sample. Then the sample tubes were tightly caped and placed in the racks in an ultrasonic bath at 60°C for one hour. After that, the racks with tubes were removed into a clean hood. Each tube was uncapped and filled to the 10.5 mL mark with 18 MΩ-cm water to match acid strength. The tubes were reweighed and 100 μL 50 ppm Cd ISTD was added. The tubes were capped again and placed in the rack followed by repeated inversions. The samples were centrifuged for 10 minutes immediately prior to running the sample.

3.4.4 CSF sampling and preparation

Ventricular CSF was collected at autopsy from 9 LAD (4 men, 5 women), 6 EAD (1 man, 5 women), and 7 MCI (3 men, 4 women) patients and 10 age-matched cognitively normal control (NC) subjects. LAD patients demonstrated progressive intellectual decline and meet NINCDS-ADRDA Workgroup criteria for the clinical diagnosis of probable AD [166]. Subjects with EAD were derived from the normal

control group and were normal on enrollment but progressed to EAD on follow-up. The clinical criteria for EAD are a) a decline in cognitive function from a previous higher level, b) declines in one or more areas of cognition in addition to memory, c) a clinical dementia rating scale score of 0.5 to 1, d) impaired activities of daily living (ADL), and e) a clinical evaluation that excludes other causes of dementia. All LAD patients met accepted criteria for the histopathologic diagnosis of AD (high likelihood NIA-Reagan Institute criteria) [167, 170, 171] and typically demonstrated Braak staging scores of VI. EAD subjects generally met high likelihood criteria for the histopathologic diagnosis of AD with Braak staging scores of V. Samples were immediately stored in preweighed and precleaned trace metal free polypropylene vials at -80 °C until used for analysis.

CSF samples were prepared in the same way as serum with changes in the amounts of sample and reagents used. More CSF sample (500µL) was used compared to serum (100µL) because of relatively low concentration of elements in CSF. 50 µL of 1.5 ppm Zn standard solution was used to spike duplicate CSF samples. 150 µL of optima HNO_3 and 50 µL of Fluka TraceSelect grade H_2O_2 were added to each sample. After acid digestion in hot water bath, each tube was uncapped and filled to the 5 mL mark with 18 MΩ-cm DI water and were added 50 µL 50 ppm Cd ISTD.

3.4.5 Brain tissue sampling and preparation

3.4.5.1 Human Brain sampling and preparation

Human tissue samples from the hippocampus and parahippocampal gyrus (HPG), superior and middle temporal gyrus (SMTG), and cerebellum (CER) were obtained from short postmortem interval (PMI) autopsies of 4 subjects with MCI, 6 subjects with EAD, and 8 age-matched control subjects using pure titanium knives (NIH

assurance number 00005295). Samples were immediately placed in liquid nitrogen at autopsy and stored in preweighed and precleaned trace metal free polypropylene vials at -80 °C until used for analysis.

3.4.5.2 Mouse Brain sampling and preparation

A mouse model that approximates significant elevated zinc transporter protein 1 (ZnT-1) levels in late Alzheimer's disease (LAD) was developed by Dr. Lovell. The mice used in these studies were generated by crossing mice expressing mutant Amyloid Precursor Protein/Presenilin 1 (APP/PS1) with ZnT-1 overexpressing mice. APP/PS1 mice have been shown to develop amyloid plaques beginning at 6 months of age and are widely used as a model of senile plaque formation in AD [172, 173]. By back crossing the progeny of APP/PS1 and ZnT-1 overexpressing mice for 7 generations, a stable line expressing APP/PS1/ZnT-1 was established. Mice expressing mutant APP/PS1 but with normal ZnT-1 were used for comparison. The mice were provided a normal diet and were housed in the Laboratory Animal Resources facility at the University of Kentucky. The facility has been AAALAC accredited since 1966 and has a current PHS Animal Welfare Assurance # A3336-01. Mice were housed by sex (4/cage) in small mouse cages and provided food and water ad libitum. All routine veterinarian care was provided through consultation with staff veterinarians. The studies did not involve significant discomfort for the animals. For euthanasia, the mice were exposed to a lethal dose of Halothane anesthesia followed by cervical dislocation consistent with the Panel on Euthanasia of the American Veterinary Medical Association and the University of Kentucky Animal Use and Care Committee (IACUC # 625M2004). Cerebellum samples were removed from 6 month old APP/PS1/ZnT-1 (3 Male, 3 Female), APP/PS1 (4M, 4F), and wildtype (4M, 4F) mice.

Samples were immediately placed in preweighed and precleaned trace metal free polypropylene vials and stored at -80 °C until used for analysis.

The sample vials were allowed to warm to room temperature inside a sealed plastic bag to avoid condensation. All samples were then refrozen and freeze dried with the lids open for several days in an ATR Heto vacuum freeze drier until the change in the sample weight was less than 3%. At this point, the samples were reweighed to obtain dry weight. It varies from 0.00243 to 0.04519 g for human brain samples and varies from 0.0078 to 0.03053 g for mouse brain samples.

Fisher brand Optima grade concentrated nitric acid (HNO_3, 1 mL) was added to vials immediately before digestion. Any brain sample that adhered to the vial walls was broken up with a disposable plastic pipette tip and then transferred to the 20 mL Teflon digestion vial inserts along with all of the acid. Fluka brand TraceSelect grade hydrogen peroxide solution (H_2O_2, 1 mL) was added to rinse the sample vial and then transferred into the digestion inserts. The inserts were placed in Teflon digestion vessels and 10 mL 18 MΩ-cm DI H_2O were added to the digestion vessels outside of the inserts. A picture of digestion insert and vessel is shown in Fig. 3.8.

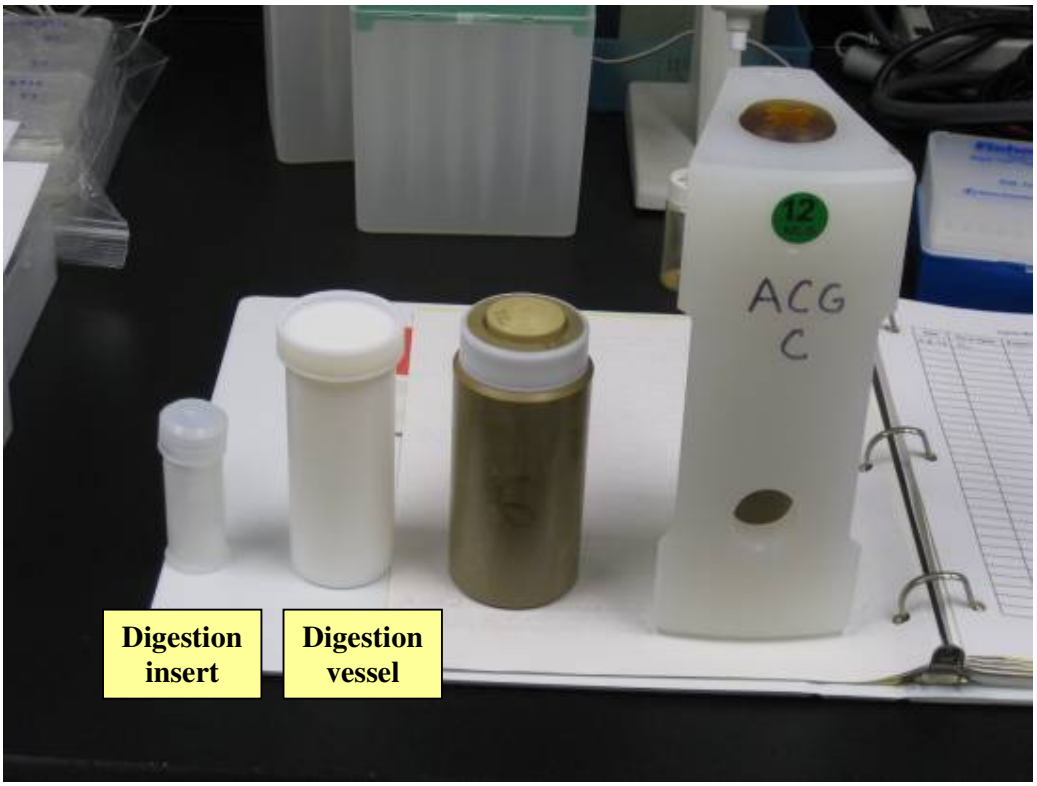

Figure 3.8 A picture of digestion insert and vessel.

The digestion vessels were then sealed and the digestion mixture was heated in a microwave at 300W/140°C for 10 minutes and 400W/180°C for 25 minutes. After digestion, the vessels were cooled to room temperature for 45 minutes before opening. This method produced clear digestates of the brain tissue. Two quality control (QC) samples of NIST SRM 1577 bovine liver (approx. 25 mg) were processed and analyzed along with each digestion set (N=12),. Two digestion vessel blanks were also prepared with each digestion set in order to measure the analyte backgrounds in the vessels and reagents. After digestion, the digestates were transferred to precleaned trace metal free polypropylene tubes by rinsing with18 MΩ-cm water. Each digestate was diluted to 10 mL and then gravimetrically diluted by a factor of 3 to make Zn concentrations less than 200 ppb in the tubes. 100 µL of 1 ppm internal standards

(ISTD) Cd was added to all the diluted solutions prior to analysis in order to compensate for any instrumental and/or matrix effects.

3.4.6 Analytical Procedures

Single element Zn standards (0, 2, 5, 10, 20, 50, 100, 200 ppb) were prepared for calibration of the inductively coupled plasma mass spectrometer (ICP-MS). One hundred μL of 1 ppm internal standard Cd was added to each standard. VG Axiom High Resolution ICP-MS (HR-ICP-MS) analysis was performed at the Research Reactor Center at the University of Missouri. The Zero point standard and quality control standards of known zinc concentration were analyzed every 8 samples during the analyses to measure background and to monitor instrument response. To prevent protein deposition and minimize nebulizer clogging, the sample probe was flushed with concentrated HNO_3 for 15 seconds followed by 45 seconds normal washing after each sample. Typical instrument parameters are shown in Table 3.4.

Table 3.4 Instrumental operating conditions for the Axiom HR-ICP-MS

RF power (W)	1400
Plasma gas (Ar) flow (L/min)	14
Auxiliary gas (Ar) flow (L/min)	1.2
Nebulizer	Micro-flow PFA (100 µL/minute) Meinhardt type nebulizer
Nebulizer gas flow	Optimized daily for max. intensity
Spray chamber	Cyclonic spray chamber (water cooled for extra sensitivity and stability)
Dwell time (ms)	10
Points/Peak Width	20
Peak Width	5
Resolution	6000
Washout time (s)	60
Sampler/skimmer cone	Nickel
Detector	Continuous dynode electron multiplier

4. Results

4.1 Introduction to Statistical Analysis to Compare Group Means

4.1.1 Comparison of two groups

4.1.1.1 Independent-samples *t*-test

If the two groups are independent, that is, observations in one group do not relate in some way to those in the other group, independent-sample *t*-test can be used to test if the means of two groups are the same with random error. The independent-samples *t*-test examines the difference between the group means and determines with some probability whether this difference is significant or simply due to chance.

4.1.1.2 Paired-samples *t*-test

The paired-samples *t*-test is generally used when measurements are taken from the same subject before and after some manipulation. The number of points in each group must be the same, and they must be organized in pairs, in which there is a definite relationship between each pair of data points.

If the data were taken as random samples, independent-samples *t*-test should be used even if the number of data points in each group is the same. Sometimes, even if data are related in pairs, the paired *t*-test is still inappropriate. A simple rule is if a given data point in group one could be paired with any data point in group two, the paired *t*-test should not be used.

4.1.1.3 Three assumptions for *t*-test

1. Normality: the scores on the dependent variable are normally distributed in each group. This assumption can be checked using the Kolmogorov-Smirnov test [175].

2. Homogeneity of Variance: the population variances are equal for the two groups. Levene's test [176] can be used to test this assumption.

3. Independence of the Observations: each observation's score on the dependent variable is not affected by other observations in the same group. This could occur when there are cluster variables. For example, observations from the same region may be more similar to each other. If we have data from different regions and the region variable is not considered in the analysis, all the observations are not independent of one another. In this example, the region is a cluster variable.

4.1.1.4 Calculations and Decisions

t statistic: $t = \frac{\bar{x}_1 - \bar{x}_2}{\sqrt{s_p^2(1/n_1 + 1/n_2)}}$, with $(n_1 + n_2 - 2)$ degrees of freedom (df) [174]

where $\bar{x}_1$ and $\bar{x}_2$ are the two group means;

n_1 and n_2 are the sample sizes of group one and group two respectively;

and $s_p^2 = [(n_1 - 1)s_1^2 + (n_2 - 1)s_2^2]/(n_1 + n_2 - 2)$ is the pooled estimate of the assumed common population variance for the groups (the homogeneity of variance assumption). The denominator is called the standard error of the difference. The calculated t statistic is compared with tabulated t values at the predefined alpha level (e.g. α=0.05). If the calculated t exceeds the tabulated *t* value, the conclusion is reached that there is a statistically significant difference between the two groups on

the dependent variable. If the calculated *t* does not exceed the tabulated *t* value, the conclusion is reached that there is no significant difference between the two groups at the confidence level (e.g. α=0.05) on the dependent variable.

If a statistical package (e.g. SPSS) is used, there is no need to use the t table to arrive at the conclusion. Instead, the *p* value (denoted as "Sig." in SPSS output) can be compared directly to the predefined alpha. If $p < \alpha$, there is a statistically significant difference between the two groups; otherwise, there is no significant difference.

If the assumption of equal variance is violated, some adjustment is made and SPSS reports the results for both when the assumption is met and when the assumption is violated.

4.1.2 More than Two Groups - Analysis of Variance (ANOVA)

One may often want to compare more than two groups (3 or more) to determine if significant differences exist between the groups on the dependent variable. To do this, another statistical procedure, called Analysis of Variance (ANOVA), is employed. ANOVA can also differentiate between more than 1 grouping variable. For example, if we would like to test the difference between females and males, in addition to the differences between AD groups, two-way ANOVA can be applied. In SPSS, ANOVA is under the umbrella category of analyses called "General Linear Model".

4.1.2.1 Three assumptions in ANOVA

1. Normality: Observations are normally distributed on the dependent variable in each group. This assumption can be checked using the Kolmogorov-Smirnov test.

2. Homogeneity of Variance: population variances for groups are equal. SPSS uses Levene's test to check this assumption.

3. Independence of Observations: each observation's score on the dependent variable is not affected by other observations in the same group. This could occur when there are cluster variables.

4.1.2.2 Violation of assumptions in ANOVA

4.1.2.2.1 Violation of normality

ANOVA is robust to non-normality. Sometimes, the data are not normally distributed. The distribution may be non-symmetric (skewed), too peaked or too flat. When the data do not follow a normal distribution because the distribution is somewhat skewed, we can still use the results from ANOVA. However, platykurtotic (flat) distributions affect power of detecting significant differences, especially with small sample sizes [177]. There are several ways to check normality.

1. Visual displays of the data for each group (e.g., with histograms)

2. Descriptive statistics (e.g., skew and kurtosis)

3. Use the Kolmogorov-Smirnov test.

For assumption check, we want the test to be nonsignificant.

4.1.2.2.2 Violation of Homogeneity of Variance

ANOVA performs acceptably when this assumption is violated if groups are equal in size [178]. It becomes a problem when group sizes are extremely unequal and this assumption of homogeneity of variance is violated. SPSS uses Levene's test to check

homogeneity of variance. When the homogeneity of variance assumption is violated, there are still several ways to use ANOVA.

1. Run an ANOVA that does not assume equal variances, such as the Kruskal-Wallis test [179].

2. Use a more stringent alpha level (e.g., 0.01, 0.001)

3. Conduct a variance stabilizing transformation (e.g., square root or natural log) of the dependent variable

4.1.2.2.3 Violation of independence of observations

Independence requires that the observations within groups not be influenced by each other. For example, if the selection of one observation depends on another observation, or if an observation's response depends on the response of another observation, the two observations are not independent. This is usually fulfilled by proper design of the study such as randomly selecting samples and randomly assigning subjects to treatments.

4.1.2.3 Interaction in ANOVA

An interaction is present when the effects of one independent variable (grouping variable) on the dependent variable change at different levels of the second independent variable (grouping variable). For example, if the AD group differences change as observations are males or females, there is an interaction between the grouping variables sex and AD group. If an interaction exists, simple effects are important. A simple effect is the effect of one grouping variable at one level of another grouping effect. For example, the effect of AD group only for males is a simple effect. The effect of AD group only for females is another simple effect. Care

should be taken to examine the effect of one grouping variable (e.g. AD group) at a single level of the other grouping variable (e.g. sex).

4.1.2.4 Post-Hoc Procedures

When a significant effect of a variable is found and this variable only has two levels, we know that the significant difference is between the two groups formed by this grouping variable. When a grouping variable has more than two levels/groups, post-hoc procedures can find where the significant group differences exist after finding a significant overall difference. For example, from ANOVA analysis, we may conclude that the several AD groups are different but we are not sure if the two AD groups in any pair differ significantly. It is likely that one AD group is different from another but not the rest of the groups. SPSS provides two categories of post-hoc procedures. One assumes homogeneity of variance (equal variance) among groups. When this assumption is violated, there are post-hoc procedures that do not assume homogeneity of variance (equal variance).

4.2 Laser ablation of crown ether complex standards

4.2.1 Method validation (Precision and Reproducibility of Thin Film Standards)

Table 4.1 represents the relative standard deviations obtained from different concentrations of the zinc crown ether standards. These analyses were performed with a 10 μm diameter laser spot and each point is the average of the integration of 4 successive 30 μm long line scans. In all of the thin film zinc standards, the precision is 10%RSD or less. The precision of these standards is also reproducible over time. The multiple analyses with the 10 μm diameter laser spot were performed on separate days

over a two month period.

Table 4.1 The relative standard deviations (%RSD) of zinc metal crown ether standards over a 2 month period

Concentrations (ppm)	7-16-05	9-17-05	9-19-05	9-20-05
6.9	8.8	8.1	6.3	6.8
13.9	/	3.7	5.1	6.0
17.7	3.2	7.6	7.8	5.1
25.9	7.4	7.7	3.1	2.5
39.6	8.1	5.9	3.7	4.2

4.3 Laser ablation of soft tissue samples

4.3.1 Laser ablation of MCI Senile Plaques (SP)

Antibody 10D-5 was used to visualize SP according to the procedure developed by Lovell et al. [66]. The zinc concentration was 2 ng/cm^2 in the 10D-5 antibody deposit, and 47 to 196 ng/cm^2 in SP [66]. The staining method does not artificially concentrate trace Zn in SP.

The prepared human brain tissue samples mounted on glass slides were examined. SPs were visually identified through microscopic lenses provided with the laser ablation unit at a magnification of 100X. All samples were tested for ^{66}Zn in the SPs. The sample demographic information is listed in Table 4.2.

Comparison of data for all subjects combined showed no significant differences in age between NC and MCI. Braak scores showed a significant disease progression with

significantly higher scores in MCI patients (3.4 ± 1.9) compared to the NC subject (0). PMI is significantly higher for MCI patients (4.3 ± 0.5) compared to the NC subject (2.5).

Table 4.2 Senile plaque sample subject demographic data

Group	Age (years)	Braak	PMI (hours)
	Average ± SD	Average ± SD	Average ± SD
NC (1 subject)	89	0	2.5
MCI (5 subjects)	90.8 ± 5.4	3.4 ± 1.9	4.3 ± 0.5

PMI: postmortem interval

Using a 10 μm diameter laser spot two ~30 μm long line scans were taken in the neuropil surrounding the plaque and one scan was taken inside the plaque. Figure 4.1 is a picture of one of the brain tissue sections that was analyzed. The dark areas are the senile plaques (SP) and the lighter areas are the neuropil (represented by letter N). The plaques chosen for analysis in this study ranged from about 20- 50 μm in diameter. These larger plaques were chosen so that multiple scans from the same plaque could be performed. Depending on how many plaques exist in each sample, 9 to 12 separate plaques (SP) and 18-24 adjacent neuropil (N) samples were analyzed from each MCI subject. There were 19-24 scans taken in each control and the control showed no SP presence. Figure 4.2 illustrates the response signal from the ablation measurements. The ^{66}Zn signal from the plaque is higher than the signal from the neuropil, and both signals are well above background which remains virtually constant throughout the scan.

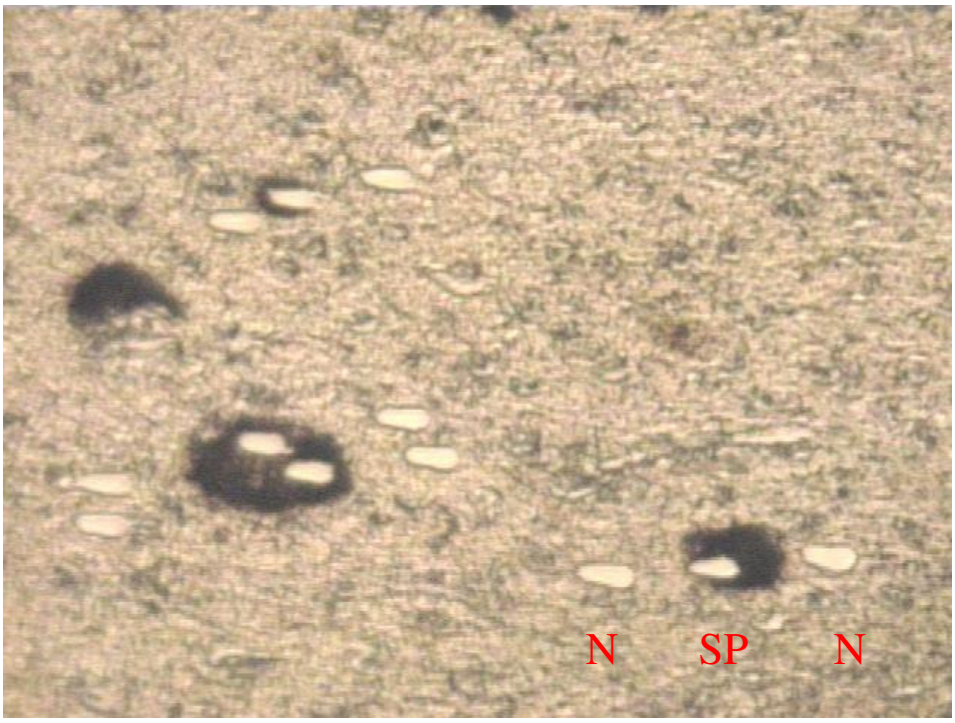

Figure 4.1 Example of the brain tissue section that was analyzed.

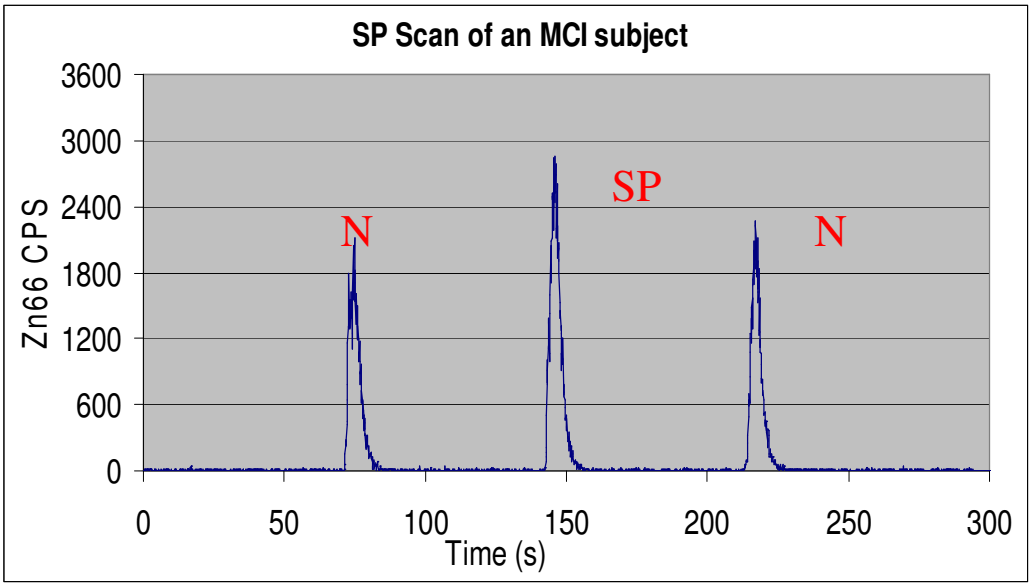

Figure 4.2 Zinc signal response from SP ablation of an MCI tissue section.

Table 4.3 is the average Zn concentrations in each MCI SP and neuropil. Table 4.4 is the average Zn concentrations in one control subject. These concentrations have been adjusted for signal fluctuation of the 25.9 ppm Zn standard throughout the day.

The brain tissue sections that were tested for Zn resulted in an average concentration of 154 ± 59 ppm in the SP (9-12 different plaques per subject for five subjects) and 58 ± 22 ppm average concentrations in the surrounding neuropil. Examination of the neuropil of the control subject indicates a zinc concentration of 62 ± 6 ppm.

Table 4.3 Average and standard deviation of the zinc concentrations (ppm) in MCI SP and MCI Neuropil

Zinc (ppm)	Number of plaques analyzed per subject	MCI SP (Average ± SD)	MCI Neuropil (Average ± SD)
MCI 1	12	201±40	90±18
MCI 2	12	102±25	40±4
MCI 3	12	229±53	64±7
MCI 4	10	145±33	59±5
MCI 5	9	95±20	35±3
Average ± SD		154±59	58±22

Table 4.4 Average and standard deviation of the zinc concentrations (ppm) in Control Neuropil

Zinc (ppm)	Number of spots analyzed per subject	Control Neuropil (Average ± SD)
Control 1	23	54±13
Control 1	19	65±6
Control 1	24	65±22
Average ± SD		62 ± 6

Statistical analysis of the data was performed using Student's *t*-test and the

commercially available software SPSS15. Random effect, one-way ANOVA was used to check if the SPs or Neuropils from each subject were independent. The *p* values (=0.005 for SP, *p*=0.004 for N) confirmed that the SPs or Neuropils from the same subject were not independent. The average SP value and average Neuropil value were then calculated for each subject and used in later analysis.

A paired *t*-test was used to determine if the MCI SPs were significantly different than MCI neuropils at the 95% confidence interval. Analysis of these MCI brain tissue sections demonstrated that zinc is significantly elevated in the MCI SPs (*p*=0.008), compared to the surrounding MCI neuropil. A two-sample *t*-test (independent) was used to determine if the MCI neuropils were significantly different than Control neuropils at the 95% confidence interval. The variances of MCI neuropils and Control neuropils were equal (*p*=0.173). There was no significant difference in the Zn concentrations between the MCI neuropils and the control neuropils (*p*=0.769).

4.3.2 Laser ablation of MCI Neurofibrillary Tangles (NFT)

MC1 staining method was used to visualize NFT in the LA-ICPMS measurements. To investigate whether or not the staining method was artificially concentrating trace Zn in NFT, samples of all reagents used in the staining process were dried and analyzed. The zinc concentration in the MC1 antibody deposit was 0.098 ppb, which is significantly lower than Zn concentration in NFT.

The prepared human MCI brain tissue samples mounted on glass slides were examined. NFTs were visually identified through microscopic lenses provided with the laser ablation unit at a magnification of 100X. All the samples were tested for ^{66}Zn

in the NFTs. The sample demographic information is listed in Table 4.5. Comparison of data for all subjects combined showed no significant differences in age between NC and MCI. There are also no significant differences in PMI between the two groups. Braak scores showed a significant disease progression related increase with significantly higher scores in MCI patients (3.3 ± 1.0) compared to NC subjects (1.6 ± 1.0).

Table 4.5 Neurofibrillary tangle sample subject demographic data

Group	Age (years)	Braak	PMI
	Average ± SD	Average ± SD	Average ± SD
NC (5 subject)	88.2 ± 2.8	1.6 ± 1.1	2.3 ± 1.0
MCI (7 subjects)	91.9 ± 2.8	3.3 ± 0.8	2.9 ± 1.0

The tangles chosen for analysis in this study ranged from about 20- 50 μm in diameter. These larger tangles were chosen so that multiple scans from the same NFT could be performed. Using a 10 μm diameter laser spot two ~30 μm long line scans were taken in the neuropil surrounding the NFT and one scan was taken inside the NFT. Figure 4.3 is a picture of one the brain tissue sections that was analyzed, the dark areas are the NFT and the lighter areas are the neuropil (N). Figure 4.4 shows the signal counts after the ablation. For one sample ID there are 10-14 separate tangles and 20-28 neuropil samples analyzed from one AD subject. There were 20-28 scans taken in each control and the control showed no NFT presence. The signal from the tangle is much higher than the signal from the neuropil, and both signals are well above background which remains virtually constant throughout the scan.

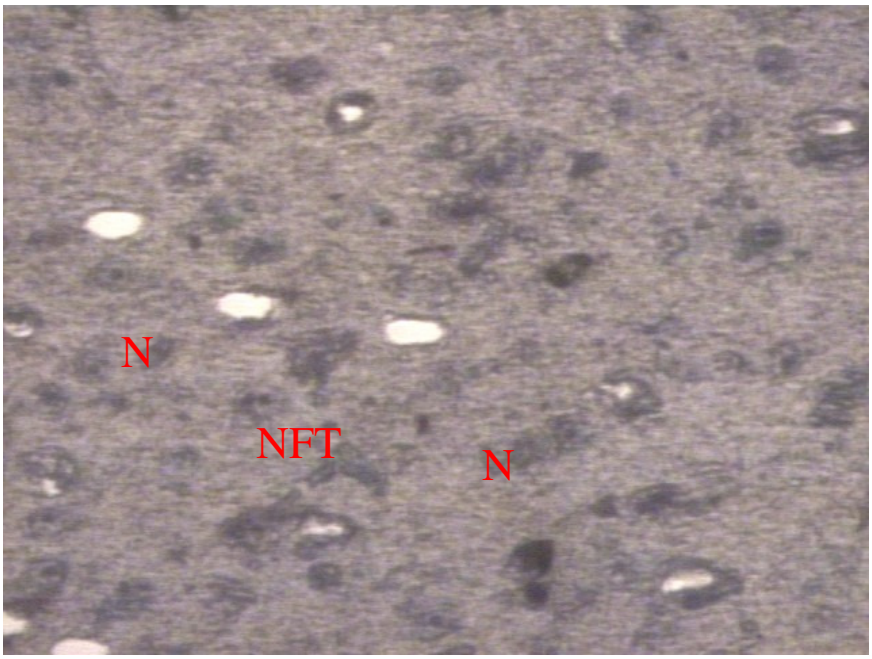

Figure 4.3 Example of the brain tissue section after being ablated.

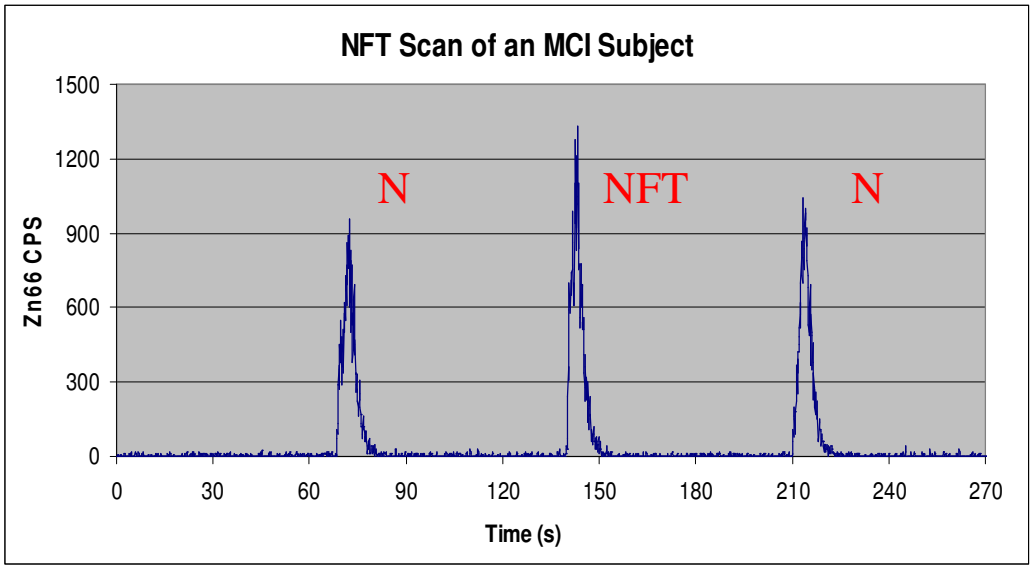

Figure 4.4 Zinc signal response from NFT ablation of an MCI tissue section.

The average Zn concentrations in each AD NFT, neuropil and control neuropil is given in Table 4.6. Each individual sample ID average is the average of 8-14 different

identified NFTs. The average Zn concentration in each control subject is given in Table 4.7. These concentrations have been adjusted for signal fluctuation of the 25 .9 ppm standard throughout the day. The brain tissue sections that were tested for Zn resulted in an average concentration of 178 ± 34 ppm in the NFT and 133 ± 24 ppm average concentrations in the surrounding neuropil. Examination of the neuropil of the control subjects indicates a zinc concentration of 146 ± 85 ppm.

Table 4.6 Average and standard deviation of the zinc concentrations (ppm) in MCI NFT and MCI Neuropil

Zn	Number of NFT analyzed per subject	MCI Neuropil (ppm)	MCI NFT (ppm)
MCI 1	9	86±10	112±15
MCI 2	12	141±26	205±45
MCI 3	13	141±21	188±31
MCI 4	14	127±11	180±36
MCI 5	10	164±32	217±53
MCI 6	13	138±15	168±19
MCI 7	11	134±24	174±27
Average ± SD		133 ± 24	178 ± 34

Table 4.7 Average and standard deviation of the zinc concentrations (ppm) in Control Neuropil

Zn	Number of spots analyzed per subject	Control Neuropil (ppm)
Control 1	20	109±12
Control 2	20	195±15
Control 3	20	79±9
Control 4	20	78±8
Control 5	20	271±14
Average ± SD		146 ± 85

Statistical analysis of the data was performed using Student's t-test and the commercially available software SPSS15. Random effect one-way ANOVA was used to check if the SPs or Neuropils from each subject were independent. The *p* values (p=0 for NFT, p=0 for N) confirmed that the NFTs and Neuropils from the same subject were not independent. The average NFT value and average Neuropil value were then calculated for each subject and used in later analysis.

A paired *t*-test was used to determine if the MCI NFTs were significantly different than MCI neuropils at the 95% confidence interval. Analysis of these MCI brain tissue sections demonstrated that zinc is significantly elevated in the MCI NFTs, compared to the surrounding MCI neuropil (p=0). A two-sample *t*-test (independent) was used to determine if the MCI neuropils were significantly different than Control neuropils at the 95% confidence interval. The variances of MCI neuropils and Control neuropils were unequal (p=0.03). There was no significant difference in the Zn concentrations between the MCI neuropils and the control neuropils (p=0.434).

4.4 Bulk Brain Tissue Analysis

4.4.1 Mouse Brain

4.4.1.1 Method validation

The calibration standard solutions yielded a linear response for Zn over the concentration range of 0 ~ 200 ppb ($r^2 \geq 0.999$). Zn concentrations in the blank solutions were less than 0.6 ppb. Zn concentrations in the samples in the final solutions ranged from 15.3 to 45.6 ppb. When blank subtraction was performed, the blank signal was less than 5% of the total sample signal in all cases. The relative standard deviation of the measured Zn concentrations was less than 2% in 5 measurements of a 50 ppb Zn standard solution and less than 2% in 3 measurements of a bovine liver 1577 quality control sample over the course of a day. The detection limit of the instrument was 0.2 ppb and was calculated as 3 times the standard deviation of the analytical signal from the blank solution. Using Cd as the internal standard, the recovery of Zn in NIST SRM bovine liver 1577 was 103.8 ± 4.9 %, which is around 20% higher than the recovery by using Sc, Y and In as internal standards. The concentrations of Zn in the original mouse brain samples ranged from 52.2 to 78.2 ppm after recovery adjustment.

4.4.1.2 Statistial analysis method

One-Sample Kolmogorov-Smirnov test was used to test if the data were normally distributed. Levene's Test of Equality of Error Variances was used to test if the error variance of the dependent variable was equal across groups. Since the equal variances assumption of Zn concentrations was not met, the statistical analyses were performed on the natural log transformed data. When the concentrations are converted to natural

log, the requirements for normal distribution and equal variances are met for all samples. General Linear Model (Univariate: Two Factor ANOVA) was then used.

4.4.1.3 Comparison of all subjects

Zinc concentrations in the original mouse brain samples by groups are shown in Table 4.8. The APP/PS1/ZnT-1 group has a marginally significantly higher Ln(Zn) than WT (p=0.066) group.

Table 4.8 Zinc concentrations (ppm) in the original mouse brain samples by groups

Group	Range	Average ± SD
WT (4M, 4F)	52.2 ~ 78.2	64.7 ± 9.5
APP/PS1 (4M, 5F)	61.0 ~ 75.4	69.3 ± 5.7
APP/PS1/ZnT-1 (3M, 3F)	64.4 ~ 76.0	71.4 ± 4.2

4.4.1.4 Comparison of data segregated by sex

Zinc concentrations in the original mouse brain samples by group and sex are shown in Table 4.9. For each sex, there are no significant differences between the two groups.

Table 4.9 Zinc concentrations (ppm) in the original mouse brain samples by sex and group

Group	Male		Female	
	Average ± SD	Range	Average ± SD	Range
WT (4M, 4F)	63.0 ± 9.5	55.6 ~ 76.9	66.4 ± 10.7	52.2 ~ 78.2
APP/PS1(4M, 5F)	63.7 ± 2.7	61.0 ~ 67.4	73.8 ± 1.4	71.7 ~ 75.4
APP/PS1/ZnT-1 (3M, 3F)	71.6 ± 2.9	69.0 ~ 74.7	71.1± 6.0	64.4 ~ 76.0

4.4.2 Human Brain

4.4.2.1 Method validation

The calibration standard solutions yielded a linear response for Zn over the concentration range of 0 ~ 200 ppb ($r^2 \geq 0.999$) as shown in Figure 4.5. Zn concentrations in the blank solutions were less than 0.5 ppb. Zn concentrations in the samples in the final solutions ranged from 20.8 to 34.7 ppb. When blank subtraction was performed, the blank signal was less than 3% of the total sample signal in all cases. The relative standard deviation of the measured Zn concentrations was less than 2% in 4 measurements of a 50 ppb Zn standard solution and less than 4% in 4 measurements of a bovine liver 1577 quality control sample over the course of a day. The detection limit of the instrument was 0.3 ppb and was calculated as 3 times the standard deviation of the analytical signal from the blank solution. The recovery of Zn in SRM bovine liver 1577 was 103.5 ± 5.1 %. The concentrations of Zn in the original human brain samples ranged from 39.3 to 152.8 ppm after recovery adjustment.

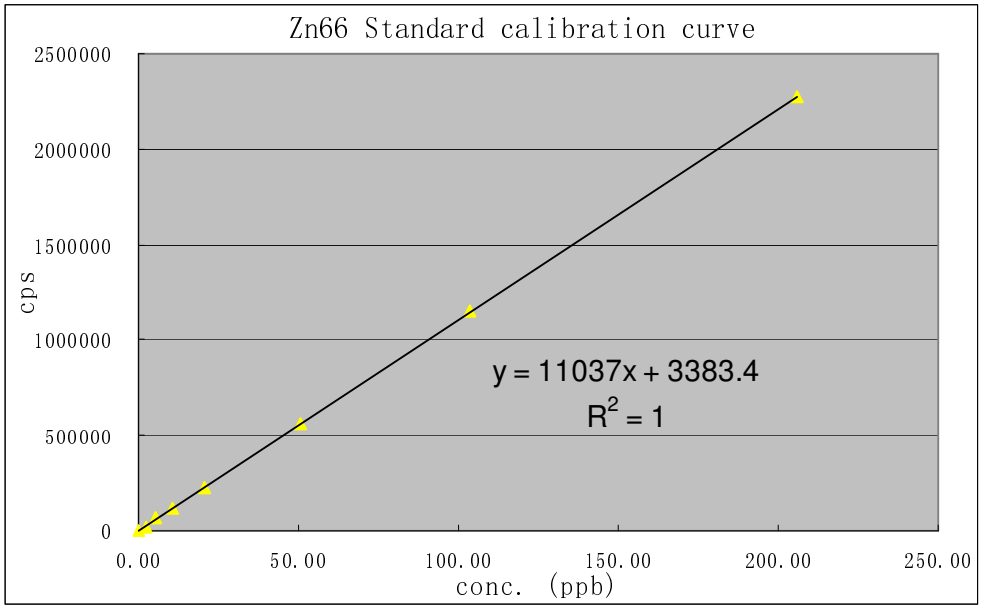

Figure 4.5 Zn calibration curve for human brain study.

4.4.2.2 Statistical analysis method

One-Sample Kolmogorov-Smirnov Test was used to test if the data were normally distributed. Levene's Test of Equality of Error Variances was used to test if the error variance of the dependent variable was equal across groups. In order to account for the non-normal distribution of the Zn concentrations in human cerebellum, the statistical analyses were performed on the natural log transformed data for cerebellum Zn. When the concentrations are converted by natural log, the requirements for normal distribution and equal variances are met for human cerebellum Zn. Since the original concentrations of Zn in human HPG and SMTG show normal distribution and equal variances, they were used for statistical analysis directly. General Linear Model (Univariate: Two Factor ANOVA) was used.

4.4.2.3 Comparison of all subjects

Comparison of data for all subjects combined showed no significant differences in age between the three groups (Table 4.10). There are also no significant differences in PMI between the three groups. Braak scores showed a significant disease progression related increase with significantly higher scores in MCI patients (3.3 ± 0.5) compared to NC subjects (0.9 ± 0.8). Patients with EAD also showed significantly higher Braak scores (4.6 ± 0.6) compared to MCI patients.

Table 4.10 Human brain subject demographic data

Group	Age (years)	Braak	PMI (hours)
	Average ± SD	Average ± SD	Average ± SD
NC (3M, 5F)	86.6 ± 7.0	0.9 ± 0.8	2.9 ± 0.7
MCI (1M, 3F)	89.3 ± 4.9	3.3 ± 0.5	3.2 ± 1.3
EAD (4M, 1F)	87.8 ± 4.7	4.6 ± 0.6	3.3 ± 1.1

Zinc concentrations in the original human brain samples by groups are shown in Table 4.11 For human cerebellum, there is no significant difference among the three groups (Control, MCI and EAD) in Ln(Zn), $F(3,20)=0.893$, $p=0.462$.

For human hippocampus, there are increases of Zn in MCI compared to control but the differences are not significant.

For human SMTG, there is a significant increase of Zn in MCI compared to control, $p=0.043$.

Table 4.11 Zinc concentrations (ppm) in the original human brains by groups

Group	Cerebellum		Hippocampus		SMTG	
	Average ± SD	Range	Average ± SD	Range	Average ± SD	Range
Control	80±7	70 ~ 90	71±14	54 ~ 93	67±12	48 ~ 88
MCI	77±18	56 ~ 90	86±30	51 ~ 114	94±30	59 ~ 114
EAD	95±34	64 ~ 153	73±25	48 ~ 114	80±12	39 ~ 111

Superior and middle temporal gyrus (SMTG)

4.5 Serum

4.5.1 Method validation

The calibration standard solutions yielded a linear response for Zn over the concentration range of 0 ~ 100 ppb ($r^2 \geq 0.999$). Zn concentrations in the blank solutions were less than 0.4 ppb. Zn concentrations in the sample tubes ranged from 1.9 to 22.0 ppb with an average of 8.4 ppb and a standard deviation of 2.6 ppb. When blank subtraction was performed, the blank signal was less than 10% of the total sample signal in all cases except one. The relative standard deviation of the measured Zn concentrations was less than 5% in 6 measurements of a 10 ppb Zn standard solution over the course of a day. The detection limit of the instrument was 0.2 ppb and was calculated as 3 times the standard deviation of the analytical signal from the blank solution. The amounts of the spiked Zn were approximately 200% of the Zn in the spiked samples and the recovery ranged from 89% to 109%. The concentrations of Zn in the original human serum samples ranged from 0.58 to 1.20 ppm after recovery adjustment.

4.5.2 Statistical analysis method

One-Sample Kolmogorov-Smirnov Test was used to test if the data were normally distributed. Levene's Test of Equality of Error Variances was used to test if the error variance of the dependent variable was equal across groups. Since the original concentrations of Zn in human serum show normal distribution and equal variances, they were used for statistical analysis directly. General Linear Model (Univariate: Two Factor ANOVA) was used.

4.5.3 Comparison of all subjects

Comparison of data for all subjects combined showed no significant differences in age between the three groups (Table 4.12). Mini-Mental State Examination (MMSE) and Clinical Dementia Rating scale (CDR) scores showed a disease progression related change with significantly higher CDR scores in MCI (0.5 ± 0.1) and probable AD patients (1.4 ± 0.9) compared to NC subjects (0 ± 0). MMSE scores showed a significant disease progression related decrease with significantly lower scores in AD patients (18.0 ± 9.4) compared to NC subjects (28.8 ± 0.4). Patients with MCI also showed lower MMSE scores (27.7 ± 1.9), although the difference was not statistically significant. Zinc concentrations in the original serum samples by groups are shown in Table 4.13. Serum Zn concentrations for all subjects showed no significant differences between the 3 groups.

Table 4.12 Serum sample subject demographic data

Group	N	Age (years)	CDR	MMSE
		Average ± SD	Average ± SD	Average ± SD
All NC	9M, 7F	77.9 ± 6.9	0 ± 0	28.8 ± 0.4
All MCI	9M, 10F	78.4 ± 7.2	0.5 ± 0.1	27.7 ± 1.9
All AD	9M, 9F	80.3 ± 7.0	1.4 ± 0.9	18.0 ± 9.4

Table 4.13 Zinc concentrations (ppm) in the original serum samples by groups

Group	Range	Average ± SD
NC (9M, 7F)	0.62 ~ 1.13	0.87 ± 0.15
MCI (9M, 10F)	0.63 ~ 1.09	0.84 ± 0.13
AD (8M, 9F)	0.58 ~ 1.05	0.82 ± 0.12

4.5.4 Comparison of data segregated by sex

Demographic data for the subject populations separated by sex are shown in Table 4.14. There were no significant differences in age for men compared to women for any of the 3 subject groups. Similarly, there were no differences in age for men between the subject groups. CDR scores showed a significant disease progression-related increase for both men and women with significant elevations for men (0.4 ± 0.18) and women (0.5 ± 0.0) with MCI and men (1.4 ± 1.2) and women (1.4 ± 0.6) with AD compared to NC men (0± 0) and NC women (0 ± 0). MMSE scores for women showed a significant decrease for MCI patients (26.7 ± 1.6) and mild to moderate AD patients (18.5 ± 9.3) compared to NC subjects (29.6 ± 0.5). MMSE scores in men with MCI (28.9 ± 1.2) were not significantly different than NC men (28.2 ± 1.8). Mild to moderate AD patients showed a significant decrease in

MMSE (17.2 ± 8.1) compared to MCI and NC subjects. MMSE scores between sexes showed a significant decrease in women with MCI compared to men with MCI. Zinc concentrations (ppm) in the original serum samples by sex and group are shown in Table 4.15. Serum Zn concentrations by sex showed a statistically significant decrease ($p < 0.05$) of Zn in men with MCI (0.77 ± 0.10 ppm) compared to NC men (0.91 ± 0.13 ppm) that rebounded to NC levels in subjects with AD (0.84 ± 0.08 ppm). In contrast, serum Zn levels between the 3 groups for women were not significantly different. Serum Zn was significantly lower ($p < 0.05$) in men with MCI compared to women with MCI. Correlation coefficients between serum Zn concentrations and MMSE or CDR scores were not significant.

Table 4.14 Serum sample subject demographic data by sex

Group	N	Age (years)	CDR	MMSE
		Average ± SD	Average ± SD	Average ± SD
NC Men	9	77.9 ± 4.8	0 ± 0	28.2 ± 1.8
NC Women	7	77.9 ± 9.5	0 ± 0	29.6 ± 0.5
MCI Men	9	77.8 ± 4.4	0.4 ± 0.2	28.9 ± 1.2
MCI Women	10	79.2 ±9.3	0.5 ± 0.0	26.7 ± 1.6
AD Men	9	79.6 ± 7.0	1.4 ± 1.2	17.2 ± 8.1
AD Women	9	81.0 ± 7.4	1.4 ± 0.6	18.5 ± 9.3

NC = normal control; MCI = mild cognitive impairment; AD = mild to moderate Alzheimer's disease; CDR = Clinical Dementia Rating scale; MMSE = Mini-Mental State Examination.

Table 4.15 Zinc concentrations (ppm) in the original serum samples by sex and group

Group	Male		Female	
	Average ± SD	Range	Average ± SD	Range
NC (9M, 7F)	0.91 ± 0.13	0.71 ~ 1.13	0.82 ± 0.18	0.62 ~ 1.09
MCI (9M, 10F)	0.77 ± 0.10	0.63 ~ 0.93	0.90 ± 0.13	0.75 ~ 1.09
AD (8M, 9F)	0.84 ± 0.08	0.74 ~ 0.97	0.79 ± 0.15	0.58 ~ 1.05

NC = normal control; MCI = mild cognitive impairment; AD = mild to moderate Alzheimer's disease

4.6 CSF

4.6.1 Method validation

The calibration standard solutions yielded a linear response for Zn over concentration range of 0 ~ 100 ppb ($r^2 \geq 0.999$). Zn concentrations in the blank solutions were less than 0.2 ppb. Zn concentrations in the sample tubes ranged from 0.84 to 46.77 ppb with an average of 10.1 ppb and a standard deviation of 10.9 ppb. While blank subtraction was performed, the blank signal was less than 10% of the total sample signal in all cases except one. The relative standard deviation of the measured Zn concentrations was less than 6% in 5 measurements of a 5 ppb Zn standard solution in a day. The detection limit (DL) of the instrument was 0.2 ppb. DL was calculated as 3 times the standard deviation of the analytical signal from the blank solution. The amounts of the spiked Zn were approximately 200% of the Zn in the spiked samples and the recovery ranged from 107% to 115%. The concentration of Zn in the original human CSF samples ranged from 7.8 to 463.5 ppb after recovery adjustment.

4.6.2 Statistical analysis method

Subject demographic data were compared using analysis of variance (ANOVA) with the commercially available SPSS15. One-way ANOVA was also used to test if there was a significant difference in Zn concentrations among all the groups. One-Sample Kolmogorov-Smirnov Test was used to test if Zn concentrations were normally distributed. Levene's Test of Equality of Error Variances was used to test if the error variance of the dependent variable was equal across groups. To meet the requirements for normal distribution, Zn concentrations were transformed to their natural log. Because the equal variances assumption of ANOVA for the transformed natural log data was still not met, Dunnett T3's post hoc test [180] was used to perform pairwise comparisons with unequal variances.

4.6.3 Comparison of all subjects

CSF sample subject demographic information is shown in Table 4.16. Comparison of data for all subjects combined showed no significant differences in age between each two groups. There were no statistically significant sex or group differences in PMI. Braak scores showed a disease progression related decrease from LAD to EAD to MCI to NC. Zn concentrations (ppb) in the original CSF samples by groups are shown in Table 4.17. Without considering sex, comparison of CSF Ln[Zn] showed a statistically significant ($p < 0.05$) decrease of Ln[Zn] in MCI patients (35 ± 13 ppb) compared to NC subjects (176 ± 158 ppb) and a marginally significant ($p < 0.07$) decrease of Ln[Zn] in MCI patients compared to LAD patients (102 ± 72 ppb). Ln[Zn] in EAD CSF was also lower than NC subjects although the difference was not statistically significant. Correlation analyses of CSF Zn concentrations and Braak staging scores across all subjects showed a statistically significant ($p < 0.05$) increase

in Braak score with decreasing CSF Zn concentration.

Table 4.16 CSF sample subject demographic data

Group	Sex	Age (years)	PMI (h)	Braak Score
		Average ± SD	Average ± SD	Average ± SD
NC	4M, 5F	85.6 ± 7.3	3.0 ± 0.9	0.9 ± 0.8
MCI	3M, 4F	90.7 ± 3.7	2.9 ± 1.0	3.7 ± 0.8
EAD	1M, 5F	86.5 ± 6.7	2.9 ± 1.1	4.8 ± 0.4
LAD	4M, 6F	83.6 ± 8.4	3.0 ± 0.5	6.0 ± 0

NC = normal control; MCI = mild cognitive impairment; EAD = early Alzheimer's disease; LAD = late stage Alzheimer's disease

Table 4.17. Zn concentrations (ppb) in the original CSF samples by groups

Group	Range (ppb)	Average ± SD (ppb)
NC (4M, 5F)	24 ~ 464	176 ± 158
MCI (3M, 4F)	8 ~ 47	35 ± 13
EAD (1M, 5F)	30 ~ 67	49 ± 13
LAD (4M, 6F)	34 ~ 233	102 ± 72

4.6.4 Comparison of data segregated by sex

Demographic data for the subject populations separated by sex are shown in Table 4.18. Women MCI are significantly older than the women NC or women LAD group. There are no other significant pairwise differences in age for women. For men, there are no other significant pairwise differences in age. There were no differences in PMI between the subject groups for either sex. For women, Braak scores showed a disease

progression related decrease from LAD to EAD to MCI to NC. For men, NC group had significantly lower Braak scores than any of the other groups. LAD group had significantly higher Braak scores than the MCI group. In fact, there was no significant sex difference in age, PMI or Braak score, even when each group was examined separately.

Zn concentrations (ppb) in the original CSF samples by group and sex are shown in Table 4.19. For males, the MCI group had a significantly lower Ln(Zn) than the Control (p=0.007) or LAD group (p=0.003). For females, the MCI group had a marginally significantly lower Ln(Zn) than the Control (p=0.06). There was no significant sex difference in Ln(Zn) without considering Group.

Table 4.18 CSF sample subject demographic data by sex

Group	N	Age (years)	PMI (h)	Braak Score
		Average ± SD	Average ± SD	Average ± SD
NC Men	4	85.8 ± 8.1	3.3 ± 0.7	0.8 ± 1.0
NC Women	5	85.4 ± 7.6	2.7 ± 1.0	1.0 ± 0.7
MCI Men	3	88.7 ± 2.9	2.6 ± 0.8	3.7 ± 0.6
MCI Women	4	92.3 ± 3.8	3.2 ± 1.2	3.5 ± 1.0
EAD Men	1	88.0	2.8	5.0
EAD Women	5	86.2 ± 7.4	2.9 ± 1.2	4.8 ± 0.4
LAD Men	4	85.8 ± 9.4	3.2 ± 0.6	6.0 ± 0
LAD Women	6	82.2 ± 8.2	2.8 ± 0.4	6.0 ± 0

a. There is only one male sample in EAD. SD is not applicable.

NC = normal control; MCI = mild cognitive impairment; EAD = early Alzheimer's disease; LAD = late stage Alzheimer's disease

Table 4.19 Zn concentrations (ppb) in the original CSF samples by sex and group

Group	Male		Female	
	Average ± SD	Range	Average ± SD	Range
NC (4M, 5F)	191 ± 194	27 ~ 464	163 ± 145	24 ~ 395
MCI (3M, 4F)	27 ± 17	8 ~ 42	41 ± 6	33 ~ 47
EAD (1M, 5F)	53[a]	53	48 ± 7	29 ~ 67
LAD (4M, 6F)	145 ± 35	121 ~ 197	73. ± 79	34 ~ 233

a. There is only one male sample in EAD. SD is not applicable

5. Discussion

5.1 Laser ablation

For the LA-ICPMS studies, all of the reported relative standard deviations are without the normalization of the signal with an internal standard such as ^{13}C or ^{12}C, used in other LA-ICP-MS studies [133]. The relative standard deviations reported in this investigation are comparable to the relative standard deviations achieved by previous studies using internal standards to correct for signal fluctuations, as demonstrated in Table 5.1.

The experiments of Feldmann et al. utilized a 266 nm laser at 100% power, a cryogenically cooled ablation chamber, frozen soft tissues, and the resulting data was then normalized using carbon as an internal standard. A homogenized CRM pig liver paste (containing ~ 70% water) was used to standardize the method in these experiments with a sample thickness of ~ 1-2 mm. The sheep liver samples that were tested were only ~35 µm thick. The thinner sheep liver samples showed decreased reproducibility compared to the thicker pig paste samples most likely due to less material being ablated from the surface of the thinner samples. The carbon normalization method was used to correct for the difference in standard and tissue thicknesses but did not significantly reduce the variability in the zinc signals. More importantly, the authors did not demonstrate that the pig paste was homogenous at the micron level. The Spurr's standards used in our LA-ICP-MS experiment were tested with a 213 nm laser at 40 -60% power, without ablation chamber cooling or carbon normalization of the signal. The Spurr's standards were ~12 µm thick films which serve as a comparative thickness to the AD tissue samples that were ~10 µm thick. It

is important in our analysis to use a standard and tissue sample with an equivalent thickness since the ablation efficiency depends on the thickness of the sample film [181].

Table 5.1 Comparison between the relative standard deviation of the standard sample used for Feldmann et al. [133], cryogenically cooled ablation chamber soft tissue studies with normalization by carbon ratio and the Spurr's standard sample utilized in our LA-HR-ICPMS without ablation chamber cooling or carbon normalization of the signal

Metal	Concentration *ppm*	Standard	# of Lines	Line Length *μm*	Spot Size *μm*	Scan Speed *μm/s*	%RSD *Metal*	%RSD *Metal /Carbon*
^{66}Zn	43	CRM Pig Liver	1	1500	50	25	12	5.2
^{66}Zn	40	Spurr's	4	30	10	10	3.7-8.1	

LA-HR-ICPMS can be used to probe fine structures inside soft biological tissues, without the destruction of the entire sample. The laser power used in these studies to ablate the tissue and standards does not produce any Zn signal from a blank glass slide. This technique allows for the AD samples to be prepared as normal pathology tissue sections, a significant advance over other microprobe techniques. For example, in micro-PIXE analysis, the backing materials should only consist light elements that have low bremsstrahlung background [182]. And in SEM analysis the sample must be carbon coated.

The LA-HR-ICPMS analysis of the thin homogeneous matrix-matched metal crown ethers film standards with a 10 μm diameter laser spot resulted in a linear response for Zn over a concentration range of 1-40 ppm. The 10 μm diameter laser spot analysis of

the thin film standards yielded limit of detection of 87 ppb for zinc, which is well below the 1 ppm level achievable by other methods such as LAMMA and μ-PIXE. While this LOD is not required for zinc analysis, it does present powerful opportunities to examine brain tissue samples for potentially toxic trace metals like lead or mercury which are anticipated to be present at much lower levels. This is important in testing the finite pathological features associated with AD since the SPs and NFTs of Alzheimer's disease patients are generally 10-30 μm in diameter.

Carbon was not used as internal standard in the analysis. The ICP-MS system used in this work is not a time of flight system. This limits our analysis to one isotope at a time. With the high resolution system we have the capability of analyzing iron in the thin film standards and AD tissue samples. This is an advantage over the other LA-ICP-MS instruments discussed which cannot achieve the resolution needed to accurately test for iron because of the ArO^+ inteference.

5.2 LA-HR-ICPMS analysis of Zn in MCI SP and NFT

With the developed LA-HR-ICPMS method, Zn levels in MCI SP, MCI neuropil and control neuropil were quantified. As demonstrated in Table 5.2 the zinc concentrations in SP obtained by LA-HR-ICP-MS are higher than those obtained by μ-PIXE [65]. However, the subjects analyzed in this study by LA-ICPMS are in MCI, the transitional stage between normal and late Alzheimer's disease. The study by Lovell et al analyzed subjects from late Alzheimer's disease. Also, only five subjects were tested in this study opposed to the nine subjects tested in the μ-PIXE study [65]. Previous studies observed a significant increase of Zn in AD SP compared to AD neuropil [62, 63, 65, 66]. We also observed a significant increase of Zn in MCI SP compared to MCI neuropil. However, we did not observe a significant increase of Zn in MCI

neuropil compared to normal neuropil. The studies by Lovell M.A. et al. [65] and Robertson J.D. et al. [66] using micro-PIXE have shown significant increases of Zn in AD neuropil compared to normal control neuropil. This difference is most likely due to the fact that the Braak scores of the subjects in our study ranged from 3 to 4, which is considered MCI patients only. Neuropil is a major component of brain tissue [183] and the Zn concentrations may not change too much in the early stage of AD.

Table 5.2 Comparison of the concentrations of zinc obtained from the testing of senile plaques using μ-PIXE and LA-ICP-MS. The μ-PIXE data was obtained by testing 9 separate subjects, 10 plaques per subject. The LA-ICP-MS was obtained for zinc by analyzing 5 subjects, 9-12 plaques per subject

Zinc	μ-PIXE (ppm)		LA-ICP-MS (ppm)
	Mean +/- S.E.M.		Mean +/- S.E.M.
AD SP	69.0 ± 18.4 [a]	MCI SP	154 ± 27 [c]
AD Neuropil	51.4 ± 11.0 [b]	MCI Neuropil	58 ± 10
Control neuropil	22.6 ± 2.8	Control Neuropil	62 ± 4

S.E.M.: standard error of the mean

[a] $p < 0.05$ (AD SP values vs. AD neuropil)

[b] $p < 0.05$ (AD neuropil vs. control neuropil)

[c] $p < 0.05$ (MCI SP values vs. MCI neuropil)

This finding is of interest in view of reports by Bush et al. [26] that indicate Zn at concentrations of 300 nM can rapidly destabilize Aβ and lead to fibril formation. The ß-amyloid protein possesses high and low affinity binding sites for Zn. The affinity of the Zn^{2+} binding sites on $A\beta_{1-40}$ are 100 nM and 1.3 uM, indicating that they might be occupied under phyisioliogical condidtions. Zn selective chelators markedly enhance the resolubilization of Aβ deposits from post-mortem AD brain samples, supporting

the hypothesis that Zn ions play a significant role in assembling these deposits. In vitro precipitation of Aβ by Zn^{2+} can be completely reversed by chelation and in postmortem AD brain selective Zn chelators can induce the resolubilization of Aβ from plaques [184].

With the developed LA-HR-ICPMS method, we also quantified Zn levels in MCI NFT, MCI neuropil and control neuropil and found a significant increase of Zn in MCI NFT compared to MCI neuropil. To our knowledge, this is the first study of Zn in MCI NFT by laser ablation ICP-MS. NFT is the other pathological feature used to diagnose definitive AD cases besides SP. There is still a debate whether Aß or tau abnormalities initiate the disease cascade [185]. While the majority of researchers agree with the amyloid cascade hypothesis, the amyloid plaques do not correlate well with neuron loss [186]. The major component of paired helical filaments that forms NFT is tau protein. Under normal conditions, tau is bound to microtubules and helps assemble and stabilize the microtubules that convey cell organelles, glycoproteins and other important materials through the neuron [97]. During the course of AD, tau becomes detached from microtubules and aggregates into NFTs, which may disturb the normal process [32]. Zinc was found to induce an increase of many kinases that phosphorylate tau [187, 188]. We observed a significant increase of Zn in MCI NFT compared to normal control and it is possible that Zn disruption may interact with kinases that phosphorylate tau to contribute to the course of AD.

5.3 Mouse Brain study

The mouse model used that generates significant elevated ZnT-1 and ZnT-6 levels in LAD was developed in Dr. Lovell's lab. Preliminary characterization of

APP/PS1/ZnT-1 mice shows ~20% overexpression of ZnT-1 and, as an unexpected advantage, ~20% increased ZnT-6 expression. Because ZnT-1 functions to remove cytoplasmic Zn to the extracellular space, it is possible that introduction of increased ZnT-1 expression into the APP/PS1 mouse model of Aß deposition would lead to accelerated production, oligomerization, and deposition of Aß. Zn was also quantified to see if there is a correlation between Zn and ZnT-1 in mouse brain. However, no alternation in Zn concentrations was observed in the related brain regions. One possibility is that localized zinc concentration changes occur only within degenerating neurons. The Zn changes in neurons will not significantly change the brain Zn. Current knowledge of the role of Zn in the progression of AD is far from satisfactory. Measuring tissue levels of Zn may not be able to see the change in specific degenerating neurons and more rigorous methods are needed to determine if any changes are localized to specific brain regions or neurons.

5.4 Human brain study

In our Zn studies in human brains, we observed a significant increase of Zn in MCI subjects compared to controls in SMTG. For HPG, there is also an increase in MCI compared to controls although the difference is not significant.

There are numerous studies in Zn levels in Alzheimer's disease subjects. Studies that did not find zinc elevations in AD brain either used small sample sizes or used formalin fixed tissue which artificially lowers zinc levels because of denatured zinc binding sites [60]. Using instrumental neutron activation analysis (INAA), Wenstrup et al showed a significant elevation of Zn in AD brain compared to normal controls in isolated subcellular fractions (whole brain, nuclei, mitochondria, microsomes) of

temporal lobe [25]. Samudralwar et al reported significantly elevated Zn in olfactory regions of 98 AD patients, compared with 56 normal age-matched control subjects [62]. Deibel et al showed a significant increase in Zn in AD hippocampus and amygdala areas [63]. Cornett et al analyzed Zn in seven brain regions from 58 AD patients and 21 control subjects and observed a statistically significant elevation of Zn in multiple regions in AD brain compared with controls [64]. In addition to INAA studies, Danscher et al used micro-PIXE to measure Zn in cryostat sections of brain tissue from AD patients and from normal control subjects and showed an increase in zinc in the hippocampal and amygdalar regions [24]. Using ICP-MS, Religa et al found that there was a significant, more than twofold increase of zinc in the AD-affected cortex compared with normal control group [189]. They also found that the elevated zinc levels in cortex in AD are biochemically linked to Aß burden and to dementia severity (CDR) [189].

Alzheimer's disease is a chronic disorder with a slowly progressive course that is characterized by an inevitable deterioration in cognitive function. The brains of patients with Alzheimer's disease show extensive neuronal loss, the accumulation of ß-amyloid, and extracellular senile plaques and intracellular neurofibrillary tangles in the hippocampus and frontal and temporal cortexes. Minor pathological changes may appear decades before clinical symptoms occur, and they may also be found in middle-aged and elderly persons without obvious symptoms of the disorder. To develop new methods to prevent and treat Alzheimer's disease, there must be a better understanding of the possible underlying mechanisms from MCI to LAD. Previous studies in brain Zn levels have been focused on late stage AD subjects. There is not much information about Zn levels in MCI subjects. In our Zn studies, we observed a significant increase of Zn in MCI subjects compared to control in SMTG. For HPG

samples, we also observed an increase of Zn in MCI compared to control although the difference was not statistically significant. Our studies indicate that Zn homeostasis is altered early in the progression of AD and may play a role in the pathogenesis of AD.

5.5 Serum and CSF study

This serum study is the first to analyze Zn concentrations in well characterized subjects in the progression of AD from MCI to mid stage disease. Our results show no significant differences in Zn when all subjects were compared. However, when the subjects were analyzed by sex, we observed a statistically significant decrease in Zn concentration in men with MCI compared to men who are neurologically normal and women with MCI. In addition, Zn concentrations in men increased to control levels in probable AD subjects. Our current serum data are consistent with previous studies [49, 69, 70] that showed no significant differences between control and AD serum Zn levels but are in contrast to a previous study of postmortem serum from a small number of LAD and control subjects [72] when subjects of both sexes were combined.

The reasons for decreased serum Zn in male MCI compared with female MCI are unclear. However, a previous study of ZnT-1 in the brain of a small number of MCI subjects suggested a more pronounced decrease of ZnT-1 in men compared to women with MCI supporting a relationship between extra-parenchymal Zn and ZnT-1 levels in brain [111].

Zinc has been studied less in CSF than in serum. The main source of Zn^{2+} to the brain parenchyma is the blood-brain barrier. The transfer of Zn^{2+} also occurs at a slower rate across the blood-cerebrospinal fluid (CSF) barrier. The CSF study is also the first

study of Zn concentrations in well characterized subjects in the progression of AD from MCI to early and late stage AD. Without considering sex, our data show the MCI group had a significantly lower Ln(Zn) than the Control or LAD group. For males, the MCI group had a significantly lower Ln(Zn) than the Control or LAD group. For females, the MCI group had a marginally significant lower Ln(Zn) than the Control group. There was no significant sex difference in Ln(Zn) without considering sex. The decrease of serum Zn in male MCI is consistent with the decreases of CSF Ln(Zn) in male MCI and whole MCI groups.

5.6 Possible Zn roles in AD

Although several studies indicate alterations in Zn levels in the AD brain, direct evidence for its role in the pathogenesis of AD has been lacking. A possible role for Zn in the pathogenesis of AD is inferred from several experimental models and the effects of Zn on processing of the amyloid precursor protein (APP) and aggregation of amyloid beta peptide (Aß). APP synthesis is regulated by Zn-containing transcription factors (NF-κß and sp1) and although Zn is essential for their activity [190-193], it is not known whether the activity *in vivo* is regulated by Zn availability. The Zn analysis in SP and NFT of AD brain in this study found significant increases of Zn in SP and NFT compared to surrounding neuropils. In the Zn studies in human brains, we showed a significant increase of Zn in MCI subjects compared to controls in SMTG and a marginally significant increase in HPG. It is possible that elevated Zn may lead to increased levels of the transcription factors. In addition to the potential influence of Zn on APP expression, it serves to influence processing of the protein. Normal processing of APP by α-secretase cleavage leads to formation of sAPP, a neurotrophic

factor. Additional proteolytic processing of APP by ß-secretase (BACE) at the ß-cleavage site [194-198] and the γ-secretase complex at the γ-secretase site (reviewed [199]) leads to formation of Aß, a 40 or 42 amino acid peptide that is the major component of SP in AD [200]. Further support for a role of alterations in APP processing in AD comes from genetic analyses of subjects with early onset familial AD who demonstrate mutations in APP, PS-1 or PS-2 that lead to increased Aß deposition in brain [201]. Additionally, high Zn concentrations can inhibit matrix metalloproteinase-2 (MMP-2) [202], which is able to partially degrade soluble $Aß_{1-42}$ *in vitro* [203]. This inhibition of MMP-2 could lead to an increase in amyloidogenic Aß levels. In addition to its effect on APP processing, several reports indicate that Zn at low physiological concentrations [26, 204-207] induces Aß aggregation, although later studies indicate that higher Zn concentrations are required [31, 32] for significant aggregation.

With the developed LA-HR-ICPMS method, Zn levels in MCI SP, MCI NFT, MCI neuropil and control neuropil were quantified. There are significant increases of Zn in MCI SP and MCI NFT compared to surrounding neuropils. As to bulk Zn analysis, the decrease of serum Zn in male MCI is consistent with the decreases of CSF Ln(Zn) in male MCI and whole MCI groups. In our Zn studies in human brains, we observed a significant increase of Zn in MCI subjects compared to control in SMTG. There is also a marginally significant increase of Zn in MCI subjects compared to control in HPG. Our studies indicate that Zn homeostasis is altered early in the progression of AD.

The results of our current serum and CSF Zn study are of interest in light of previous *in vivo* studies that show systemic Zn deficiencies lead to diminished ZnT-1 levels and increased brain Zn suggesting a compensatory response of brain capillary epithelial cells to increase Zn uptake in the presence of diminished extra-parenchymal Zn [74, 112].

Analysis of Zn concentrations in brain specimens from a small number of subjects of each group showed a significant elevation of Zn in specimens of superior and middle temporal gyrus (SMTG) and a marginally significant elevation of Zn in hippocampus/parahippocampal gyrus (HPG) in MCI patients compared to NC subjects. Our current serum, CSF and human brain data are consistent with previous *in vivo* animal studies that show systemic Zn deficiencies lead to diminished brain ZnT-1 levels and increased brain Zn [74, 112], suggesting brain capillary epithelial cells increase Zn uptake in the presence of diminished extra-parenchymal Zn to maintain Zn stores. This increase in brain Zn may particularly affect Aβ processing and deposition and contribute to disease progression.

APPENDICES

Appendix I. Serum sample demographic data and Zn concentrations (ppm)

Group	Sex	Age	Zn (ppm)
NC 1	F	83	1.09
NC 2	F	67	0.88
NC 3	F	93	0.64
NC 4	F	84	0.62
NC 5	F	69	1.00
NC 6	F	71	0.81
NC 7	F	78	0.68
NC 8	M	77	0.92
NC 9	M	71	1.01
NC 10	M	74	0.74
NC 11	M	73	0.89
NC 12	M	80	0.91
NC 13	M	86	0.95
NC 14	M	82	0.71
NC 15	M	78	0.93
NC 16	M	81	1.13
MCI 1	F	85	0.79
MCI 2	F	82	0.75
MCI 3	F	66	0.78
MCI 4	F	82	0.93
MCI 5	F	91	1.08
MCI 6	F	91	1.00
MCI 7	F	71	1.09
MCI 8	F	83	0.75
MCI 9	F	66	0.98
MCI 10	F	75	0.86
MCI 11	M	71	0.75
MCI 12	M	73	0.67
MCI 13	M	77	0.86
MCI 14	M	80	0.68
MCI 15	M	74	0.79
MCI 16	M	84	0.87
MCI 17	M	82	0.63
MCI 18	M	81	0.74
MCI 19	M	78	0.93
AD 1	F	90	0.77
AD 2	F	84	0.98
AD 3	F	85	0.88
AD 4	F	83	0.79
AD 5	F	69	0.61
AD 6	F	75	1.04
AD 7	F	69	0.70

AD 8	F	84	0.80
AD 9	F	78	0.58
AD 10	M	89	0.74
AD 11	M	65	0.85
AD 12	M	74	0.75
AD13	M	79	0.87
AD 14	M	86	0.80
AD15	M	83	0.91
AD 16	M	81	0.97
AD 17	M	78	0.72
AD 18	M	81	0.86

Appendix II. CSF sample demographic data and Zn concentrations (ppm)

Group	Sex	Braak	Age	PMI	Zn (ppb)
Control 1	F	1	86	1.75	23.5
Control 2	F	2	90	4.00	69.3
Control 3	F	1	76	2.00	136.5
Control 4	F	1	80	2.25	192.7
Control 5	F	0	95	3.50	395.0
Control 6	M	2	87	2.42	27.0
Control 7	M	1	74	4.00	81.9
Control 8	M	0	90	3.50	463.5
Control 9	M	0	92	3.25	192.3
MCI 1	F	3	97	2.75	44.0
MCI 2	F	3	91	5.00	46.5
MCI 3	F	3	93	2.75	39.7
MCI 4	F	5	88	2.25	32.9
MCI 5	M	4	87	3.50	42.4
MCI 6	M	4	92	2.00	7.8
MCI 7	M	3	87	2.25	29.3
EAD 1	F	5	83	2.25	46.0
EAD 2	F	5	96	1.60	39.1
EAD 3	F	5	91	4.75	29.4
EAD 4	F	4	84	2.75	66.6
EAD 5	F	5	77	3.00	57.4
EAD 6	M	5	88	2.75	52.8
LAD 1	F	6	90	2.80	35.8
LAD 2	F	6	75	2.33	41.5
LAD 3	F	6	70	3.25	45.7
LAD 4	F	6	86	3.25	232.9
LAD 5	F	6	90	2.75	34.0
LAD 6	F	6	82	2.50	48.4
LAD 7	M	6	73	2.75	131.7
LAD 8	M	6	95	4.00	121.0
LAD 9	M	6	90	3.25	197.1
LAD 10	M	6	85	2.75	131.8

Appendix III. Human brain sample demographic data and Zn concentrations (ppm)

	Sex	Braak	Age	PMI	CER Zn (ppm)	SMTG Zn (ppm)	HPG Zn (ppm)
Control 1	F	1	76	2.00	80.7	63.5	92.8
Control 2	F	1	80	2.25	76.8	74.2	55.5
Control 3	F	0	95	3.50	71.6	48.1	66.7
Control 4	F	2	93	2.75	89.6	60.6	83.6
Control 5	F	1	86	3.75	82	66.8	78.1
Control 6	M	0	90	3.50	83.4	88	60.6
Control 7	M	0	92	3.25	82.9	69.9	54.1
Control 8	M	2	81	2.00	69.9	60.6	72.5
MCI 1	F	3	91	5.00	-	59.2	51.3
MCI 2	F	3	93	2.75	56.2	109.4	51.3
MCI 3	F	3	82	3.00	83.9	114.2	113.9
MCI 4	M	4	91	2.00	90.2	-	70.8
EAD 1	F	5	91	4.75	96.6	110.7	47.8
EAD 2	M	5	88	2.75	152.8	77.4	61.7
EAD 3	M	4	80	3.00	63.8	80.9	80.9
EAD 4	M	5	88	3.75	79.1	89	114.1
EAD 5	M	4	92	2.00	99.3	39.3	75.2

CER - Cerebellum

SMTG - Superior and middle temporal gyrus

HPG - Hippocampus and parahippocampal gyrus

Appendix IV. Mouse brain sample information and Zn concentrations (ppm)

Mouse type	Sex	Zn (ppm)
WT 1	F	52.2
WT 2	F	67
WT 3	F	68
WT 4	F	78.2
WT 5	M	55.6
WT 6	M	59.6
WT 7	M	76.9
WT 8	M	60
APP/PS1 1	F	73.1
APP/PS1 2	F	74.4
APP/PS1 3	F	75.4
APP/PS1 4	F	74.5
APP/PS1 5	F	71.7
APP/PS1 6	M	61
APP/PS1 7	M	67.4
APP/PS1 8	M	63.6
APP/PS1 9	M	62.6
App/PS1/ZnT1 1	F	74.7
App/PS1/ZnT1 2	F	71.2
App/PS1/ZnT1 3	F	69
App/PS1/ZnT1 4	M	76
App/PS1/ZnT1 5	M	72.9
App/PS1/ZnT1 6	M	64.4

WT – Wild type

APP/PS1 – Amyloid precursor protein/preseniline 1

APP/PS1/ZnT1 - Amyloid precursor protein/ preseniline 1/Zn transporter 1

Appendix V. Subject demographic data for Zn study in senile plaques

	Age	Sex	PMI	Braak Stage
MCI 1	91	F	5.00	3
MCI 2	100	F	4.25	4
MCI 3	88	M	3.00	3
MCI 4	86	M	2.00	3
MCI 5	89	M	7.00	4
Control 1	89	M	2.5	0

Appendix VI. Subject demographic data for Zn study in neurofibrillary tangles

	Age	Sex	PMI	Braak Stage
MCI 1	92	F	3.00	2
MCI 2	91	F	5.00	3
MCI 3	95	F	2.15	3
MCI 4	88	M	3.00	3
MCI 5	96	M	3.00	4
MCI 6	90	M	2.20	4
MCI 7	91	M	2.00	4
Control 1	85	F	1.66	2
Control 2	92	F	4.00	2
Control 3	89	M	1.50	3
Control 4	89	M	2.50	0
Control 5	86	M	1.75	1

Appendix VII. Zinc concentrations (ppm) in MCI SP and neuropil

Braak Score =3			Braak Score = 3			Braak Score = 3		
MCI 1	**Neu**	**SP**	**MCI 2**	**Neu**	**SP**	**MCI 3**	**Neu**	**SP**
	71	278		48	132		74	205
	99	250		37	78		57	222
	112	231		34	89		62	162
	83	174		45	139		62	244
	52	197		39	92		61	224
	87	206		36	131		68	231
	103	169		43	102		73	262
	96	197		35	105		73	169
	113	222		40	105		59	320
	100	140		37	118		63	248
	78	155		40	65		58	152
	81	194		41	67		56	310
Average	90	201		39	102		64	229
Stdev	18	40		4	25		7	53

Braak Score = 4			Braak Score = 4		
MCI 4	**Neu**	**SP**	**MCI 5**	**Neu**	**SP**
	55	180		40	99
	62	136		33	130
	60	179		31	89
	57	131		32	86
	67	153		37	62
	55	147		39	74
	51	89		37	98
	59	127		34	107
	69	186		33	110
	59	118			
Average	59	145		35	95
Stdev	6	33		3	20

SP – Senile plaques

Neu – Neuropil

Appendix VIII. Zinc concentrations (ppm) in control neuropil

R-862	Neu	R-862	Neu	R-862	Neu
	26		70		115
	39		68		100
	57		63		99
	49		66		110
	60		72		91
	73		78		76
	59		69		67
	42		58		70
	50		58		49
	55		58		51
	54		57		50
	64		67		41
	66		65		76
	41		61		57
	50		59		50
	49		69		46
	64		59		47
	65		64		47
	72		72		61
	83				55
	43				51
	47				50
	45				59
					53
Average	54		65		65
Stdev	13		6		22

Appendix IX. Zinc concentrations (ppm) in MCI NFT and neuropil

Sample	Neu	NFT	Sample	Neu	NFT	Sample	Neu	NFT	Sample	Neu	NFT
MCI 1	104	137	MCI 2	114	143	MCI 3	112	144	MCI 4	122	170
	90	114		126	150		113	141		123	142
	81	101		138	197		132	177		123	188
	84	125		128	156		118	158		121	159
B=2	79	83	B=3	123	230	B=3	127	199	B=3	115	140
	90	104		118	299		143	189		117	142
	85	107		133	181		126	154		113	153
	81	112		134	197		140	215		126	191
	69	109		141	165		147	228		129	169
	98	125		200	234		150	234		134	196
				176	236		148	191		133	202
				132	240		154	191		139	176
				176	231		178	225		126	230
							180	192		153	265
Average				141	204		141	188		127	180
SD	86	112		26	45		21	31		10	36

Sample	Neu	NFT	Sample	Neu	NFT	Sample	Neu	NFT
MCI 5	120	163	MCI 6	140	195	MCI 7	120	169
	124	149		128	149		118	171
	118	155		133	180		117	138
	136	193		127	196		119	160
B=4	131	206	B=4	148	170	B=5	161	234
	160	163		152	196		166	178
	136	164		148	193		162	184
	134	161		149	161		172	193
	158	181		172	220		110	172
	157	173		174	248		113	128
	141	141		189	292		124	178
				212	330		132	188
				202	236			
				225	271			
Average	138	168		164	217		134	174
SD	15	19		32	53		23	27

NFT – Neurofibrillary Tangles

Neu - Neuropil

Appendix X. Zinc concentrations (ppm) in control neuropil

Control 1	Neu	Control 2	Neu	Control 3	Neu	Control 4	Neu	Control 5	Neu
	87		206		77		82		271
	97		179		77		90		260
	112		183		77		81		247
	105		186		77		69		275
	95		173		79		81		288
	96		179		71		74		280
	117		204		82		79		269
	104		189		71		81		268
	98		226		78		82		283
	114		193		86		72		263
	108		194		76		77		271
	100		212		77		99		245
	116		185		86		74		276
	120		206		73		71		293
	106		187		74		83		285
	123		224		114		81		260
	123		190		75		73		261
	123		187		75		72		272
	112		211		77		71		259
	129		185		73		64		295
Average	109		195		79		78		271
SD	11		15		9		8		14

REFERENCES

1. Evans, D. A.; Funkenstein, H. H.; Albert, M. S.; Scherr, P. A.; Cook, N. R.; Chown, M. J.; Hebert, L. E.; Hennekens, C. H.; Taylor, J. O., Prevalence of Alzheimer's disease in a community population of older persons. Higher than previously reported. *Journal of the American Medical Association* **1989,** 262, (18), 2551-2556.

2. Hebert, L. E.; Scherr, P. A.; Bienias, J. L.; Bennett, D. A.; Evans, D. A., Alzheimer disease in the US population: Prevalence estimates using the 2000 census. *Archives of Neurology* **2003,** 60, (8), 1119-1122.

3. Ciarleglio, L. J.; Bennett, R. L.; Williamson, J.; Mandell, J. B.; Marks, J. H., Genetic counseling throughout the life cycle. *Journal of Clinical Investigation* **2003,** 112, (9), 1280-1286.

4. St. George-Hyslop, P. H., The molecular genetics of Alzheimer's disease. In *Alzheimer's disease*, Terry, R. D.; Katzman, R.; Bick, L. L., Eds. Raven Press: New York, 1994; pp 345-352.

5. Levy-Lahad, E.; Wasco, W.; Poorkaj, P.; Romano, D. M.; Oshima, J.; Pettingell, W. H.; Yu, C. E.; Jondro, P. D.; Schmidt, S. D.; Wang, K.; Crowley, A. C.; Fu, Y. H.; Guenette, S. Y.; Galas, D.; Nemens, E.; Wijsman, E. M.; Bird, T. D.; Schellenberg, G. D.; Tanzi, R. E., Candidate gene for the chromosome 1 familial Alzheimer's disease locus. *Science* **1995,** 269, (5226), 973-977.

6. Corder, E. H.; Saunders, A. M.; Strittmatter, W. J.; Schmechel, D. E.; Gaskell, P. C.; Small, G. W.; Roses, A. D.; Haines, J. L.; Pericak-Vance, M. A., Gene dose of apolipoprotein E type 4 allele and the risk of Alzheimer's disease in late onset families. *Science* **1993,** 261, (5123), 921-923.

7. Mortimer, J. A.; Van Duijn, C. M.; Chandra, V.; Fratiglioni, L.; Graves, A. B.; Heyman, A.; Jorm, A. F.; Kokmen, E.; Kondo, K.; Rocca, W. A.; Shalat, S. L.; Soininen, H.; Hofman, A., Head trauma as a risk factor for Alzheimer's disease: A collaborative re-analysis of case-control studies. *International Journal of Epidemiology* **1991,** 20, (SUPPL. 2).

8. Snowdon, D. A.; Greiner, L. H.; Markesbery, W. R., Linguistic ability in early life and the neuropathology of Alzheimer's disease and cerebrovascular disease: Findings from the Nun Study. In *Annals of the New York Academy of Sciences*, 2000; Vol. 903, pp 34-38.

9. Snowdon, D. A.; Kemper, S. J.; Mortimer, J. A.; Greiner, L. H.; Wekstein, D. R.; Markesbery, W. R., Linguistic ability in early life and cognitive function and Alzheimer's disease in late life: Findings from the Nun Study. *Journal of the American Medical Association* **1996,** 275, (7), 528-532.

10. Leibson, C. L.; Rocca, W. A.; Hanson, V. A.; Cha, R.; Kokmen, E.; O'Brien, P. C.; Palumbo, P. J., Risk of dementia among persons with diabetes mellitus: A population-based cohort study. *American Journal of Epidemiology* **1997,** 145, (4), 301-308.

11. Ott, A.; Stolk, R. P.; Van Harskamp, F.; Pols, H. A. P.; Hofman, A.; Breteler, M. M. B., Diabetes mellitus and the risk of dementia: The Rotterdam Study. *Neurology* **1999,** 53, (9), 1937-1942.

12. Peila, R.; Rodriguez, B. L.; Launer, L. J., Type 2 diabetes, APOE gene, and the risk for dementia and related pathologies: The Honolulu-Asia Aging Study. *Diabetes* **2002,** 51, (4), 1256-1262.

13. Jick, H.; Zornberg, G. L.; Jick, S. S.; Seshadri, S.; Drachman, D. A., Statins and the risk of dementia. *Lancet* **2000,** 356, (9242), 1627-1631.

14. Skoog, I.; Lernfelt, B.; Landahl, S.; Palmertz, B.; Andreasson, L. A.; Nilsson, L.; Persson, G.; Ode?n, A.; Svanborg, A., 15-year longitudinal study of blood pressure and dementia. *Lancet* **1996,** 347, (9009), 1141-1145.

15. Ott, A.; Breteler, M. M. B.; De Bruyne, M. C.; Van Harskamp, F.; Grobbee, D. E.; Hofman, A., Atrial fibrillation and dementia in a population-based study: The Rotterdam study. *Stroke* **1997,** 28, (2), 316-321.

16. Merchant, C.; Tang, M. X.; Albert, S.; Manly, J.; Stern, Y.; Mayeux, R., The influence of smoking on the risk of Alzheimer's disease. *Neurology* **1999,** 52, (7), 1408-1412.

17. Ott, A.; Slooter, A. J. C.; Hofman, A.; Van Harskamp, F.; Witteman, J. C. M.; Van Broeckhoven, C.; Van Duijn, C. M.; Breteler, M. M. B., Smoking and risk of dementia and Alzheimer's disease in a population-based cohort study: The Rotterdam Study. *Lancet* **1998,** 351, (9119), 1840-1843.

18. Seshadri, S.; Beiser, A.; Selhub, J.; Jacques, P. F.; Rosenberg, I. H.; D'Agostino, R. B.; Wilson, P. W. F.; Wolf, P. A., Plasma homocysteine as a risk factor for dementia and Alzheimer's disease. *New England Journal of Medicine* **2002,** 346, (7), 476-483.

19. Gustafson, D.; Rothenberg, E.; Blennow, K.; Steen, B.; Skoog, I., An 18-year follow-up of overweight and risk of Alzheimer disease. *Archives of Internal Medicine* **2003,** 163, (13), 1524-1528.

20. Petersen, R. C.; Smith, G. E.; Waring, S. C.; Ivnik, R. J.; Tangalos, E. G.; Kokmen, E., Mild cognitive impairment: Clinical characterization and outcome. *Archives of Neurology* **1999,** 56, (3), 303-308.

21. Petersen, R. C.; Morris, J. C., Clinical features. In *Mild Cognitive Impairment*, Petersen, R. C.; . Eds. Oxford University: New York, 2003; pp 15-39.

22. Bennett, D. A.; Wilson, R. S.; Schneider, J. A.; Evans, D. A.; Beckett, L. A.;

Aggarwal, N. T.; Barnes, L. L.; Fox, J. H.; Bach, J., Natural history of mild cognitive impairment in older persons. *Neurology* **2002,** 59, (2), 198-205.

23. DeCarli, C., Mild cognitive impairment: Prevalence, prognosis, aetiology, and treatment. *The Lancet Neurology* **2003,** 2, (1), 15-21.

24. Danscher, G.; Jensen, K. B.; Frederickson, C. J.; Kemp, K.; Andreasen, A.; Juhl, S.; Stoltenberg, M.; Ravid, R., Increased amount of zinc in the hippocampus and amygdala of Alzheimer's diseased brains: A proton-induced X-ray emission spectroscopic analysis of cryostat sections from autopsy material. *Journal of Neuroscience Methods* **1997,** 76, (1), 53-59.

25. Wenstrup, D.; Ehmann, W. D.; Markesbery, W. R., Trace element imbalances in isolated subcellular fractions of Alzheimer's disease brains. *Brain Research* **1990,** 533, (1), 125-131.

26. Bush, A. I.; Pettingell, W. H.; Multhaup, G.; Paradis, M. D.; Vonsattel, J. P.; Gusella, J. F.; Beyreuther, K.; Masters, C. L.; Tanzi, R. E., Rapid induction of Alzheimer Abeta amyloid formation by zinc. *Science* **1994,** 265, (5177), 1464-1467.

27. Glabe, C. G., Common mechanisms of amyloid oligomer pathogenesis in degenerative disease. *Neurobiology of Aging* **2006,** 27, (4), 570-575.

28. Klein, W. L.; Krafft, G. A.; Finch, C. E., Targeting small A beta oligomers: The solution to an Alzheimer's disease conundrum? *Trends in Neurosciences* **2001,** 24, (4), 219-224.

29. Walsh, D. M.; Klyubin, I.; Fadeeva, J. V.; Cullen, W. K.; Anwyl, R.; Wolfe, M. S.; Rowan, M. J.; Selkoe, D. J., Naturally secreted oligomers of amyloid ? protein potently inhibit hippocampal long-term potentiation in vivo. *Nature* **2002,** 416, (6880), 535-539.

30. Wisniewski, H. M.; Narang, H. K.; Terry, R. D., Neurofibrillary tangles of paired helical filaments. *Journal of the Neurological Sciences* **1976,** 27, (2), 173-181.

31. Clements, A.; Allsop, D.; Walsh, D. M.; Williams, C. H., Aggregation and metal-binding properties of mutant forms of the amyloid Abeta peptide of Alzheimer's disease. *Journal of Neurochemistry* **1996,** 66, (2), 740-747.

32. Esler, W. P.; Stimson, E. R.; Jennings, J. M.; Ghilardi, J. R.; Mantyh, P. W.; Maggio, J. E., Zinc-induced aggregation of human and rat beta-amyloid peptides in vitro. *Journal of Neurochemistry* **1996,** 66, (2), 723-732.

33. Folstein, M. F.; Folstein, S. E.; McHugh, P. R., 'Mini mental state'. A practical method for grading the cognitive state of patients for the clinician. *Journal of Psychiatric Research* **1975,** 12, (3), 189-198.

34. Morris, J. C., The Clinical Dementia Rating (CDR): Current version and scoring rules. *Neurology* **1993,** 43, (11), 2412-2414.

35. Bentue-Ferrer, D.; Tribut, O.; Polard, E.; Allain, H., Clinically Significant Drug Interactions with Cholinesterase Inhibitors: A Guide for Neurologists. *CNS Drugs* **2003,** 17, (13), 947-963.

36. Livingston, G.; Katona, C., The place of memantine in the treatment of Alzheimer's disease: A number needed to treat analysis. *International Journal of Geriatric Psychiatry* **2004,** 19, (10), 919-925.

37. Van Marum, R. J., Current and future therapy in Alzheimer's disease. *Fundamental and Clinical Pharmacology* **2008,** 22, (3), 265-274.

38. St George-Hyslop, P. H.; Tanzi, R. E.; Polinsky, R. J., The genetic defect causing familial Alzheimer's disease maps on chromosome 21. *Science* **1987,** 235, (4791), 885-890.

39. Sommer, B., Alzheimer's disease and the amyloid cascade hypothesis: Ten years on. *Current Opinion in Pharmacology* **2002,** 2, (1), 87-92.

40. Coyle, J. T.; Puttfarcken, P., Oxidative stress, glutamate, and neurodegenerative disorders. *Science* **1993,** 262, (5134), 689-695.

41. Markesbery, W. R.; Ehmann, W. D., Trace element alterations in Alzheimer's disease. In *Alzheimer's disease*, Terry, R. D.; Katzman, R., Eds. Raven Press: New York, 1994.

42. Haass, C.; De Strooper, B., The presenilins in Alzheimer's disease - Proteolysis holds the key. *Science* **1999,** 286, (5441), 916-919.

43. Vetrivel, K. S.; Zhang, Y. W.; Xu, H.; Thinakaran, G., Pathological and physiological functions of presenilins. *Molecular Neurodegeneration* **2006,** 1, (1).

44. Vasto, S.; Candore, G.; Listi, F.; Balistreri, C. R.; Colonna-Romano, G.; Malavolta, M.; Lio, D.; Nuzzo, D.; Mocchegiani, E.; Di Bona, D.; Caruso, C., Inflammation, genes and zinc in Alzheimer's disease. *Brain Research Reviews* **2008,** 58, (1), 96-105.

45. Bour, A.; Grootendorst, J.; Vogel, E.; Kelche, C.; Dodart, J. C.; Bales, K.; Moreau, P. H.; Sullivan, P. M.; Mathis, C., Middle-aged human apoE4 targeted-replacement mice show retention deficits on a wide range of spatial memory tasks. *Behavioural Brain Research* **2008,** 193, (2), 174-182.

46. Bird, T. D., Genetic Factors in Alzheimer’s Disease. *N Engl J Med* **2005,** 352, (9).

47. Cherny, R.; Atwood, C. S.; Xilinas, M. E.; Gray, D. N.; Jones, W. D.; McLean, C. A.; Barnham, K. J.; Volitakis, I.; Fraser, F. W.; Kim, Y.; Huang, X.; Goldstein, L. E.; Moir, R. D.; Lim, J. T.; Beyreuther, K.; Zheng, H.; Tanzi, R. E.; Masters, C. L.; Bush, A. I., Treatment with copper-zinc chelator markedly and rapidly inhibits beta-amyloid accumulation in Alzheimer's disease transgenic mice. *Neuron* **2001,** 30, 641-642.

48. Giannakopoulos, P.; Herrmann, F. R.; Bussie?re, T.; Bouras, C.; Ko?vari, E.; Perl, D.

P.; Morrison, J. H.; Gold, G.; Hof, P. R., Tangle and neuron numbers, but not amyloid load, predict cognitive status in Alzheimer's disease. *Neurology* **2003,** 60, (9), 1495-1500.

49. Haines, A.; Iliffe, S.; Morgan, P.; Dormandy, T.; Wood, B., Serum aluminium and zinc and other variables in patients with and without cognitive impairment in the community. *Clinica Chimica Acta* **1991,** 198, (3), 261-266.

50. Forbes, W. F.; Hill, G. B., Is exposure to aluminum a risk factor for the development of Alzheimer disease? - Yes. *Archives of Neurology* **1998,** 55, (5), 740-741.

51. Munoz, D. G., Is exposure to aluminum a risk factor for the development of Alzheimer disease? - No. *Archives of Neurology* **1998,** 55, (5), 737-739.

52. Brewer, G. J., Iron and copper toxicity in diseases of aging, particularly atherosclerosis and Alzheimer's disease. *Experimental Biology and Medicine* **2007,** 232, (2), 323-335.

53. Cheung, K. H.; Shineman, D.; Mu?ller, M.; Ca?rdenas, C.; Mei, L.; Yang, J.; Tomita, T.; Iwatsubo, T.; Lee, V. M. Y.; Foskett, J. K., Mechanism of Ca2+ Disruption in Alzheimer's Disease by Presenilin Regulation of InsP3 Receptor Channel Gating. *Neuron* **2008,** 58, (6), 871-883.

54. Dreses-Werringloer, U.; Lambert, J. C.; Vingtdeux, V.; Zhao, H.; Vais, H.; Siebert, A.; Jain, A.; Koppel, J.; Rovelet-Lecrux, A.; Hannequin, D.; Pasquier, F.; Galimberti, D.; Scarpini, E.; Mann, D.; Lendon, C.; Campion, D.; Amouyel, P.; Davies, P.; Foskett, J. K.; Campagne, F.; Marambaud, P., A Polymorphism in CALHM1 Influences Ca2+ Homeostasis, Ab Levels, and Alzheimer's Disease Risk. *Cell* **2008,** 133, (7), 1149-1161.

55. Green, K. N.; LaFerla, F. M., Linking Calcium to Ab and Alzheimer's Disease. *Neuron* **2008,** 59, (2), 190-194.

56. Burnet, F. M., A possible role of zinc in the pathology of dementia. *Lancet* **1981,** 1, (8213), 186-188.

57. Andrasi, E.; Nadasdi, J.; Molnar, Z.; Bezur, L.; Ernyei, L., Determination of main and trace element contents in human brain by NAA and ICP-AES methods. *Biological Trace Element Research* **1990,** 26-27, 691-698.

58. Andrasi, E.; Suhajda, M.; Saray, I.; Bezur, L.; Ernyei, L.; Reffy, A., Concentration of elements in human brain: Glioblastoma multiforme. *Science of the Total Environment* **1993,** 139-140, 399-402.

59. Corrigan, F. M.; Reynolds, G. P.; Ward, N. I., Hippocampal tin, aluminum and zinc in Alzheimer's disease. *Biometals* **1993,** 6, (3), 149-154.

60. Deng, Q. S.; Turk, G. C.; Brady, D. R.; Smith, Q. R., Evaluation of brain element composition in Alzheimer's disease using inductively-coupled plasma mass spectrometry. *Neurobiol. Aging* **1994,** 15, (SUPPL.).

61. Ehmann, W. D.; Markesbery, W. R.; Alauddin, M., Brain trace elements in Alzheimer's disease. *Neurotoxicology* **1986,** 7, (1), 197-206.

62. Samudralwar, D. L.; Diprete, C. C.; Ni, B. F.; Ehmann, W. D.; Markesbery, W. R., Elemental imbalances in the olfactory pathway in Alzheimer's disease. *Journal of the Neurological Sciences* **1995,** 130, (2), 139-145.

63. Deibel, M. A.; Ehmann, W. D.; Markesbery, W. R., Copper, iron, and zinc imbalances in severely degenerated brain regions in Alzheimer's disease: Possible relation to oxidative stress. *Journal of the Neurological Sciences* **1996,** 143, (1-2), 137-142.

64. Cornett, C. R.; Markesbery, W. R.; Ehmann, W. D., Imbalances of trace elements related to oxidative damage in Alzheimer's disease brain. *Neurotoxicology* **1998,** 19, (3), 339-346.

65. Lovell, M. A.; Robertson, J. D.; Teesdale, W. J.; Campbell, J. L.; Markesbery, W. R., Copper, iron and zinc in Alzheimer's disease senile plaques. *Journal of the Neurological Sciences* **1998,** 158, (1), 47-52.

66. Robertson, J. D.; Crafford, A. M.; Markesbery, W. R.; Lovell, M. A., Disruption of zinc homeostasis in Alzheimer's disease. *Nuclear Instruments and Methods in Physics Research, Section B: Beam Interactions with Materials and Atoms* **2002,** 189, (1-4), 454-458.

67. Lee, J. Y.; Cole, T. B.; Palmiter, R. D.; Suh, S. W.; Koh, J. Y., Contribution by synaptic zinc to the gender-disparate plaque formation in human Swedish mutant APP transgenic mice. *Proceedings of the National Academy of Sciences of the United States of America* **2002,** 99, (11), 7705-7710.

68. Palmiter, R. D.; Cole, T. B.; Quaife, C. J.; Findley, S. D., ZnT-3, a putative transporter of zinc into synaptic vesicles. *Proceedings of the National Academy of Sciences of the United States of America* **1996,** 93, (25), 14934-14939.

69. Molina, J. A.; Jimenez-Jimenez, F. J.; Aguilar, M. V.; Meseguer, I.; Mateos-Vega, C. J.; Gonzalez-Munoz, M. J.; De Bustos, F.; Porta, J.; Orti-Pareja, M.; Zurdo, M.; Barrios, E.; Martinez-Para, M. C., Cerebrospinal fluid levels of transition metals in patients with Alzheimer's disease. *Journal of Neural Transmission* **1998,** 105, (4-5), 479-488.

70. Shore, D.; Henkin, R. I.; Nelson, N. R., Hair and serum copper, zinc, calcium, and magnesium concentrations in Alzheimer-type dementia. *Journal of the American Geriatrics Society* **1984,** 32, (12), 892-895.

71. Jeandel, C.; Nicolas, M. B.; Dubois, F.; Nabet-Belleville, F.; Penin, F.; Cuny, G., Lipid peroxidation and free radical scavengers in Alzheimer's disease. *Gerontology* **1989,** 35, (5-6), 275-282.

72. Rulon, L. L.; Robertson, J. D.; Lovell, M. A.; Deibel, M. A.; Ehmann, W. D.; Markesbery, W. R., Serum zinc levels and Alzheimer's disease. *Biological Trace Element*

Research **2000,** 75, (1-3), 79-85.

73. Gonzalez, C.; Martin, T.; Cacho, J.; Brenas, M. T.; Arroyo, T.; Garcia-Berrocal, B.; Navajo, J. A.; Gonzalez-Buitrago, J. M., Serum zinc, copper, insulin and lipids in Alzheimer's disease epsilon 4 apolipoprotein E allele carriers. *European Journal of Clinical Investigation* **1999,** 29, (7), 637-642.

74. Takeda, A., Zinc homeostasis and functions of zinc in the brain. *Biometals* **2001,** 14, (3-4), 343-351.

75. Shi, L. Z.; Zheng, W., Establishment of an in vitro brain barrier epithelial transport system for pharmacological and toxicological study. *Brain Research* **2005,** 1057, (1-2), 37-48.

76. Strazielle, N.; Preston, J. E., Transport across the choroid plexuses in vivo and in vitro. *Methods in molecular medicine* **2003,** 89, 291-304.

77. Zheng, W., Toxicology of choroid plexus: Special reference to metal-induced neurotoxicities. *Microscopy Research and Technique* **2001,** 52, (1), 89-103.

78. Zheng, W.; Deane, R.; Redzic, Z.; Preston, J. E.; Segal, M. B., Transport of L-[125I]thyroxine by in situ perfused ovine choroid plexus: Inhibition by lead exposure. *Journal of Toxicology and Environmental Health - Part A* **2003,** 66, (5), 435-451.

79. Zheng, W.; Aschner, M.; Ghersi-Egea, J. F., Brain barrier systems: A new frontier in metal neurotoxicological research. *Toxicology and Applied Pharmacology* **2003,** 192, (1), 1-11.

80. Hershey, C. O.; Hershey, L. A.; Varnes, A., Cerebrospinal fluid trace element content in dementia: Clinical, radiologic, and pathologic correlations. *Neurology* **1983,** 33, (10), 1350-1353.

81. Molina, J. A.; Jime?nez-Jime?nez, F. J.; Aguilar, M. V.; Meseguer, I.; Mateos-Vega, C. J.; Gonza?lez-Mun?oz, M. J.; De Bustos, F.; Porta, J.; Orti?-Pareja, M.; Zurdo, M.; Barrios, E.; Marti?nez-Para, M. C., Cerebrospinal fluid levels of transition metals in patients with Alzheimer's disease. *Journal of Neural Transmission* **1998,** 105, (4-5), 479-488.

82. Sahu, R. N.; Pandey, R. S.; Subhash, M. N.; Arya, B. Y. T.; Padmashree, T. S.; Srinivas, K. N., CSF zinc in Alzheimer's type dementia. *Biological Psychiatry* **1988,** 24, (4), 480-482.

83. Kapaki, E.; Segditsa, J.; Papageorgiou, C., Zinc, copper and magnesium concentration in serum and CSF of patients with neurological disorders. *Acta Neurologica Scandinavica* **1989,** 79, (5), 373-378.

84. Rao, K. S. J.; Shanmugavelu, P.; Shankar, S. K.; Devi, R. P. R.; Rao, R. V.; Menon, S. P. R. B., Trace elements in the cerebrospinal fluid in Alzheimer's disease. *Alzheimer's*

Reports **1999,** 2, (6), 333-338.

85. Kovatsi, L.; Touliou, K.; Tsolaki, M.; Kazis, A., Cerebrospinal fluid levels of calcium, magnesium, copper and zinc in patients with Alzheimer's disease and mild cognitive impairment. *Trace Elements and Electrolytes* **2006,** 23, (4), 247-250.

86. Bettger, W. J.; O'Dell, B. L., A critical physiological role of zinc in the structure and function of biomembranes. *Life Sciences* **1981,** 28, (13), 1425-1438.

87. Golden, B. E., Zinc in cell division and tissue growth: Physiological aspects. In *Zinc in Human Biology*, Mills, C. F., Ed. Springer-Verlag: London, 1989; pp 119-127.

88. Vallee, B. L.; Falchuk, K. H., The biochemical basis of zinc physiology. *Physiological Reviews* **1993,** 73, (1), 79-118.

89. Frederickson, C. J.; Hernandez, M. D.; McGinty, J. F., Translocation of zinc may contricute to seizure-induced death of neurons. *Brain Research* **1989,** 480, (1-2), 317-321.

90. Takeda, A., Movement of zinc and its functional significance in the brain. *Brain Research Reviews* **2000,** 34, (3), 137-148.

91. Lehmann, H. M.; Brothwell, B. B.; Volak, L. P.; Bobilya, D. J., Zinc status influences zinc transport by porcine brain capillary endothelial cells. *Journal of Nutrition* **2002,** 132, (9), 2763-2768.

92. Bertoni-Freddari, C.; Fattoretti, P.; Casoli, T.; Di Stefano, G.; Giorgetti, B.; Balietti, M., Brain aging: The zinc connection. *Experimental Gerontology* **2008,** 43, (5), 389-393.

93. Haug, F. M. S., Electron microscopical localization of the zinc in hippocampal mossy fibre synapses by a modified sulfide silver procedure. *Histochemie* **1967,** 8, (4), 355-368.

94. Frederickson, C. J.; Klitenick, M. A.; Manton, W. I.; Kirkpatrick, J. B., Cytoarchitectonic distribution of zinc in the hippocampus of man and the rat. *Brain Research* **1983,** 273, (2), 335-339.

95. Perez-Clausell, J.; Danscher, G., Intravesicular localization of zinc in rat telencephalic boutons. A histochemical study. *Brain Research* **1985,** 337, (1), 91-98.

96. Perez-Clausell, J.; Danscher, G., Release of zinc sulphide accumulations into synaptic clefts after in vivo injection of sodium sulphide. *Brain Research* **1986,** 362, (2), 358-361.

97. Mohandas, B.; Colvin, R. A., The role of zinc in Alzheimer's disease. *Recent Res. Devel. Physiol.* **2004,** 2, 225-245.

98. Yu, W. H.; Lukiw, W. J.; Bergeron, C.; Niznik, H. B.; Fraser, P. E., Metallothionein III is reduced in Alzheimer's disease. *Brain Research* **2001,** 894, (1), 37-45.

99. Uchida, Y.; Takio, K.; Titani, K.; Ihara, Y.; Tomonaga, M., The growth inhibitory factor that is deficient in the Alzheimer's disease brain is a 68 amino acid metallothionein-like protein. *Neuron* **1991,** 7, (2), 337-347.

100. Uchida, Y.; Ihara, Y.; Tomonaga, M., Alzheimer's disease brain extract stimulates the survival of cerebral cortical neurons from neonatal rats. *Biochemical and Biophysical Research Communications* **1988,** 150, (3), 1263-1267.

101. Law, W.; Kelland, E. E.; Sharp, P.; Toms, N. J., Characterisation of zinc uptake into rat cultured cerebrocortical oligodendrocyte progenitor cells. *Neuroscience Letters* **2003,** 352, (2), 113-116.

102. Huang, L.; Kirschke, C. P.; Zhang, Y.; Yan, Y. Y., The ZIP7 gene (Slc39a7) encodes a zinc transporter involved in zinc homeostasis of the Golgi apparatus. *Journal of Biological Chemistry* **2005,** 280, (15), 15456-15463.

103. Colvin, R. A.; Fontaine, C. P.; Laskowski, M.; Thomas, D., Zn2+ transporters and Zn2+ homeostasis in neurons. *European Journal of Pharmacology* **2003,** 479, (1-3), 171-185.

104. Jia, Y.; Jeng, J. M.; Sensi, S. L.; Weiss, J. H., Zn2+ currents are mediated by calcium-permeable AMPA/kainate channels in cultured murine hippocampal neurones. *Journal of Physiology* **2002,** 543, (1), 35-48.

105. Koh, J. Y., Zinc toxicity on cultured cortical neurons: Involvement of N-methyl-D-aspartate receptors. *Neuroscience* **1994,** 60, (4), 1049-1057.

106. Cheng, C.; Reynolds, I. J., Calcium-sensitive fluorescent dyes can report increases in intracellular free zinc concentration in cultured forebrain neurons. *Journal of Neurochemistry* **1998,** 71, (6), 2401-2410.

107. Eide, D. J., Zinc transporters and the cellular trafficking of zinc. *Biochimica et Biophysica Acta - Molecular Cell Research* **2006,** 1763, (7), 711-722.

108. Langmade, S. J.; Ravindra, R.; Daniels, P. J.; Andrews, G. K., The transcription factor MTF-1 mediates metal regulation of the mouse ZnT1 gene. *Journal of Biological Chemistry* **2000,** 275, (44), 34803-34809.

109. Palmiter, R. D., Protection against zinc toxicity by metallothionein and zinc transporter 1. *Proceedings of the National Academy of Sciences of the United States of America* **2004,** 101, (14), 4918-4923.

110. Palmiter, R. D.; Findley, S. D., Cloning and functional characterization of a mammalian zinc transporter that confers resistance to zinc. *EMBO Journal* **1995,** 14, (4), 639-649.

111. Lovell, M. A.; Smith, J. L.; Xiong, S.; Markesbery, W. R., Alterations in zinc transporter protein-1 (ZnT-1) in the brain of subjects with mild cognitive impairment,

early, and late-stage Alzheimer's disease. *Neurotoxicity research* **2005,** 7, (4), 265-271.

112.Chowanadisai, W.; Kelleher, S. L.; Lo?nnerdal, B., Zinc deficiency is associated with increased brain zinc import and LIV-1 expression and decreased ZnT-1 expression in neonatal rats. *Journal of Nutrition* **2005,** 135, (5), 1002-1007.

113.Cherny, R. A.; Legg, J. T.; McLean, C. A.; Fairlie, D. P.; Huang, X.; Atwood, C. S.; Beyreuther, K.; Tanzi, R. E.; Masters, C. L.; Bush, A. I., Aqueous dissolution of Alzheimer's disease Abeta amyloid deposits by biometal depletion. *Journal of Biological Chemistry* **1999,** 274, (33), 23223-23228.

114.Suh, S. W.; Jensen, K. B.; Jensen, M. S.; Silva, D. S.; Kesslak, P. J.; Danscher, G.; Frederickson, C. J., Histochemically-reactive zinc in amyloid plaques, angiopathy, and degenerating neurons of Alzheimer's diseased brains. *Brain Research* **2000,** 852, (2), 274-278.

115.Stoltenberg, M.; Bruhn, M.; S 鴌 dergaard, C.; Doering, P.; West, M. J.; Larsen, A.; Troncoso, J. C.; Danscher, G., Immersion autometallographic tracing of zinc ions in Alzheimer beta-amyloid plaques. *Histochemistry and Cell Biology* **2005,** 123, (6), 605-611.

116.Miller, L. M.; Wang, Q.; Telivala, T. P.; Smith, R. J.; Lanzirotti, A.; Miklossy, J., Synchrotron-based infrared and X-ray imaging shows focalized accumulation of Cu and Zn co-localized with b-amyloid deposits in Alzheimer's disease. *Journal of Structural Biology* **2006,** 155, (1), 30-37.

117.Lee, J. Y.; Mook-Jung, I.; Koh, J. Y., Histochemically reactive zinc in plaques of the Swedish mutant beta-amyloid precursor protein transgenic mice. *The Journal of neuroscience : the official journal of the Society for Neuroscience* **1999,** 19, (11).

118.Friedlich, A. L.; Lee, J. Y.; Van Groen, T.; Cherny, R. A.; Volitakis, I.; Cole, T. B.; Palmiter, R. D.; Koh, J. Y.; Bush, A. I., Neuronal Zinc Exchange with the Blood Vessel Wall Promotes Cerebral Amyloid Angiopathy in an Animal Model of Alzheimer's Disease. *Journal of Neuroscience* **2004,** 24, (13), 3453-3459.

119.Lovell, M. A.; Smith, J. L.; Markesbery, W. R., Elevated zinc transporter-6 in mild cognitive impairment, Alzheimer disease, and Pick disease. *Journal of Neuropathology and Experimental Neurology* **2006,** 65, (5), 489-498.

120. Smith, J. L.; Xiong, S.; Markesbery, W. R.; Lovell, M. A., Altered expression of zinc transporters-4 and -6 in mild cognitive impairment, early and late Alzheimer's disease brain. *Neuroscience* **2006,** 140, (3), 879-888.

121. Vanhoe, H., A review of the capabilities of ICP-MS for trace element analysis in body fluids and tissues. *Journal of Trace Elements and Electrolytes in Health and Disease* **1993,** 7, (3), 131-139.

122. Patriarca, M., The contribution of inductively coupled plasma mass spectrometry

to biomedical research. *Microchemical Journal* **1996,** 54, (3), 262-271.

123. Subramanian, K. S., Determination of metals in biofluids and tissues: Sample preparation methods for atomic spectroscopic techniques. *Spectrochimica Acta - Part B Atomic Spectroscopy* **1996,** 51, (3 PART B), 291-319.

124. Pruszkowski, E.; Neubauer, K.; Thomas, R., An Overview of Clinical Applications by Inductively Coupled Plasma Mass Spectrometry. *Atomic Spectroscopy* **1998,** 19, (4), 111-115.

125. Chen, H.; Cao, S.; Zeng, X., Application of inductively coupled plasma mass spectrometry in biological samples analysis. *Fenxi Huaxue* **2001,** 29, (5), 596-600.

126. Panicaut, B.; Bonnefoy, C.; Moesch, C.; Lachatre, G., Inductively coupled plasma mass spectrometry. Perspectives in analysis and in biology. *Spectrome?trie de masse a? plasma couple? par induction (ICP-MS). Potentialite?s en analyse et en biologie* **2006,** 64, (5), 312-327.

127. Parsons, P. J.; Barbosa Jr, F., Atomic spectrometry and trends in clinical laboratory medicine. *Spectrochimica Acta - Part B Atomic Spectroscopy* **2007,** 62, (9), 992-1003.

128. Becker, J. S.; Zoriy, M. V.; Dehnhardt, M.; Pickhardt, C.; Zilles, K., Copper, zinc, phosphorus and sulfur distribution in thin section of rat brain tissues measured by laser ablation inductively coupled plasma mass spectrometry: Possibility for small-size tumor analysis. *Journal of Analytical Atomic Spectrometry* **2005,** 20, (9), 912-917.

129. Good, P. F.; Perl, D. P.; Lovell, M. A.; Ehmann, W. D.; Markesbery, W. R., Laser microprobe mass analysis in Alzheimer's disease [2]. *Annals of Neurology* **1993,** 34, (3), 413-415.

130. Lovell, M. A.; Ehmann, W. D.; Markesbery, W. R., Laser microprobe analysis of brain aluminum in Alzheimer's disease. *Annals of Neurology* **1993,** 33, (1), 36-42.

131. Thong, P. S. P.; Makjanic, J.; Watt, F., A review of nuclear microscopy and applications in medicine. *Singapore Medical Journal* **1996,** 37, (5), 527-531.

132. Chandra, S., SIMS ion microscopy as a novel, practical tool for subcellular chemical imaging in cancer research. *Applied Surface Science* **2003,** 203-204, 679-683.

133. Feldmann, J.; Kindness, A.; Ek, P., Laser ablation of soft tissue using a cryogenically cooled ablation cell. *Journal of Analytical Atomic Spectrometry* **2002,** 17, (8), 813-818.

134. Lovell, M. A.; Ehmann, W. D.; Markesbery, W. R., Quantitation in laser microprobe mass spectrometry (LMMS) as applied to biological tissue analysis. *J. Trace Microprobe Tech.* **1992,** 10, (2-3), 109-124.

135. Becker, J. S.; Zoriy, M.; Dobrowolska, J.; Matusch, A., Laser ablation inductively coupled plasma mass spectrometry (LA-ICP-MS) in elemental imaging of biological tissues and in proteomics. *Journal of Analytical Atomic Spectrometry* **2007,** 22, (7), 736-744.

136. Dobrowolska, J.; Dehnhardt, M.; Matusch, A.; Zoriy, M.; Palomero-Gallagher, N.; Koscielniak, P.; Zilles, K.; Becker, J. S., Quantitative imaging of zinc, copper and lead in three distinct regions of the human brain by laser ablation inductively coupled plasma mass spectrometry. *Talanta* **2008,** 74, (4), 717-723.

137. Kindness, A.; Sekaran, C. N.; Feldmann, J., Two-Dimensional Mapping of Copper and Zinc in Liver Sections by Laser Ablation - Inductively Coupled Plasma Mass Spectrometry. *Clinical Chemistry* **2003,** 49, (11), 1916-1923.

138. Spurr, A. R., Choice and preparation of standards for X ray microanalysis of biological materials with special reference to macrocyclic polyether complexes. *J.MICROSC.BIOL.CELL.* **1975,** 22, (2-3), 287-302.

139. Becker, J. S.; Zoriy, M. V.; Pickhardt, C.; Palomero-Gallagher, N.; Zilles, K., Imaging of copper, zinc, and other elements in thin section of human brain samples (hippocampus) by laser ablation inductively coupled plasma mass spectrometry. *Analytical Chemistry* **2005,** 77, (10), 3208-3216.

140. Jackson, B.; Harper, S.; Smith, L.; Flinn, J., Elemental mapping and quantitative analysis of Cu, Zn, and Fe in rat brain sections by laser ablation ICP-MS. *Analytical and Bioanalytical Chemistry* **2006,** 384, (4), 951-957.

141. Riondato, J.; Vanhaecke, F.; Moens, L.; Dams, R., Determination of trace and ultratrace elements in human serum with a double focusing magnetic sector inductively coupled plasma mass spectrometer. *Journal of Analytical Atomic Spectrometry* **1997,** 12, (9), 933-937.

142. Nelms, S., Determination of copper, zinc, and selenium in human serum samples. *American Biotechnology Laboratory* **2003,** 21, (11), 39.

143. Diem, K.; Lentner., C., *Scientific tables* 7th ed.; Ardsley, N.Y. : Geigy Pharmaceuticals: 1974.

144. Thompson, J.; Ward, N. I.; Gooddy, W., Elemental analysis of cerebrospinal fluid (CSF) by inductively coupled plasma mass spectrometry (ICP-MS). **1991**, 33/7-33/8.

145. Krachler, M., Microwave digestion methods for the determination of trace elements in brain and liver samples by inductively coupled plasma mass spectrometry. *Fresenius' Journal of Analytical Chemistry* **1996,** 355, (2), 120-128.

146. Kassu, A.; Yabutani, T.; Mulu, A.; Tessema, B.; Ota, F., Serum Zinc, Copper, Selenium, Calcium, and Magnesium Levels in Pregnant and Non-Pregnant Women in

Gondar, Northwest Ethiopia. *Biological Trace Element Research* **2007**, 1-10.

147. Kassu, A.; Yabutani, T.; Mahmud, Z. H.; Mohammad, A.; Nguyen, N.; Huong, B. T. M.; Hailemariam, G.; Diro, E.; Ayele, B.; Wondmikun, Y.; Motonaka, J.; Ota, F., Alterations in serum levels of trace elements in tuberculosis and HIV infections. *European Journal of Clinical Nutrition* **2006,** 60, (5), 580-586.

148. Helal, A. I.; Zahran, N. F.; Rashad, A. M., Isotopes and concentrations of Zn in human blood and serum by ICP-MS. *International Journal of Mass Spectrometry* **2002,** 213, (2-3), 217-224.

149. Dombovari, J.; Varga, Z.; Becker, J. S.; Matyus, J.; Kakuk, G.; Papp, L., ICP-MS determination of trace elements in serum samples of healthy subjects using different sample preparation methods. *Atomic Spectroscopy* **2001,** 22, (4), 331-335.

150. Alimonti, A.; Petrucci, F.; Fioravanti, S.; Laurenti, F.; Caroli, S., Assessment of the content of selected trace elements in serum of term and pre-term newborns by inductively coupled plasma mass spectrometry. *Analytica Chimica Acta* **1997,** 342, (1), 75-81.

151. Lambert, M. P.; Barlow, A. K.; Chromy, B. A.; Edwards, C.; Freed, R.; Liosatos, M.; Morgan, T. E.; Rozovsky, I.; Trommer, B.; Viola, K. L.; Wals, P.; Zhang, C.; Finch, C. E.; Krafft, G. A.; Klein, W. L., Diffusible, nonfibrillar ligands derived from Ab1-42 are potent central nervous system neurotoxins. *Proceedings of the National Academy of Sciences of the United States of America* **1998,** 95, (11), 6448-6453.

152. Gellein, K.; Skogholt, J. H.; Aaseth, J.; Thoresen, G. B.; Lierhagen, S.; Steinnes, E.; Syversen, T.; Flaten, T. P., Trace elements in cerebrospinal fluid and blood from patients with a rare progressive central and peripheral demyelinating disease. *Journal of the Neurological Sciences* **2008,** 266, (1-2), 70-78.

153. Krachler, M.; Rossipal, E.; Micetic-Turk, D., Concentrations of trace elements in sera of newborns, young infants, and adults. *Biological Trace Element Research* **1999,** 68, (2), 121-135.

154. Melo, T. M.; Larsen, C.; White, L. R.; Aasly, J.; Sjoakk, T. E.; Flaten, T. P.; Sonnewald, U.; Syversen, T., Manganese, copper, and zinc in cerebrospinal fluid from patients with multiple sclerosis. *Biological Trace Element Research* **2003,** 93, (1-3), 1-8.

155. Lyon, T. D. B.; Fell, G. S.; McKay, K.; Scott, R. D., Accuracy of multi-element analysis of human tissue obtained at autopsy using inductively coupled plasma mass spectrometry. *Journal of Analytical Atomic Spectrometry* **1991,** 6, (7), 559-564.

156. Lyon, T. D. B.; Fell, G. S., Trace elements in autopsy tissue. *Food Chemistry* **1992,** 43, (4), 299-306.

157. Panayi, A. E.; Spyrou, N. M.; Iversen, B. S.; White, M. A.; Part, P., Determination of cadmium and zinc in Alzheimer's brain tissue using Inductively

Coupled Plasma Mass Spectrometry. *Journal of the Neurological Sciences* **2002,** 195, (1), 1-10.

158. Gelinas, Y.; Lafond, J.; Schmit, J. P., Multielemental analysis of human fetal tissues using inductively coupled plasma-mass spectrometry. *Biological Trace Element Research* **1997,** 59, (1-3), 63-74.

159. Bocca, B.; Conti, M. E.; Pino, A.; Mattei, D.; Forte, G.; Alimonti, A., Simple, fast, and low-contamination microwave-assisted digestion procedures for the determination of chemical elements in biological and environmental matrices by sector field ICP-MS. *International Journal of Environmental Analytical Chemistry* **2007,** 87, (15), 1111-1123.

160. Bocca, B.; Forte, G.; Petrucci, F.; Senofonte, O.; Violante, N.; Alimonti, A., Development of methods for the quantification of essential and toxic elements in human biomonitoring. *Annali dell'Istituto Superiore di Sanita* **2005,** 41, (2), 165-170.

161. Bocca, B.; Lamazza, A.; Pino, A.; De Masi, E.; Iacomino, M.; Mattei, D.; Rahimi, S.; Fiori, E.; Schillaci, A.; Alimonti, A.; Forte, G., Determination of 30 elements in colorectal biopsies by sector field inductively coupled plasma mass spectrometry: Method development and preliminary baseline levels. *Rapid Communications in Mass Spectrometry* **2007,** 21, (11), 1776-1782.

162. Campbell, M. J.; Torvenyi, A., Non-spectroscopic suppression of zinc in ICP-MS in a candidate biological reference material (IAEA 392 Algae). *Journal of Analytical Atomic Spectrometry* **1999,** 14, (9), 1313-1316.

163. Houk, R. S., Mass spectrometry of inductively coupled plasmas. *Analytical Chemistry* **1986,** 58, (1).

164. McCurdy, E.; Potter, D., Optimising ICP-MS for the determination of trace metals in high matrix samples. *Spectroscopy Europe* **2001,** 13, (3).

165. Stewart, I. I.; Olesik, J. W., The effect of nitric acid concentration and nebulizer gas flow rates on aerosol properties and transport rates in inductively coupled plasma sample introduction. *Journal of Analytical Atomic Spectrometry* **1998,** 13, (11), 1249-1256.

166. McKhann, G.; Drachman, D.; Folstein, M., Clinical diagnosis of Alzheimer's disease: Report of the NINCDS-ADRDA work group under the auspices of Department of Health and Human Services Task Force on Alzheimer's disease. *Neurology* **1984,** 34, (7), 939-944.

167. Morris, J. C.; Heyman, A.; Mohs, R. C.; Hughes, J. P.; Van Belle, G.; Fillenbaum, G.; Mellitis, E. D.; Clark, C., The Consortium to Establish a Registry for Alzheimer's Disease (CERAD). Part I. Clinical and neuropsychological assessment of Alzheimer's disease. *Neurology* **1989,** 39, (9), 1159-1165.

168. Buschke, H.; Kuslansky, G.; Katz, M.; Stewart, W. F.; Sliwinski, M. J.; Eckholdt, H. M.; Lipton, R. B., Screening for dementia with the Memory Impairment Screen. *Neurology* **1999,** 52, (2), 231-238.

169. Markesbery, W. R.; Schmitt, F. A.; Kryscio, R. J.; Davis, D. G.; Smith, C. D.; Wekstein, D. R., Neuropathologic substrate of mild cognitive impairment. *Archives of Neurology* **2006,** 63, (1), 38-46.

170. National, National institute on aging and Reagan institute working group on diagnostic criteria for the neuropathological assessment of Alzheimer's disease. *Neurobiol Aging* **1997,** 18(S4), S1-S2.

171. Mirra, S. S.; Heyman, A.; McKeel, D.; Sumi, S. M.; Crain, B. J.; Brownlee, L. M.; Vogel, F. S.; Hughes, J. P.; Van Belle, G.; Berg, L., The Consortium to Establish a Registry for Alzheimer's Disease (CERAD). Part II. Standardization of the neuropathologic assessment of Alzheimer's disease. *Neurology* **1991,** 41, (4), 479-486.

172. Flood, D. G.; Reaume, A. G.; Dorfman, K. S.; Lin, Y. G.; Lang, D. M.; Trusko, S. P.; Savage, M. J.; Annaert, W. G.; De Strooper, B.; Siman, R.; Scott, R. W., FAD mutant PS-1 gene-targeted mice: increased A beta 42 and A beta deposition without APP overproduction. *Neurobiol Aging* **2002,** 23, (3), 335-48.

173. Kawarabayashi, T.; Younkin, L. H.; Saido, T. C.; Shoji, M.; Ashe, K. H.; Younkin, S. G., Age-dependent changes in brain, CSF, and plasma amyloid ? protein in the Tg2576 transgenic mouse model of Alzheimer's disease. *Journal of Neuroscience* **2001,** 21, (2), 372-381.

174. Kanji, G. K., *100 Statistical Tests* Sage Publications Ltd: 1999; p 224.

175. Chakravarti, I. M.; Laha, R. G.; Roy, J., *Handbook of methods of applied statistics* Wiley: New York, 1967.

176. Levene, H., In *Contributions to Probability and Statistics: Essays in Honor of Harold Hotelling*, Olkin, I., Ed. Stanford University Press: Stanford, CA, 1960.

177. Glass, G. V., Peckham, P.D., & Sanders, J. R., Consequences of failure to meet assumptions underlying the fixed effects analysis of variance and covariance. *Review of Educational Research* **1972**, (42), 51.

178. Milligan, G. W., Wong, D. S., & Thompson, P. A., Robustness properties of nonorthogonal analysis of variance. *Psychological Bulletin* **1987,** 101, (3), 7.

179. Siegel, D.; Castellan, N. J., Jr., *Nonparametric statistics for the behavioral sciences* 2nd ed.; McGraw-Hill: New York, 1988.

180. Meyers, L. S., Gamst, G., & Guarino, A. J. ; p.429, *Applied multivariate research: Design and interpretation*. Thousand Oaks, CA: Sage. : 2006.

181. Lam, K. K. K.; Chan, W. T., Novel laser sampling technique for inductively coupled plasma atomic emission spectrometry. *Journal of Analytical Atomic Spectrometry* **1997,** 12, (1), 7-12.

182. Lowe, T.; Chen, Q.; Fernando, Q.; Keith, R.; Gandolfi, A. J., Elemental analysis of renal slices by proton-induced X-ray emission. *Environmental Health Perspectives* **1993,** 101, (4), 302-308.

183. Carpenter, M. B., *Human Neuroanatomy*. Williams & Wilkins: 1983; p 872.

184. Cherny, R. A.; Legg, J. T.; McLean, C. A.; Fairlie, D. P.; Huang, X.; Atwood, C. S.; Beyreuther, K.; Tanzi, R. E.; Masters, C. L.; Bush, A. I., Aqueous dissolution of Alzheimer's disease Ab amyloid deposits by biometal depletion. *Journal of Biological Chemistry* **1999,** 274, (33), 23223-23228.

185. Mudher, A.; Lovestone, S., Alzheimer's disease - Do tauists and baptists finally shake hands? *Trends in Neurosciences* **2002,** 25, (1), 22-26.

186. Schmitz, C.; Rutten, B. P. F.; Pielen, A.; Scha?fer, S.; Wirths, O.; Tremp, G.; Czech, C.; Blanchard, V.; Multhaup, G.; Rezaie, P.; Korr, H.; Steinbusch, H. W. M.; Pradier, L.; Bayer, T. A., Hippocampal Neuron Loss Exceeds Amyloid Plaque Load in a Transgenic Mouse Model of Alzheimer's Disease. *American Journal of Pathology* **2004,** 164, (4), 1495-1502.

187. An, W. L.; Bjorkdahl, C.; Liu, R.; Cowburn, R. F.; Winblad, B.; Pei, J. J., Mechanism of zinc-induced phosphorylation of p70 S6 kinase and glycogen synthase kinase 3b in SH-SY5Y neuroblastoma cells. *Journal of Neurochemistry* **2005,** 92, (5), 1104-1115.

188. Harris, F. M.; Brecht, W. J.; Xu, Q.; Mahley, R. W.; Huang, Y., Increased tau phosphorylation in apolipoprotein E4 transgenic mice is associated with activation of extracellular signal-regulated kinase. Modulation by zinc. *Journal of Biological Chemistry* **2004,** 279, (43), 44795-44801.

189. Religa, D.; Strozyk, D.; Cherny, R. A.; Volitakis, I.; Haroutunian, V.; Winblad, B.; Naslund, J.; Bush, A. I., Elevated cortical zinc in Alzheimer disease. *Neurology* **2006,** 67, (1), 69-75.

190. Zabel, U.; Schreck, R.; Baeuerle, P. A., DNA binding of purified transcription factor NF-kappa B. Affinity, specificity, Zn2+ dependence, and differential half-site recognition. *Journal of Biological Chemistry* **1991,** 266, (1), 252-260.

191. Zeng, J.; Heuchel, R.; Schaffner, W.; Kagi, J. H. R., Thionein (apometallothionein) can modulate DNA binding and transcription activation by zinc finger containing factor Sp1. *FEBS Letters* **1991,** 279, (2), 310-312.

192. Zeng, J.; Vallee, B. L.; Kagi, J. H. R., Zinc transfer from transcription factor IIIA fingers to thionein clusters. *Proceedings of the National Academy of Sciences of the*

United States of America **1991,** 88, (22), 9984-9988.

193. Yang, J. P., Inhibition of the DNA-binding activity of NF-kB by gold compounds in vitro. *FEBS Letters* **1995,** 361, (1), 89-96.

194. Hussain, I.; Powell, D.; Howlett, D. R.; Tew, D. G.; Meek, T. D.; Chapman, C.; Gloger, I. S.; Murphy, K. E.; Southan, C. D.; Ryan, D. M.; Smith, T. S.; Simmons, D. L.; Walsh, F. S.; Dingwall, C.; Christie, G., Identification of a novel aspartic protease (Asp 2) as beta-secretase. *Molecular and Cellular Neurosciences* **1999,** 14, (6), 419-427.

195. Sinha, S.; Anderson, J. P.; Barbour, R.; Basi, G. S.; Caccaveffo, R.; Davis, D.; Doan, M.; Dovey, H. F.; Frigon, N.; Hong, J.; Jacobson-Croak, K.; Jewett, N.; Keim, P.; Knops, J.; Lieberburg, I.; Power, M.; Tan, H.; Tatsuno, G.; Tung, J.; Schenk, D.; Seubert, P.; Suomensaari, S. M.; Wang, S.; Walker, D.; Zhao, J.; McConlogue, L.; John, V., Purification and cloning of amyloid precursor protein ?-secretase from human brain. *Nature* **1999,** 402, (6761), 537-540.

196. Vassar, R.; Bennett, B. D.; Babu-Khan, S.; Kahn, S.; Mendiaz, E. A.; Denis, P.; Teplow, D. B.; Ross, S.; Amarante, P.; Loeloff, R.; Luo, Y.; Fisher, S.; Fuller, J.; Edenson, S.; Lile, J.; Jarosinski, M. A.; Biere, A. L.; Curran, E.; Burgess, T.; Louis, J. C.; Collins, F.; Treanor, J.; Rogers, G.; Citron, M., Beta-Secretase cleavage of Alzheimer's amyloid precursor protein by the transmembrane aspartic protease BACE. *Science* **1999,** 286, (5440), 735-741.

197. Yan, R.; Bienkowski, M. J.; Shuck, M. E.; Miao, H.; Tory, M. C.; Pauley, A. M.; Brashler, J. R.; Stratman, N. C.; Matthew, W. R.; Buhl, A. E.; Carter, D. B.; Tomaselli, A. G.; Parodi, L. A.; Heinrikson, R. L.; Gurney, M. E., Membrane-anchored aspartyl protease with Alzheimer's disease ?-secretase activity. *Nature* **1999,** 402, 531-537.

198. Lin, X.; Koelsch, G.; Wu, S.; Downs, D.; Dashti, A.; Tang, J., Human aspartic protease memapsin 2 cleaves the beta-secretase site of beta-amyloid precursor protein. *Proceedings of the National Academy of Sciences of the United States of America* **2000,** 97, (4), 1456-1460.

199. Sisodia, S. S.; St George-Hyslop, P. H., Gamma-secretase, Notch, Abeta and Alzheimer's disease: Where do the presenilins fit in? *Nature Reviews Neuroscience* **2002,** 3, (4), 281-290.

200. Selkoe, D. J., Translating cell biology into therapeutic advances in Alzheimer's disease. *Nature* **1999,** 399, (SUPPL.).

201. Selkoe, D. J.; Schenk, D., Alzheimer's Disease: Molecular Understanding Predicts Amyloid-Based Therapeutics. In *Annu Rev Pharmacol Toxicol*, 2003; Vol. 43, pp 545-584.

202. Backstrom, J. R.; Miller, C. A.; Tokes, Z. A., Characterization of neutral proteinases from Alzheimer-affected and control brain specimens: Identification of calcium-dependent metalloproteinases from the hippocampus. *Journal of Neurochemistry*

1992, 58, (3), 983-992.

203. Bergeron, C.; Petrunka, C.; Weyer, L., Copper/zinc superoxide dismutase expression in the human central nervous system: Correlation with selective neuronal vulnerability. *American Journal of Pathology* **1996,** 148, (1), 273-279.

204. Bush, A. I.; Atwood, C. S.; Huang, L., Abnormal homeostasis of ph1 and zinc: the prelunde for cerebral Aß amyloid formation. *Eur Neuropsychopharmacol* **1996,** 6 (suppl 3), S2-4.

205. Bush, A. I.; Pettingell Jr, W. H.; Paradis, M. D.; Tanzi, R. E., Modulation of Abeta adhesiveness and secretase site cleavage by zinc. *Journal of Biological Chemistry* **1994,** 269, (16), 12152-12158.

206. Bush, A. I.; Pettingell, W. H.; Paradis, M. D.; Tanzi, R., Zinc and Alzheimer's disease. *Science* **1995,** 268, 1921-3.

207. Mantyh, P. W.; Ghilardi, J. R.; Rogers, S.; DeMaster, E.; Allen, C. J.; Stimson, E. R.; Maggio, J. E., Aluminum, iron, and zinc ions promote aggregation of physiological concentrations of ?-amyloid peptide. *Journal of Neurochemistry* **1993,** 61, (3), 1171-1174.

VITA

Jiang Dong was born on October 29, 1980, in Yancheng, China, where he attended elementary, middle and high schools. He received a B. S. in Chemistry from the University of Science and Technology of China (2003).